Julius-Maximilians-Universität Würzburg

Zeitliche Charakterisierung der Funktion der Blut-Nerven-Schranke und der entzündungsauflösenden Lipide als Targets bei Neuropathie

Temporal characterization of the blood nerve barrier and specialized pro resolving mediators as therapeutic targets in neuropathy

Doctoral thesis for a doctoral degree

at the Graduate School of Life Sciences,

Julius-Maximilians-Universität Würzburg,

Section Neuroscience

submitted by

Adel Ben-Kraiem

from

Toulouse, France

Würzburg 2023

Reverse page

Submitted on: the 22nd of February 2023

……...……..

Office stamp

Members of the Thesis Committee

Chairperson: Prof. Dr. Carmen Villmann

Primary Supervisor: Prof. Dr. Heike Rittner

Supervisor (Second): Prof. Dr. Robert Blum

Supervisor (Third): Prof. Dr. Claudia Sommer

Supervisor (Fourth): Prof. Dr. Paul Pauli

(If applicable)

Table of content

Zusammenfassung

Neuropathische Schmerzen betreffen 6,9 bis 10 % der Allgemeinbevölkerung. Sie entstehen durch eine Verletzung oder Erkrankung des somatosensorischen Nervensystems und deren Behandlung ist eine Herausforderung. Die derzeitigen Behandlungen sind relativ unwirksam und haben starke Nebenwirkungen. Insofern sind die Identifizierung neuer Angriffspunkte und die Entwicklung neuer Behandlungsstrategien besonders wichtig. Die Blut-Nerven-Schranke besteht aus den endoneuralen Kapillaren und dem Perineurium, die beide durch Tight Junctions versiegelt werden. Letztere werden aus Tight Junction-Proteinen wie Claudin-5 und -1 gebildet. Da die Blut-Nerven-Schranke das Nervengewebe vor äußeren Einflüssen schützt und die Homöostase aufrechterhält, führt eine Öffnung zur Diffusion von potential algetischen Mediatoren und Infiltration von Immunzellen. Dieser Prozess fördert Neuroinflammation und sensibilisiert Nozizeptoren und verstärkt letztendlich die Schmerzen. Daher könnte die Abdichtung der Blut-Nerven-Schranke bei neuropathischen Schmerzen eine mögliche Behandlung darstellen.

„Specialised proresolving mediators“, wie Lipoxin A4 und Resolvin D1, sind kleine Lipide, die an Rezeptoren wie der Formlypeptid 2 Rezeptor (FPR2) binden und Entzündungsprozesse auflösen. Insbesondere Resolvin D1 hat nicht nur entzündungshemmende und schmerzlindernde Eigenschaften, sondern wirkt auch barriereabdichtend in Lungenepithelzellen. Der Einsatz von Resolvin D1 oder möglicherweise anderer „specialised proresolving mediators“ bei neuropathischen Schmerzen könnte also die Blut-Nerven-Schranke wieder abdichten und neuropathische Schmerzen lindern. In der vorliegenden Arbeit sollte die Blut-Nerven-Schranke in einem präklinischen Modell der diabetischen Polyneuropathie und einer Nervenverletzung („chronic constriction injury“) charakterisiert und „specialised proresolving mediators“ identifiziert werden, die die Blut-Nerven-Schranke abdichten und damit neuropathische Schmerzen lindern.

Bei der diabetischen Polyneuropathie ist die Blut-Nerven-Schranke nur für kleine Moleküle durchlässig, was auf den Verlust von Claudin-1 im Perineurium und eine geringere Anzahl von gefäßassoziierten Makrophagen zurückzuführen ist. Interessanterweise tritt die Durchlässigkeit der Blut-Nerven-Schranke erst vier bis acht Wochen nach der Diabetesinduktion auf, während die mechanische Hyperalgesie bereits nach zwei Wochen messbar ist. Dies spricht eher für eine schmerzunterhaltende als für eine schmerzauslösende Rolle der Blut-Nerven-Schranke.

Bei chronic constriction injury bilden sich die mechanische und thermische Hyperalgesie im Zeitraum von drei bis sechs Wochen nach der Verletzung zurück. Hier ist der Blut-Nerven-

Schranke von Anfang an sowohl für kleine als auch für große Moleküle durchlässig. Der Schmerzrückbildungsprozess findet vor allem parallel zur Abdichtung der endoneurialen Barriere für große Moleküle wie Fibrinogen aus dem Plasma und dessen Abbau statt. Das Perineurium ist neun Wochen nach der Verletzung noch durchlässig. Metabolomanalysen zeigen, dass insbesondere Vorläufer von Resolvin D1 sowie die entsprechenden Rezeptoren wie FPR2, zu Beginn der Schmerzrückbildung hochreguliert sind. Applikation von Resolvin D1 Nanopartikeln bzw. Agonisten des FPR2 an der Verletzungsstelle vor dem Beginn der Schmerzauflösung beschleunigt sich den Prozess und Fibrinogen ist nicht mehr endoneurial nachweisbar.

Zusammenfassend ist je nach Art der Nervenschädigung die Blut-Nervenschranke unterschiedlich stark betroffen. Ein direktes mechanisches Trauma und die begleitende Inflammation führen im Gegensatz zur metabolisch-toxischen Schädigung zu einer ausgeprägteren und langanhaltenden Durchlässigkeit. Gerade bei einer Nervenläsion sind verschiedene Bereiche (Ort der Nervendurchtrennung und distale Regenerationsbereiche) unterschiedlich betroffen von der Schädigung und der Reparatur. Insofern ist Hyperalgesie nur teilweise davon beeinflusst. Möglicherweise ist die Durchlässigkeit zumindest für kleine Moleküle für längerdauernde Reparaturvorgänge wichtig. Die Permeabilität der Kapillaren ist im Nerven nicht nur von den Tight Junctions sondern auch von anderen Zellen abhängig: neben gefäßassoziierten Makrophagen könnten auch Perizyten abdichtend wirken. Endoneuriales Fibrinogen löst Schmerzen aus, der genaue Mechanismus muss noch untersucht werden. Resolvinhaltige Nanopartikeln waren besonders effektiv und könnten lokal gut eingesetzt werden, da sie körpereigene Substanzen in nichttoxischen Partikeln enthalten.

Abstract

Neuropathic pain affects 6.9 to 10% of the general population, arises from lesion or disease of the somatosensory nervous system and is still challenging to treat. Indeed, current treatments efficacy are relatively low and present strong side effects. To that extent, identifying new targets and developing new treatment strategies constitute a priority. The blood nerve barrier consists of the endoneurial micro-blood vessels and the perineurium sealed by tight junctions constituted of tight junction proteins such claudin-5 and claudin-1. As the functional blood nerve barrier allows nerve tissue protection from external elements and maintains homeostasis, a destabilization or a disruption leads to infiltration of immunocytes promoting neuroinflammation and increased inflammatory mediators that can sensitize nociceptors and enhance pain. Thus resealing the blood nerve barrier in case of neuropathic pain could be a possible treatment strategy.

Specialised proresolving mediators such lipoxin A4 and resolvin D1 are small lipids that bind to receptors such the formylpeptide recptor 2 (FPR2) and resolve inflammation. Specially resolvin D1 as anti-inflammatory and analgesic properties. Thus using resolvin D1 or eventually other specialized proresolving mediators in neuropathic pain could reseal the blood nerve barrier and resolve neuropathic pain. The present work aimed to characterize the blood nerve barrier in a preclinical model of diabetic polyneuropathy and nerve injury (chronic constriction injury) and to identify specialized proresolving mediators that seal the blood nerve barrier and thereby alleviate neuropathic pain.

In diabetic polyneuropathy, the blood nerve barrier is permeable only to small molecules, which is due to the loss of claudin-1 in the perineurium and a reduced number of blood vessel-associated macrophages. Interestingly, blood nerve barrier permeability did not occur until four to eight weeks after diabetes induction, whereas mechanical hyperalgesia was measurable as early as two weeks. This suggests a pain-maintaining rather than a pain-triggering role of the blood nerve barrier.

In case of chronic constriction injury, a resolution process of both mechanical and thermal hyperalgesia occurs between three to six weeks after injury. Here, the blood nerve barrier is permeable to both small and large molecules from the beginning. The pain recovery process occurs primarily in parallel with the sealing of the endoneurial barrier to large molecules such as fibrinogen from the plasma and its degradation. Perineurium is still permeable nine weeks after injury. Metabolomic analyses show that especially precursors of Resolvin D1 as well as its receptor FPR2, are upregulated at the beginning of pain resolution. Application of resolvin D1 loaded nanoparticles or agonists of FPR2 at the injury site before the onset of pain resolution

accelerates the process and fibrinogen is no longer detectable in the endoneurium. Depending on the nerve damage, the blood nerve barrier is affected to varying degrees. Direct mechanical trauma and the accompanying inflammation lead to a more pronounced and long-lasting permeability - independent hyperalgesia. Possibly permeability, at least for small molecules, is important for prolonged reparative processes. In the nerve, permeability of capillaries in particular depends not only on tight junctions but also on other cells: in addition to macrophages, pericytes could also have a sealing effect. Endoneurial fibrinogen triggers pain; the exact mechanism remains to be investigated. Resolvin-containing nanoparticles were particularly effective and could be used locally as they contain endogenous substances in non-toxic particles.

General Introduction

„Im Schmerz ist so viel Weisheit wie in der Lust: er gehört gleich dieser zu den arterhaltenden Kräften ersten Ranges.“

*“*In pain, there is as much wisdom as in pleasure: like the latter, it is one of the best self-preservatives of a species.*”*

Friedrich Nietzsche

Pain and its classification

From the evolutional point of view, pain has a protective role. It is supposed to be an alarm that allows an individual to escape from dangerous and harmful situations, to preserve and care about a body part while healing and to avoid repeating such experiences later on (Clauw et al 2019). Nevertheless, in some cases pain persist and is no more a protecting signal or a symptom but an ailment and an issue necessitating attention and care.

Pain arises from nociception, the neural process of encoding noxious stimuli that are received by specialized fibers (unmyelinated C fibers and thinly myelinated Aδ fibers) that sense the physiochemical properties of pain stimuli (**Fig. 1**). Noxious stimuli are for example pressure (Aδ fibers), heat, cold, and some chemicals (C fibers). These peripheral inputs are transferred by nociceptive afferents to glutamatergic synapses in the dorsal horn of the spinal cord. The sensory inputs that arrive to the dorsal horn are then transmitted by different pathways ascending to the specific processing centers of the brain (thalamic nuclei and somatosensory cortex) for pain perception. The body can not only sense pain but also control pain. To this end, a descending inhibitory pathway is activated passing through in the periaqueductal grey matter where serotoninergic neurons are found. These neurons projects to enkephalinergic neurons in the dorsal horn of the spinal cord, which by releasing enkephalin inhibit the noxious signal transmission in order to reduce pain sensation.

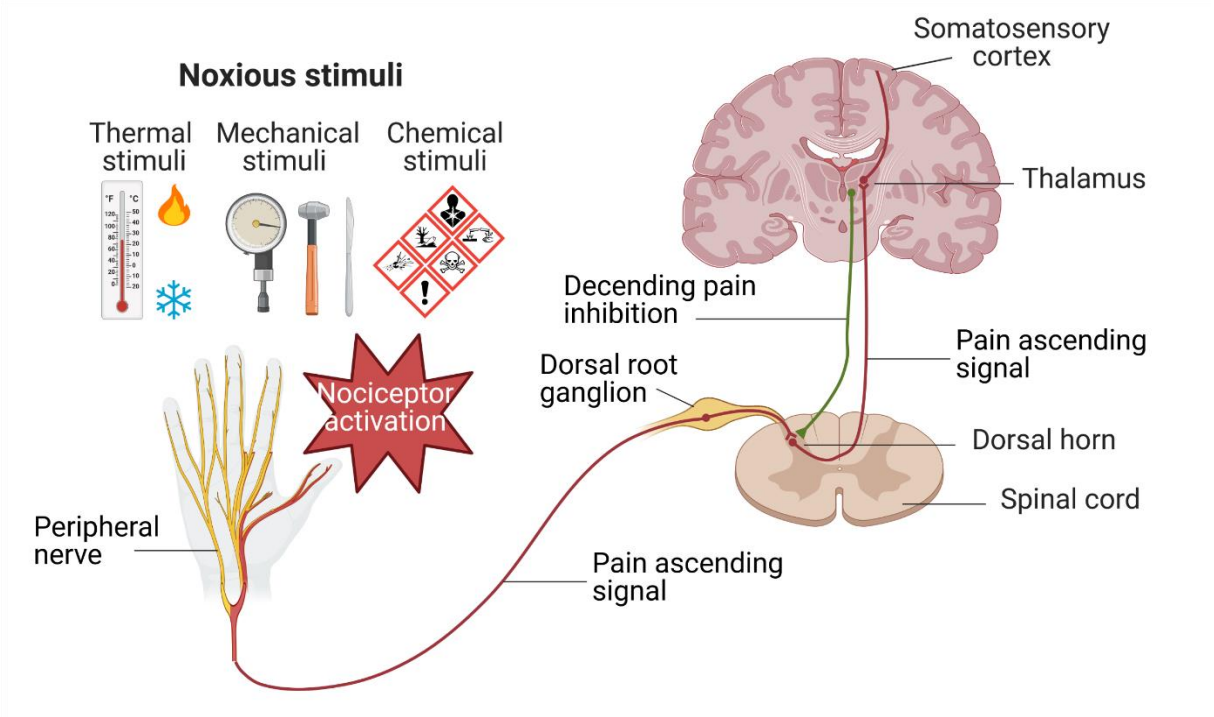

Fig. 1 Simplified diagram showing the peripheral and central nervous system pathways for pain sensation (illustration made with Biorender SCR_018361).

The international association for the study of pain (IASP) and the world health organization (WHO) agreed on a generic definition of pain as: "An unpleasant sensory and emotional experience associated with actual or potential tissue damage or described in terms of such damage." (Terminology | International Association for the Study of Pain (iasp-pain.org))

- Pain is a subjective experience perceived differently between individuals that can be affected to a certain extent by biological, physiological and social factors.
- Nociception and pain differ as the first is a sensory process directly linked to sensory neuron activity and the latest is an experience resulting from the integration of the sensory neurons activity.
- Pain is a concept learned and experienced during individuals' life.
- Full credit and respect should be given to a person reporting a painful experience.
- Pain's primary role is to alarm and allow preservation and adaptation of individuals. However its adverse effects on different aspects of one's life (social and psychological well-being) has to be considered.
- The inability to communicate clearly or verbally does not invalidate the fact that an animal-being human or not experiences pain.

Following this definition pain is a subjective phenomenon, so defining it properly has been a challenge. Pain is considered as a symptom of an underlying condition and chronic pain is defined as a disease by itself. There are many classifications of pain; the mostly used is the one referring to the pathophysiology which describes three types of pain. First nociceptive pain, described as a normal physiological response to tissue damage resulting from trauma, non-healing injury or inflammatory processes (Clauw et al 2019, Orr et al 2017, Stanos et al 2016). The International Association for the Study of Pain (IASP) defines nociceptive pain as "pain that arises from actual or threatened damage to non-neural tissue and is due to the activation of nociceptors" (https://www.iasp-pain.org/resources/terminology/?ItemNumber=1698&navItemNumber=576). There are two categories of nociceptive pain, somatic pain that refers to injuries of the musculoskeletal system and visceral pain refers to internal organ injury and is often felt indirectly (Orr et al 2017). Nociceptive pain is the most experienced. Examples include e.g. wounds, inflammation, or injuries.

Second is neuropathic pain (NP). It is defined as pain caused by a lesion or disease of the somatosensory nervous system and occurs as a result of abnormal neural activity (Clauw et al 2019, Orr et al 2017). Neuropathic pain can be described as central or peripheral, depending on whether the lesion is in the peripheral or central nervous system (Clauw et al 2019). Neuropathic pain can be acute or chronic (lasting from weeks to months) and is challenging in diagnosis and treatment (Finnerup et al 2016) Examples include diabetic polyneuropathy, thalamic stroke, spinal cord injury and phantom pain most frequently after limb amputation.

The third group is chronic or nociplastic pain. It arises from altered nociception despite no clear evidence of actual or threatened tissue damage causing the activation of peripheral nociceptors, nor evidence for disease of or lesions within the somatosensory system causing the pain (Clauw et al 2019, Orr et al 2017, Stanos et al 2016).

Neuropathic pain

Chronic pain affects more than 30% of people worldwide (Cohen et al 2021) and is more and more considered as a disease itself rather than a symptom. In my thesis, the focus will be directed to neuropathic pain. Neuropathic pain can be chronic, and affects between 6.9 to 10% of the global population (Ye et al 2018) accounting for 20 to 25% of chronic pain affected population (Bouhassira 2019). Affected patients often exhibit a wide range of symptoms such spontaneous pain, continuous or paroxysmal and evoked pain. Evoked pain can be described as allodynia or hypersensitivity when arising from normally non-noxious stimuli and hyperalgesia

when resulting in an exaggerated response to a normally noxious stimulus. Triggers for evoked pain can both be mechanical and/or thermal stimuli. Mechanical allodynia would be initiated by moving stimuli, by pressure or punctate stimuli. Thermal evoked pain from either heat or cold stimuli is predominantly due to cold allodynia/ hyperalgesia rather than heat allodynia/ hyperalgesia. Patients suffering from neuropathic pain describe it as burning pain or electric shock like pain, which differs from other types of chronic pain. Due to these symptoms patients usually experience further mischief, including sleep disturbances, anxiety, and depression (Bouhassira 2019).

To assess NP in patients some tools have been developed such as questionnaires and the quantitative sensory testing (QST). One must notice that pain intensity is measured using visual analog or numerical scales that are complemented by questionnaires such as the neuropathic pain scale, the neuropathic pain symptom inventory (NPSI), the McGill short-form questionnaire or the pain quality assessment scale. Such questionnaires are based on pain descriptors. The mostly used is the NPSI that refers to 10 pain descriptors each having a scale from 0 to 10 and cover the multiple dimensions and symptoms of neuropathic pain. This method is only based on patients' declarations and can to some extend be biased.

To another extent the QST is based on assessing sensory alterations by measuring the responses to mechanical, thermal and vibration stimuli. The QST allow to determine pain threshold of both, noxious and non-noxious stimuli. To that extent QST is considered as an objective measurement (Bouhassira 2019).

After detecting and measuring NP, treatment strategies are implemented. The first line therapy consists of antiepileptic treatments such as gabapentin and pregabalin, antidepressants like serotonin-noradrenaline-reuptake-inhibitors (SNRI) and tricyclic antidepressants. If not enough, a second line of treatment is recommended using local anesthetics like lidocaine patches, topical analgesics such capsaicin 8% patches, or weak opioids. In resistant cases third line therapy can be needed, thus implying the use of botulinum toxin A subcutaneously as myorelaxant treatment locally, strong opioids or invasive therapy (Finnerup et al 2015). Regardless of the kind of treatment, NP is still difficult to treat properly, essentially due to the low efficacy of the different treatments. For example, the number needed to treat (NNT) of the tricyclic antidepressants is 3.6, meaning that almost four patients need to be treated in order to have one patient recovering from NP which represents an efficacy a bit above 25%. For other treatments, the NNT range varies from 1.9 for botulinum toxin A, meaning an efficacy of 50% to a NNT of 10.6 for capsaicin 8% patches meaning less than 10% efficacy. Regarding tramadol and strong opioids, the NNT are respectively 4.7 and 4.3 indicating an efficacy between 20 and

25% (Finnerup et al 2015). Moreover one should not forget the side effects of these different treatments, such as drowsiness, dizziness, postural hypotension for tricyclic antidepressant, sleepiness, headaches, nausea for SNRI, or dizziness, sedation, nausea, constipation and addiction for opioids (Binder & Baron 2016).

For all these reasons developing new treatment strategies is of important need. To develop new treatments studying the molecular aspects pain in general and more precisely of neuropathic pain is a requirement, therefore lot of different animal models of pain were established. In fact as pain is multidimensional and processed both at the periphery and centrally the use of rodent model is a necessity in order to study properly all aspects of pain and their interaction from behavior level to cellular and molecular levels , which cannot be done in-vitro (Mogil et al 2010).

Models of neuropathic pain

Models of polyneuropathy

Polyneuropathies (peripheral neuropathies) are the most common type of disorder of the peripheral nervous system in adults, and specifically in the elderly, with an estimated prevalence of 5–8%, depending on age (Abboud et al 2021). Patients with common peripheral neuropathies such chemotherapy-induced (Ventzel et al 2018) or diabetic (Raputova et al 2017) polyneuropathies,(Finnerup et al 2003) exhibit a sensory loss profile (Abboud et al 2021). Recently, relevant models mimicking drug-induced peripheral neuropathy and diabetic polyneuropathy have been developed and validated. Some examples of these models are briefly discussed in the following.

Chemotherapy-induced peripheral neuropathy (CIPN) is a frequent and limiting side effect for a number of chemotherapeutic agents in ongoing oncological treatments. More 60% of patients experience acute CIPN, during their chemotherapy treatment (Sałat 2020). Many CIPN models have been established such the cisplatin-induced-neurotoxicity model (Authier et al 2003), the mouse model of oxaliplatin-induced peripheral neuropathy (Marmiroli et al 2017) and the bortezomib-induced peripheral neuropathy model (Yamamoto et al 2015). All models consist of repeated injections of the designated drug.

Diabetic polyneuropathy (DPN) is a progressive disease that leads to structural changes in the nerves causing hyperalgesia. DPN is the most common diabetes complication. In 10 to 26% of diabetic patients, DPN is painful (Raputova et al 2017). There are numerous animal models of DPN in rodents and possibly with different underlying pathophysiology. The most common metabolic model is the streptozotocin (STZ) diabetic rats and mice (Biessels et al 2014). This

model is the one studied in this thesis. Depending on the desired disease intensity, diabetes is induced by a single intraperitoneal or intravenous dose of 40–80 mg STZ/kg (rat), or 150–200 mg STZ/kg (mouse) body weight, or of lower doses given to mouse over consecutive days. STZ provoke the destruction of β-cells in the pancreas leading to a type 1 diabetes some days after injection (**Fig. 2**) (Furman 2015). Diabetes development occurs quite fast and can be regulated with insulin injection treatment. The development of neuropathy needs some time and treating with insulin slows down the process, as hyperglycemia would not be strong enough. The STZ model is one of most used models to induce diabetes due to its simplicity in implementation and monitoring in comparison to other type 1 diabetes models such the spontaneous diabetic rat model. The spontaneous diabetic rat model was developed by selecting rats that present a natural high blood glucose level and breed them until a fifth generation that is more prone to develop diabetes spontaneously (Goto et al 1976). The STZ model offers a higher diabetes incidence is high (92.5% develop severe diabetes five days after injection) while it varies between 9 to 50% of diabetes development between litters for the spontaneous diabetes rat model (Deeds et al 2011, Nakhooda et al 1978). A major limitation of the STZ model is that as it is a model of type 1 diabetes based on destruction of pancreatic islet cells and different from type 2 diabetes based on metabolic syndrome and insulin resistance of the tissue (Preguiça et al 2020). For example, the obese mouse or ob/ob mouse carries a mutation of the leptin gene, and thus cannot produce leptin leading to food overtake, obesity and later type 2 diabetes (Drel et al 2006). Although the STZ model cannot mimick the metabolic syndrome of type 2 diabetes, it has the advantage on both genetic type 2 diabetes models and other type 1 diabetes model to allow a precise control and monitoring of diabetes onset.

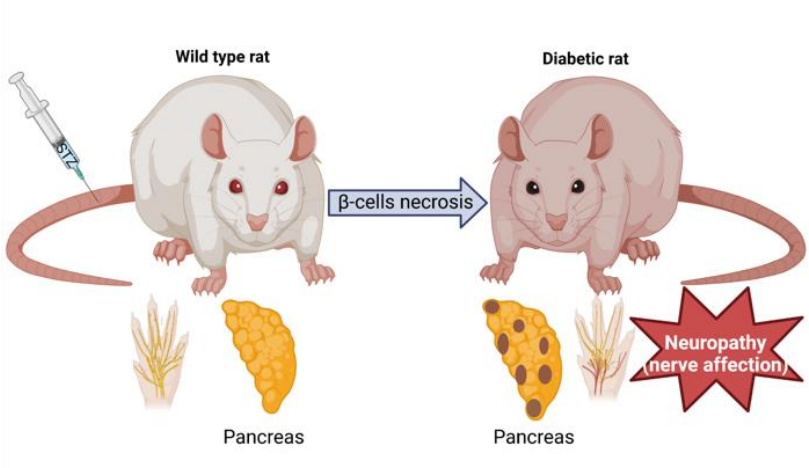

Fig. 2 Representation of diabetes induction following STZ injection in the tail vein (figure realised with Biorender SCR_018361).

Nerve injury models

Peripheral nerve traumatic injuries count for 2.8% of the trauma patients (Noble et al 1998) and those with severe cases often suffer chronic pain and eventually permanent disability (Siemionow & Brzezicki 2009). To study peripheral nerve injury, several partial nerve lesion models have been established. Indeed partial nerve lesion allows to observe and study NP but also nerve regeneration and pain resolution. Different models allows to study different injury grades with different aspects as one model cannot mimic all cases and symptoms. All these models differ in the procedure and thus in the period of the NP symptoms: The partial sciatic nerve ligation (PSNL) model was developed by Seltzer and colleagues in 1990 and is also called partial nerve injury (PNI) model (Seltzer et al 1990). Kim and Chung introduced the spinal nerve ligation (SNL) in rats in 1992 (Ho Kim & Mo Chung 1992). Spared nerve injury (SNI) was developed in 2000 (Decosterd & Woolf 2000). Chronic constriction injury (CCI) was first developed by Bennett and Xie in 1988 (Bennett & Xie 1988) (Fig. 3). It consists of four loose ligatures around the common branch of the sciatic nerve of rats or mice. The ligation of the nerve induces neuropathy as well as an inflammation (Costa et al 2005). CCI is not a permanent model. Spontaneous pain as well as pain hypersensitivity occurs 24 h after surgery and persist at least 6 weeks until recovery (Sommer et al 1995). Due to the tightness of the ligatures, a variability in responses can be observed (Wang et al 2021).

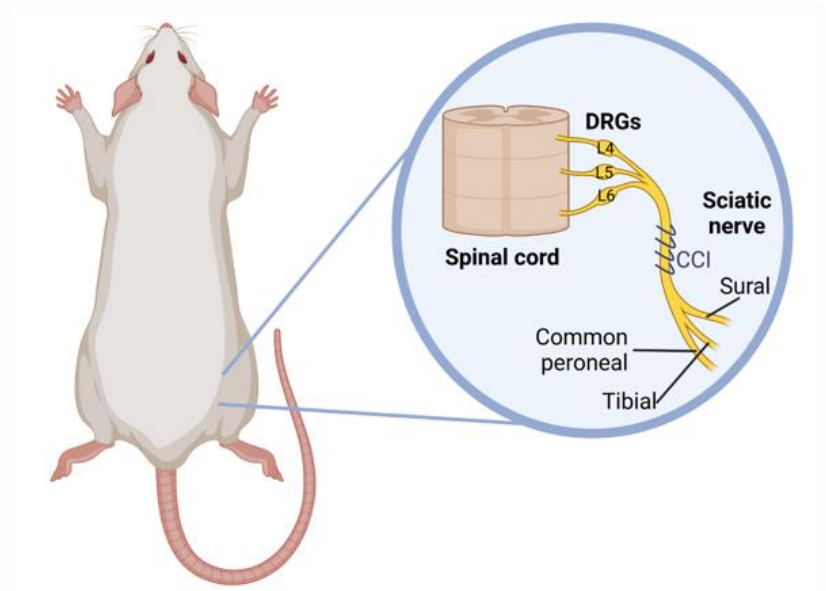

Fig. 3 Schematic representation of the CCI nerve injury model (created with Biorender SCR_018361).

In these models, pain-like behavior is a direct consequence of sciatic nerve lesion, and they are able to mimic certain neuropathic syndromes observed in patients. Typical syndroms with compression are carpal tunnel syndrome or nerve compression due to cancer or after injury. In addition, CCI is considered to be models of complex regional pain syndromes type 2 (CRPS) with sensory symptoms similar to those described in patients (e.g, touch hypersensitivity, mechanical hyperalgesia, spontaneous pain, and pain radiation as well as temperature differences and swelling). Finally, SNL models sciatica or radiculopathy (defined as pain resulting from injury or disease of the cervical, thoracic, lumbar or sacral nerve roots) (Abboud et al 2021). Thus, these models are of important need in order to study and identify new targets in the perspective of developing and finding new treatments. Indeed the recovery observed in the CCI model used in this thesis allowed us to study and describe the resolution phase in order to identify new targets and mechanisms for NP resolution.

Pain measurement in rodents

As for patients, in animal models pain-like behavior needs to be assessed. To study and understand nociceptive processes (pain) in animals several tests were developed. Pain measurement in animal models includes observation and analysis of reflexive responses to thermal (Hargreaves test) or mechanical stimuli (von Frey hair test) such as withdrawal thresholds to noxious stimuli. Reflexive measurements provide various information regarding physiological basis of nociception, identification of nociceptors and neurotransmitters, intracellular messengers and genes involved in pain behavior. Most of the reflexive behavioral tests closely mimic human evoked reactions (Gregory et al 2013) but cannot provide any information regarding spontaneous pain and affection of quality of life. Indeed, pain is a multidimensional experience that impact function and quality of life. Therefore, functional measurements (gait analysis and motor activity: CatWalk test and voluntary wheel running) can help to better understand its mechanisms (Gregory et al 2013). In the following, an overview of some behavior tests commonly implemented to assess pain-like behaviors in animal models that are also used in this thesis.

Reflexive pain tests

Reflexive pain tests are based on the observation of reflexes after stimuli induction. Thus, the von Frey hair test (**Fig. 4a**), developed in the 1890s in Würzburg by the physiologist Maximilian von Frey is used to evaluate mechanical allodynia in mice and rats. Two version of the test exist, the manual von Frey test that remains and thus despite the development of a more recent version, the second one, the electronic von Frey test. The procedure consists of placing animals in individual cages with a mesh bottom then a monofilament is applied at the plantar surface of the hind paw until it bends, delivering a constant pre-determined force. Usually, a series of filament exerting different forces are applied to determine nociceptive thresholds. Animals are considered to respond positively if they exhibit a pain-like behavior such swift paw withdrawal, paw licking or paw shacking during or right after the application of the filament (Deuis et al 2017).

In parallel the Hargreaves test (**Fig. 4b**), originally introduced in 1988, measures heat thresholds in the hind paws of mice and rats upon application of a radiant or infrared heat stimulus (Hargreaves et al 1988). During the test, animals are placed in a glass bottom enclosure underneath which a radiant or infrared heat source is positioned in a way that it is aimed at the plantar surface of the animal hind paw. The latency of paw withdrawal from application of the heat stimulus is recorded, and depending on the model of the Hargreaves system, may either be

recorded manually by the investigator or automatically by the apparatus. Calibration of the light source should be performed, that a paw withdrawal latency of 13 to 16s is obtained with naïve animals, thus providing a sufficient detection window to heat allodynia. A pre-determined cut off time of 20s is established to prevent tissue damage. The Hargreaves test allows measurement of both ipsilateral and contralateral heat thresholds; thus, each animal can serve as an internal control in unilateral pain models. Moreover, as during the procedure animals are not restrained, the probability of stress-induced response is reduced.

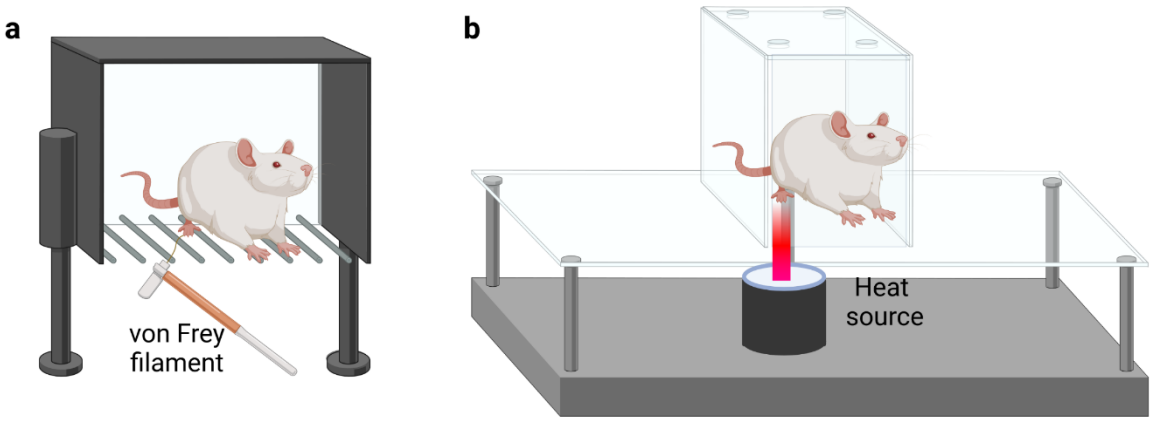

Fig. 4 Representation of reflexive Pain tests. Respectively in **(a)** von Frey hair test and in **(b)** Heargreaves test (created with Biorender SCR 018361).

Non-reflexive pain tests

Chronic pain affects quality of life, to that regard, some tests are implemented to observe and study basic function such motor activity and gait affection. For example, voluntary wheel running (**Fig. 5.a**) assesses the motor activity of animals – a natural pleasant behaviour of rodent. Rats or mice are placed in cage equipped with a running wheel with free access to food and water. When animals use the wheel, that is connected to a computer, their motor activity is monitored and subdivided in many parameters such as total covered distance, mean speed, maximal speed, mean acceleration, maximal acceleration and so on (Pitzer et al 2016). Pain expression can here be considered as a reduced motor activity. To another extent the rotarod test allows motor coordination analysis (**Fig. 5.b**). Animals are placed on a horizontal rod that rotates about its long axis; they must walk forwards to remain upright and not fall off. Both set speed and accelerating versions of the rotarod are available. The latency to fall in seconds (s)

is the measured. The less latency the animals perform the less motor coordination they have (Deacon 2013).

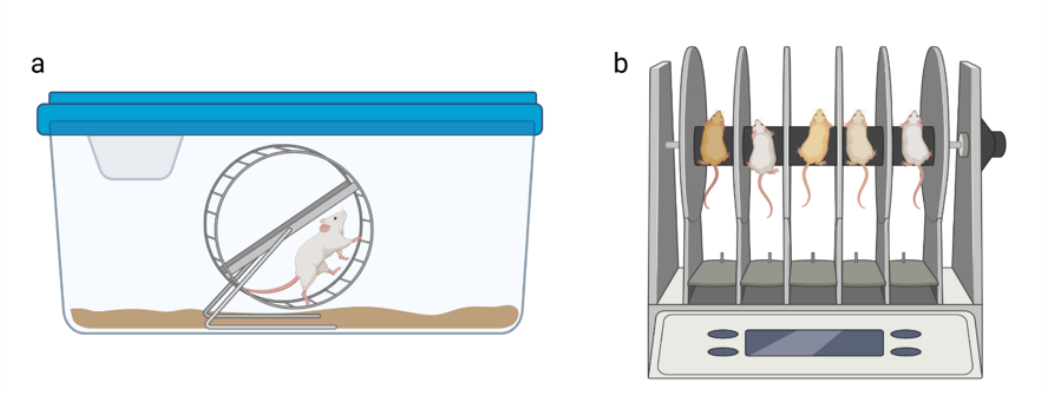

Fig. 5 Representation of non-reflexive tests. Respectively in **(a)** voluntary wheel running and in **(b)** rotarod test (created with Biorender SCR_018361).

The blood nerve barrier

The nervous system consists of its delicate structures, highly sensitive to homeostatic changes and determining basic vital functions. Hence, a variety of barriers shields it from external influence form the central level towards the periphery. These include the blood brain barrier (BBB), the blood spinal cord barrier (BSCB), the blood dorsal root ganglion barrier (BDRGB) and the blood nerve barrier (BNB). This thesis focuses on the BNB.

In the peripheral nervous system (PNS), nerves are separated from the external space by BNB (**Fig. 6**) consisting of the endoneurial micro-blood vessels and the perineurium. Cells of the perineurium, non-polarized flattened cells, are interconnected by tight junctions, gap junctions and adherens junction to preserve homeostasis. The perineurium constitutes the first defense line protecting axons against ion influx, toxins, and infections. It is also interesting to note that a reciprocal signaling between perineurial cells and Schwan cells is needed for a proper nerve ensheathment by both cell types (Kucenas et al 2008). A perturbation in the microenvironment or injury or/and BNB disruption leads to infiltration of immunocytes promoting neuroinflammation and increased inflammatory mediators that can sensitize nociceptors and enhance pain.

Originally, perineurial cells are developed in the CNS as ventral spinal cord glia cells before migrating into the periphery (Kucenas et al 2008). Claudin-1 is mainly expressed in the perineurium to maintain the perineurial barrier and permeability. Application of *Cldn1* siRNA or specific claudin-1 peptidomimetics unseal the BNB (Sauer et al 2014). Regulators of

tightness of the perineurial barrier include metalloproteinases (MMPs) like MMP9 (Hackel et al 2012b) or tissue plasminogen activator (Yang et al 2016).

The endoneurium contains endoneurial fluid, which maintains homeostasis and protection of the nerve microenvironment. Blood toxins have to be minimized and a controlled blood nerve exchange allows nourishing nerve and other tissues (Reinhold & Rittner 2017). This regulation is preserved by endothelial cells of endoneurial vessels. These vessels generate an intrinsic vasculature, occupying about 1% of the endoneurial area. They are sealed by tight junction proteins (TPJs), which are more permeable than the perineurial TJP including claudin-5, occludin and ZO-1.

Nerve injury damaging peripheral nerves leads to disruption of the BNB. After crush injury, *Cldn1*, *Cldn5* and *Ocln* are rapidly downregulated in endoneurium and perineurium (Hirakawa et al 2003). After CCI a prompt disruption of endoneurial vascular barrier correlates with a decreased expression of endothelial TJPs and an early and sustained alteration of Hedgehog signaling pathway (Moreau et al 2016). Interestingly, BNB breakdown occurs before the development of a neuropathic phenotype which evolves over days – at least after mechanical injury. Apart from the BNB, myelinated Schwann cells protect the PNS. These glial cells are wrapped around neurons in multiple sheaths to protect and isolate neurons increasing their conductance velocity. The mesaxon is a double-layered membrane of a Schwann cell that envelopes the nerve axon and connects the myelin sheaths. TJPs in Schwann cells are claudin-1, -3, -19, occludin, ZO-1 and tricellulin. During the development of Schwann cells, small clefts are left (Schmidt-Lantermann incisures), which allow communication between Schwann cell cytoplasm by connecting the inner and outer layer of the myelin sheath. TJPs found here are claudin-1, -3, -5, -12, occluding and ZO-1. Schwann cell myelination is interrupted by node of Ranvier to facilitate salutatory nerve conduction. Near the paranodal region, the barrier is sealed by claudin-1, -19, occluding, ZO-1 and tricellulin (Alanne et al 2009).

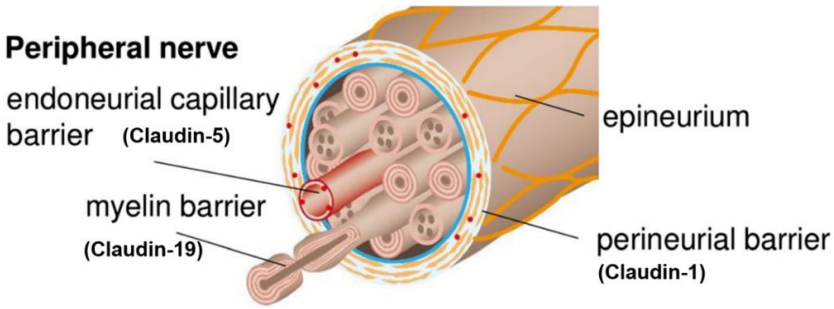

Fig. 6 Representation of the blood nerve barrier and its components. Reproduced with permission from Springer Nature, original figure with minor edits (Ben-Kraiem et al 2021).

Looking for new treatment strategies: SPMs as a possibility

Inflammation is a complex process involving various cells and protagonists. The inflammatory process has two phases. The first is an acute phase in which pro-inflammatory actors (neutrophils) are active and pro-inflammatory molecules and mediators (interleukin-1β (IL1β), Tnf α) are released leading to edema and swelling and last from min to hours. The second one called resolution phase lasts longer from hours to days and consists in activated anti-inflammatory actors (macrophages) and release of anti-inflammatory molecules and mediators (interleukin-6, -10, (IL6, IL10), leading normally to healing (**Fig. 7**). An incomplete resolution leads to chronic inflammation that in the case of nerve tissue induces NP.

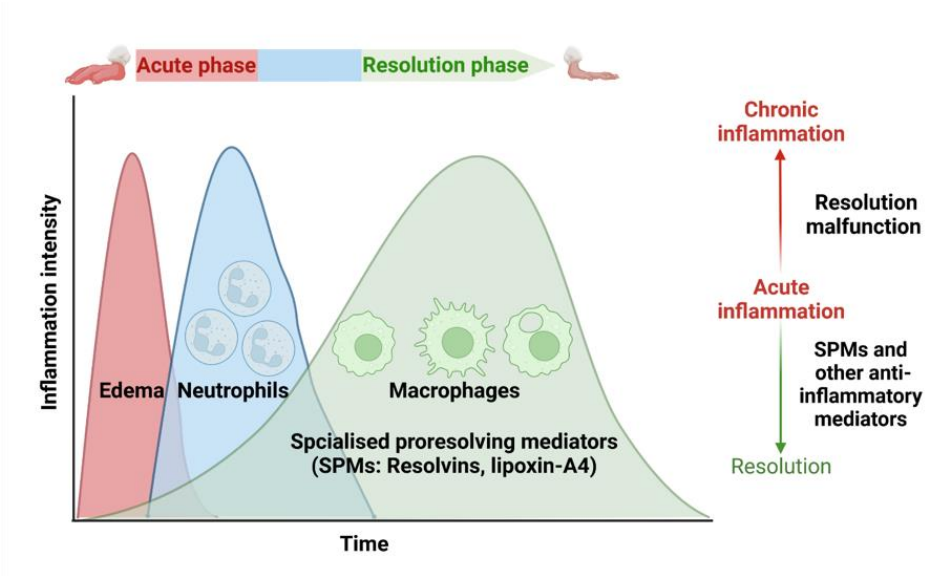

Fig. 7 Schematic representation of inflammation and its resolution (created with Biorender SCR_018361).

Searching on mechanism in resolution of acute inflammation a new genus of proresolving lipid mediators was discovered that includes separate families of molecules: lipoxins, resolvins, protectins, and maresins, collectively termed in specialized proresolving mediators (SPMs) (Serhan 2004, Serhan & Chiang 2013) (**Fig. 8**). In animal experiments, SPMs evoke anti-inflammatory mechanism and pain control (Ji et al 2011, Lim et al 2015). Resolvins, sometimes called as resolution-phase interactive products, are transcellular biosynthesized in resolving inflammatory exudates from ω-3 polyunsaturated fatty acids (PUFAs) such as eicosapentaenoic acid (EPA) and docosahexaenoic acid (DHA) and are thus denoted as E-series (RvE) and D-series (RvD) resolvins, respectively. Maresins are macrophage-derived mediators of inflammation resolution coined from macrophage mediator in resolving inflammation. Maresin

1 (Mar1), and more recently defined maresins, are12-lipoxygenase-derived metabolites of DHA, that also possess potent anti-inflammatory, pro-resolving, protective, and pro-healing properties. Mar1 enhances the uptake (e.g., stimulates the efferocytosis) of apoptotic human neutrophils by human macrophages and stimulates phagocytosis of it. Also produced out of DHA are protectins. Protectin D1 or also known as neuroprotectin D1 (NPD1) is an endogenous stereoselective lipid mediator and is mainly produced as a response to inflammatory signals. Studies showed that PD1 acts as a signaling molecule and through its ligand-receptor interaction down-regulates the expression of genes, such as NF-κB. Consequently, the pro-inflammatory gene cyclooxygenase-2 (COX-2) is down-regulated, which is responsible for the release of certain prostaglandins, a potent pro-inflammatory mediator (Mukherjee et al 2004). Additionally, there are not classic eicosanoids called lipoxins. They are derived enzymatically from arachidonic acid, an omega-6 fatty acid (Romano et al 2015). Initially, two lipoxins were identified, lipoxin A4 (LXA_4) with its receptor (ALX/FPR2) and LXB4, with evidence reducing hypersensitivity of pain and pro-inflammatory mediators from astrocytes.

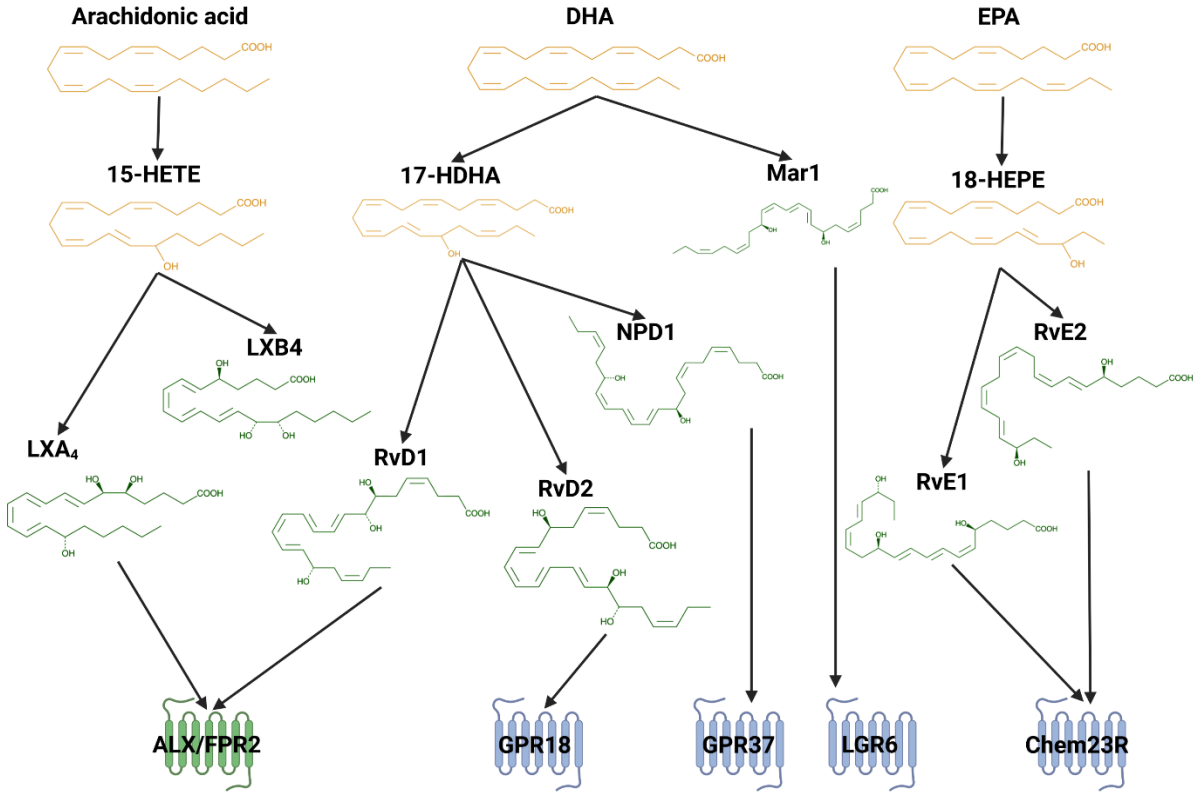

Fig. 8 Specialized proresolving mediators (SPMs) synthesis pathway and their known receptors (made with Biorender SCR 018361).

Resolvins are known to have antinociceptive properties: intraplantar and intrathecal application of RvD1 and RvE1 reduce thermal hypersensitivity without changing basal nociceptive thresholds in inflammatory pain (Huang et al 2011, Wang & Strichartz 2017, Xu et al 2010). Similarly, in several models of postsurgical pain SPMs are analgesic (Zhang et al 2018): Intrathecal administration of RvD1 before surgery ameliorates hypersensitivity (Huang et al 2011). Moreover, intrathecal post-operative treatment with NPD1, MaR1, and D-resolvins, RvD1 and RvD5, but not RvD3 and RvD4, effectively reduced mechanical hyperalgesia and cold allodynia (Zhang et al 2018). Intrathecal delivery of RvD1 at the day of thoracotomy or 4 days later, halved the spread of the mechano-sensitive area, lowered by 60% the percent of rats with tactile hypersensitivity, and reduced the drop in the threshold for a nocifensive response, along with a reduction in the occurrence of vigorous nocifensive responses (Wang & Strichartz 2017). Potential mechanisms include anti-inflammatory effect and the inhibition of different non-selective ion channels: transient receptor potential ankyrin 1 (TRPA1) and vanilloid 1, 2 and 4 (TRPV1, TRPV3 and TRPV4) expressed in DRGS as well as peripheral nerve endings in the skin and muscles (Bang et al 2010, Xu et al 2010).

Resolvins are unstable and thus that they have a limited half-life which constitute their main disadvantage. Therefore, long-acting substances are important for clinical application. Indeed, systemic application of a resolvin precursor,17(R)-hydroxy docosahexaenoic acid (17(R)-HDHA), inhibits the development and the maintenance of mechanical hyperalgesia in acute inflammation/arthritis (Lima-Garcia et al 2011) and osteoarthritis via elevation of plasma RvD2 and reduction in spinal cord astrogliosis (Huang et al 2017).

Not only inflammatory but also neuropathic pain is ameliorated by resolvins. In a rat model of non-compressive lumber disk herniation intrathecal injection of vehicle or RvD1 (10 or 100 ng) for three days was antinociceptive for up to 21 d, inhibited the up-regulation of TNF-α and IL-1β, increased the release of IL-10 and TGF-β1, and attenuated the expression of NF-kB/p65 and p-ERK in a dose-dependent manner (Liu et al 2016). In another model, chronic constriction injury (CCI), intrathecal pre-treatment of RvE1 daily for three days partially prevented the development of nerve injury-induced mechanical allodynia and up-regulation of IBA-1 (microglial marker) and TNF-α in the spinal cord dorsal horn. Furthermore, intrathecal post-treatment of RvE1, three weeks after nerve injury, transiently reduced mechanical allodynia and heat hyperalgesia (Xu et al 2010). To sum up, antinociception of resolvins by intraplantar or intrathecal application in inflammatory pain is well established but, surprisingly, in neuropathy and specifically CCI local perisciatic application of specific resolvins has not been examined before.

Only a few studies have explored barrier sealing properties of SPMs yet. Epithelial and endothelial cells were explored. Occludin and ZO-1 protein in vascular endothelia in lungs are reduced after exposure to lipopolysaccharide and normalize after systemic RvD1 treatment (Xie et al 2013). RvD1 relieves the pulmonary edema, restores pulmonary capillary permeability, and reduces disruption of tight junctions. Similarly, in salivary epithelial cells, RvD1 abolishes tight junction and cytoskeletal disruption, specifically ZO-1, caused by TNF-α. Thereby it enhances transepithelial resistance in these cells (Odusanwo et al 2012). Not only tight junctions but also adherens junction are preserved (Chattopadhyay et al 2017), because RvD1 blocks LPS-induced endothelial barrier dysfunction via blockade of adherents junction protein tyrosine phosphorylation. Mechanistically, the RvD1 shields endothelial adherens junction via activation of its receptors ALX/FPR2 and GPR32. Consistent with these observations, RvD1 also protects endothelial tight junctions' integrity and barrier function from lipopolysaccharide-induced disruption in mice arteries in vivo as well (Chattopadhyay et al 2017).

To sum up, RvD1 and RvE1 initiate the resolution of inflammation and the control of hypersensitivity via induction of anti-inflammatory signaling cascades. RvD1 binds to lipoxin A4/annexin-A1 7 receptor/formyl-peptide receptor 2 (ALX/FPR2) and reduces pain by interaction with TRPA1, RvE1 binds to chemerin receptor (ChemR23) and activates TRPV1. SPM are more potently analgesic than morphine or COX-2 inhibitors. However, it is unclear whether and how SPMs seal nerve barriers.

Aims and hypothesis

After traumatic nerve injury the BNB is opened. This leads to neuro-inflammation and influx of potentially proalgesic mediators. However, it is not known whether this is a common pathophysiological pathway in all neuropathies. SPMs have both anti-inflammatory and analgesic effects and are also able to reseal other barriers of the body after inflamation (Xie et al 2013). This opens the perspective of a possible new NP treatment strategy based SPMs to seal the BNB. Since SPMs are short-lived, challenge resides in developing long-lasting formulations.

Thus, the aims of this thesis are first to characterize the BNB and the role of TJPs in both DPN and CCI models – a metabolic and a mechanical injury-induced NP model. The metabolome then identified SPMs regulating the normal resolution process as well as the corresponding receptors. We then used this knowledge to locally apply SPMs RvD1 stabilized in nanoparticles as well as SPM analogs like BML111 in traumatic neuropathy.

We hypothesized that firstly in both, DPN and CCI, the BNB is disrupted and in CCI it reseals. We postulated, that endogenous specialized SPMs foster barrier resealing and pain relief in the healing/resolution phase after traumatic neuropathy. Secondly, we hypothesized that local RvD1 nanoparticle application reseals barriers, restores their function, and thereby resolves mechanical hyperalgesia in traumatic neuropathy.

Material and Methods

Animal models

Animal protocols (# REG 2-264 and 2-612) have been approved by the animal care committee of the provincial government of Würzburg. Both male and female Wistar rats (Janvier labs, Le Genest-St-Isle, France) weighing 150–250 g, free of pathogenic microorganisms, were housed in groups of six in cages, with enrichment tools, in a circadian light rhythm (12 h/12 h light/dark cycle, 21–25 °C, 45–55% humidity) with food and water ad libitum. All experiments were carried out during daytime at indicated time points. To habituate animals handling procedures were implemented in accordance with international guidelines for the care and use of laboratory animals (EU Directive 2010/63/EU for animal experiments). To monitor animal well-being score sheets were filled daily.

To study diabetic polyneuropathy two experimental groups were compared at different time points (four and eight weeks): vehicle and STZ (Sigma chemical) injected rats. STZ condition was established by injecting a 45 mg/kg STZ in 0.1 M citrate buffer pH 4.5 single intravenous dose (King 2012). Blood glucose measurement using Glucosmart® allowed us to characterize diabetes induction. Vehicle rats were injected with 0.1 M citrate buffer pH 4.5.

To study peripheral nerve injury, we used the CCI model. Adult male and female Wistar rats underwent surgery under brief isoflurane anesthesia (3.5%). No other analgesics were given. The common branch of the sciatic nerve at the right mid-thigh was exposed, and four loose silk ligatures (4/0) with about 1-mm spacing were tightened around the nerve. We closed the wound sewing with silk sutures (Rittner et al 2009, Sauer et al 2017). Sham animals underwent surgery under brief isoflurane anesthesia (3.5%) only. The common branch of the sciatic nerve at the right mid-thigh was exposed without any ligation and the wound was closed with silk sutures.

Behavioral testing

Mechanical hypersensitivity was determined using the von Frey test (Reinhold et al 2019, Sauer et al 2017, Sauer et al 2014). Applying a series of von Frey filaments (Aesthesio® set, UGO BASILE) we assessed and record the hind paw withdrawal threshold determining mechanical allodynia and touch sensitivity after STZ injection, CCI injury and CCI injury with BML111 or RvD1 loaded nanoparticles injection. The filaments were applied to the right hind paw plantar surface and were held for 1–3 s, until the filaments were bent to a 45° angle. Each paw was stimulated with filaments exerting different forces, with a 30-s recovery period between each application. The paw withdrawal threshold response was determined using Dixon's up and down method (Deuis et al 2017).

The Hargreaves test assessed heat hypersensitivity (IITC plantar test apparatus model 400 heated base) (Hackel et al 2012a). A radiant light source was applied on right hind paw. Measurements were repeated two times (with 30 s intervals). Averages were calculated subsequently.

Motor performance was studied using rotarod. Rats were placed on turning wheels and their performance (latency to fall from the wheel) was measured (Sauer et al 2017, Sauer et al 2014).

Motor activity was evaluated performing voluntary wheel running. Rats were housed individually in cages containing a running wheel once a week for 24 h. Unrestricted access to running wheel was continuously provided throughout the experiment and rats performance (covered distance and mean speed during 24 h) were measured by computer system (Bioseb spontaneous activity wheels reference: BIO-ACTIVW-M and BIOSEB ACTIVW-SOFT software) (Green-Fulgham et al 2022, Manglik et al 2016, Ni et al 2019, Tiwari et al 2018).

Perineural injection

All SPMs (BML111 and RvD1 nanoparticles) were injected locally at the injured sciatic nerve (right side). Male and female CCI Wistar rats were placed under brief isoflurane anesthesia (3.5%). A stimulation electrode (Pajunk Sonoplex®) was then placed in order to localize the sciatic nerve. Once the sciatic nerve localized thanks to a reflex in response to a 30 mA stimulation we could proceed with the treatment injections.

BML111 treated animals were injected twice daily with a 500 nmol of BML (CAS number 78606-80-1 ; Item:SML0215, Sigma Aldrich) in phosphate-buffered saline (PBS), once just after the baseline measurement and once after the last behavior testing six hours after the first injection thus for seven days. The vehicle group received only PBS injections.

Nanoparticles loaded with 500 nM RvD1 (CAS number 872993-05-0; Item: 10012554, Cayman Chemical) were injected in CCI rats once daily just after the baseline behavior measurement for seven days. The vehicle group received empty nanoparticles injections.

RvD1-loaded-nanoparticles preparation

The nanoparticles were prepared by our collaborators at Dr. Andrés García's lab at the Parker H. Petit Institute for Bioengineering and Bioscience in Georgia Institute of Technology, Georgia, USA.

Biotinylated polymeric polyethylene glycol–poly lactic acid-coglycolic acid (PEG-PLGA) (Nanosoft Polymers; PLGA MW = 10 KDa, PEG MW = 2 kDa) was dissolved in dimethylformamide (100 mg/mL). 3.76 μg of RvD1 (Cayman chemical, dissolved in ethanol at 0.1 mg/mL) was added to the polymer solution. From the polymer-resolvin mixture obtained

500 uL was added dropwise to 10 mL of PBS. Control unloaded-nanoparticles were prepared by dropwise addition of polymer solution (without resolvin) to PBS. The nanoparticles were stirred for four to five hours, concentrated by centrifugation using Amicon Ultra-15 centrifugal filter units, and filtered through sterile 0.45 μm syringe filters.

Permeability assessment

We assessed both permeability to small and large molecules. At the perineurial level permeability to small molecules in STZ and control rats was studied by immediately fixing harvested sciatic nerves with 4% PFA for 1 h and immersing them for 15 min in a 3% sodium fluorescein (NaFlu, 2 ml/kg; MW, 376 Da; Sigma-Aldrich) in saline solution.

To assess capillary permeability to small molecules, STZ and vehicle rats were intravenously injected with NaFlu,10%. After 30 min, the sciatic nerves were harvested and post fixated for 1 h in 4% paraformaldehyde (PFA) then placed in sucrose 10% over night. For both experiments tissues were then embedded in Tissue-Tek O.C.T compound (ref. 4583) and cut. Sections of 10 μm obtained were analyzed by microscopy (Keyence BZ-9000).

For large molecules permeability in perineurium, harvested STZ and vehicle sciatic nerves were immersed in 2 ml of Evans blue albumin (EBA, 5% bovine serum albumin (BSA) labeled with 1% Evans blue; both from Sigma Chemicals, 68 kDa) for 1 h. Then nerves were placed in sucrose 10% over night prior embedding in Tissue-Tek O.C.T compound (ref. 4583) and cut (Sauer et al 2017, Sauer et al 2014). Sections of 10 μm obtained were analyzed by microscopy (Keyence BZ-9000).

Endothelial permeability for large macromolecules was assessed using immunofluorescence directed against fibrinogen (340 kDa). Fixed in 4% PFA and embedded in O.C.T compounf STZ and control sciatic nerves tissue were cut in 10 μm sections and postfixed with ice cold acetone. Sections were permeabilized with 0.5% Triton-X100 in phosphate-buffered saline and blocked in 1% goat serum in phosphate-buffered saline and 3% bovine serum albumin in phosphate-buffered saline. Then, they were incubated with primary antibody goat anti fibrinogen (1:100 RRID: AB_10787808) over night and then incubated with secondary antibody donkey anti goat Alexa fluor 594 (1:600 RRID: AB_2762828). Stained sections were analyzed by microscopy (Keyence BZ-9000).

In the course of experiments, we brought some changes to the perineurial permeability protocol. These changes were applied on the nerve samples from CCI and Sham animals. Thus, harvested Sham and CCI nerves from the different time points got their extremities sealed with Vaseline. Then 1 mL of both EBA and NaFlu (5% BSA, 1% Evans Blue, 3% NaFlu in PBS) dye were

added on the nerves for a 15 min incubation time at room temperature in the dark. Then dye solution were taken away and samples washed with PBS and again we added 1mL of EBA only for 45 min at room temperature and in the dark. Once incubated the EBA solution was discarded and samples washed in PBS and then were fixed for two hours in PFA at 4°C still in the dark. After fixation tissue were washed a last time in PBS and then incubated in sucrose 10% overnight at 4°C before flash freezing in O.C.T compound thanks to liquid nitrogen-cooled methylbutane. Then 10 µm sections of 10 were cut and analyzed by microscopy (Keyence BZ-9000).

For the endoneurial permeability assessment after nerve injury (CCI) we perform only a fibrinogen staining on CCI and Sham harvested sciatic nerves at the different time points as described for the STZ animals.

Immunofluorescence and fluorescence microscopy

Sciatic nerves from STZ and vehicle rats frozen in O.C.T compound were sectioned and fixed with ice-cold acetone. Sections were permeabilized with 0.5% Triton-X100 in phosphate-buffered saline (PBS) and blocked in 1% goat serum in PBS and 3% bovine serum albumin in PBS. Then, they were incubated with primary antibodies mouse anti human, rat, canine claudin-1 (1:100; RRID AB_2533323), mouse anti human, rat-claudin-5 (1:100; RRID AB_2533200), rabbit anti-von Willebrand factor (vWF) (1:100; RRID:AB_2315602), mouse anti rat CD68 (RRID:AB_2291300), mouse anti rat RECA-1 (1:100; RRID:AB_935279), and rabbit anti rat CD206 (1:100; RRID:AB_1523910) overnight, following sequential incubation with secondary antibodies: donkey anti-mouse Alexa Fluor 555 (1:600; RRID:AB_2536180), goat anti-mouse FITC (1:600; RRID:AB_259378), donkey anti-rabbit Alexa Fluor 555 (1:600; RRID:AB_162543), and donkey anti-rabbit Alexa Fluor 488 (1:600, RRID:AB_2535792). DAPI 2 mg/ml in distilled water (Ref D9542, Sigma Aldrich) was used to stain nuclei. Fluorescence microscopy was performed (Keyence BZ-9000).

Frozen sciatic nerves from Sham, CCI, CCI+BML, CCI+vehicle, CCI+RvD1 and CCI+empty nanoparticles (vehicle) were sectioned and fixed with cold 4% paraformaldehyde (PFA). Section were permeabilized and blocked with 10% donkey serum in 0.3% Triton X_100, 0.1% Tween_20 in PBS. Then they were incubated over night with primary antibody goat anti fibrinogen (1:100 RRID: AB_10787808) and secondary antibody donkey anti goat Alexa fluor 594 (1:600 RRID: AB_2762828). Stained sections were analyzed by microscopy (Keyence BZ-9000). DAPI 2 mg/ml in distilled water (Ref D9542, Sigma Aldrich) was used to stain nuclei. Fluorescence microscopy was performed (Keyence BZ-9000).

Reverse transcription quantitative PCR

Total RNA was extracted from harvested sciatic nerves with Trizol (Invitrogen). 500ng of RNA per sample were transcribed to cDNA using the high capacity cDNA-kit (Applied Biosystems, Life technologies) following manufacturer's instructions. Samples were analyzed as triplicates. Relative mRNA abundances to Gapdh were calculated by the ΔΔCt method (threshold cycle value). To compare different samples, the control condition (vehicle animals / Sham) was set at 1. QPCR analysis was performed with the following primers using the Taqman method: *Cldn1* (Thermo Fischer Cat# Rn00581740_m1), *Cldn5* (Thermo Fisher cat# Rn01753146_s1), *Fpr2* (Thermo Fisher cat# Rn03037051_gH) and *Gapdh* (Thermo Fisher cat# Rn01462662_g1). QPCR analysis was carried out using the StepOnePlus Real-Time PCR System (Applied Biosystems) with the following program: fast 40 min for a run, 95 °C for 20s, and 45 cycles at 95 °C for 1 s and 60 °C for 20 s.

Western blot

Sciatic nerves were harvested eight weeks after injection of either vehicle solution or STZ. Then homogenized in RIPA lysis buffer (50 mM Tris pH 8.0; 150 mM NaCl; 0.1% SDS; 0.5% Na-deoxycholate; 1% NP40) with proteinase inhibitor (Complete, Roche Applied Science) and placed in tissue lyser for 5 min at maximal frequency of 30. Obtained homogenates were then centrifuged at 450g for 10min at 4 °C. Collected supernatants underwent centrifugation for 60 min at 20,000g at 4 °C to precipitate the membrane fraction. The cytosolic fraction in the supernatant was transferred to another tube and the precipitated membrane fraction dissolved in RIPA lysis buffer with proteinase inhibitors. We quantified Proteins with BCA protein assay reagent (Pierce, Rockford, IL, USA). Aliquots of protein were mixed with sodium dodecyl sulfate (SDS) containing buffer (Laemmli), denatured at 60 °C for 5 min then loaded in 12% SDS polyacrylamide gels, and subsequently blotted onto nitrocellulose membranes (Amersham™ catalogue number:10500001). Proteins were detected using specific antibodies: mouse anti claudin-5 1:200; RRID AB_2533200, mouse IgG HRP conjugated 1:3000 RRID: AB_330924 and—as protein loading control—β-actin HRP conjugated, 1:20,000 RRID: AB_262011. For quantification, claudin-5 band intensities were normalized to their β-actin loading control band.

After BML111 treatment experiment the same protocol as for STZ nerves was applied. Proteins were detected using specific antibodies: mouse anti claudin-5 1:200; RRID AB_2533200, mouse anti Gapdh 1:2000; RRID: AB_2107445, mouse IgG HRP conjugated 1:3000 RRID: AB_330924. Claudin-5 band intensities were normalized to their Gapdh loading-control band.

Image analysis

Working with FIJI (ImageJ) software, bioimages were analyzed. Regions of interest (ROI) were segmented manually for each image, and the fluorescence intensity (mean gray value) was measured in the determined ROIs. Three to six images were analyzed per animal, allowing the calculation of an individual mean fluorescence intensity. To quantify claudin-5 specifically in capillaries, co-staining for von Willebrand factor (vWF) were realised. Once claudin-5 and vWF got quantified following the above-described method with assurance that no changes in vWF expression was detected, we normalized claudin-5 fluorescence intensity on vWF fluorescence intensity. In order to quantify vessel-associated macrophages, sections were co-stained either for CD68 and vWF or CD206 and RECA-1. The total number of macrophages (CD68+ or CD206+) near blood vessels (vWF+ or RECA-1+) was counted and we calculated the ratio of the total number of macrophages to the total number of blood vessels.

Liquid chromatography tandem mass spectrometry (LC-Ms/Ms)

This procedure was done by our collaborators at Dr. Marco Sisignano's lab at the Pharmazentrum Frankfurt/ZAFES, Institute of Clinical Pharmacology, University Hospital, Goethe-University, D-60590 Frankfurt am Main, Germany.

Sciatic nerve from from CCI and Sham male Wistar rats at the differents time point were harvested, weighted and stored in dark eppendorf tube to avoid light exposure. They were then sent to our collaborators in a container with dry ice to maintain them cold and preserve the molecular state of the tissue. Then they proceeded LC-Ms/Ms. Briefly determination of SPMs precurssors was performed as described in detail by Toewe and colleagues (Toewe et al 2018) after some modifying method. Tissue sample homogenates extraction by solid phase extraction was achieved using Express ABN cartridges and an Extrahera (both from Biotage). Then, measurement of sample extracts were performed using an LC-MS/MS system constituted of an Agilent 1200 LC system and a 5500 QTRAP mass spectrometer from Sciex. Chiral chromatographic separation was done employing a Lux Amylose-1 column (250 x 4.6 mm, 3 µm, Phenomenex), applying water:FA (100:0.1, v/v) as solvent A and CAN:MeOH:FA (95:5:0.1, v/v/v) as solvent B in gradient elution mode. Data were acquired and evaluated using Analyst 1.6.2 and MultiQuant 3.0 softwares (both from Sciex).

Statistical analysis

Data are presented as mean ± SEM and medians and interquartile range. When two groups were compared a t test (parametric data) or Mann-Whitney non-parametric test were applied. One-

or two-way ANOVA or repeated measurements (RM), two-way ANOVA and Friedman's nonparametric test were used in case of multiple measurements with one or two variables (e.g., time and treatment), as described in the figure legends. Differences were considered significant if $p < 0.05$.

Results

Descriptive study on the role of tight junction proteins and blood vessel associated macrophages in induced diabetic polyneuropathy in sciatic nerve in rats

All data presented in this part are reproduced with permission from Springer Nature, original text and figures with minor edits corresponds to Ben-Kraiem A, Sauer RS, Norwig C, Popp M, Bettenhausen AL Sobhy Atalla M, Brack A, Blum R, Doppler K and Rittner H L. 2021. Selective blood-nerve barrier leakiness with claudin-1 and vessel-associated macrophage loss in diabetic polyneuropathy. Journal of Molecular Medicine (Ben-Kraiem et al 2021).

Mechanical hypersensitivity and motor alteration in STZ diabetic Wistar rats

First, we validated the model by measuring glycemia and observed a four-times increased level for all STZ-injected rats one week after injection and a seven-times higher level four to eight weeks after injection (**Fig. 9a, b**). We then confirmed neuropathic changes by detecting mechanical hypersensitivity starting at two weeks after STZ by von Frey hair test (**Fig. 9c**) in line with the previous findings (Fox et al 1999). In addition, the performance time on the rotarod, measuring motor function, was altered in STZ-treated rats (**Fig. 9d**).

Fig. 1

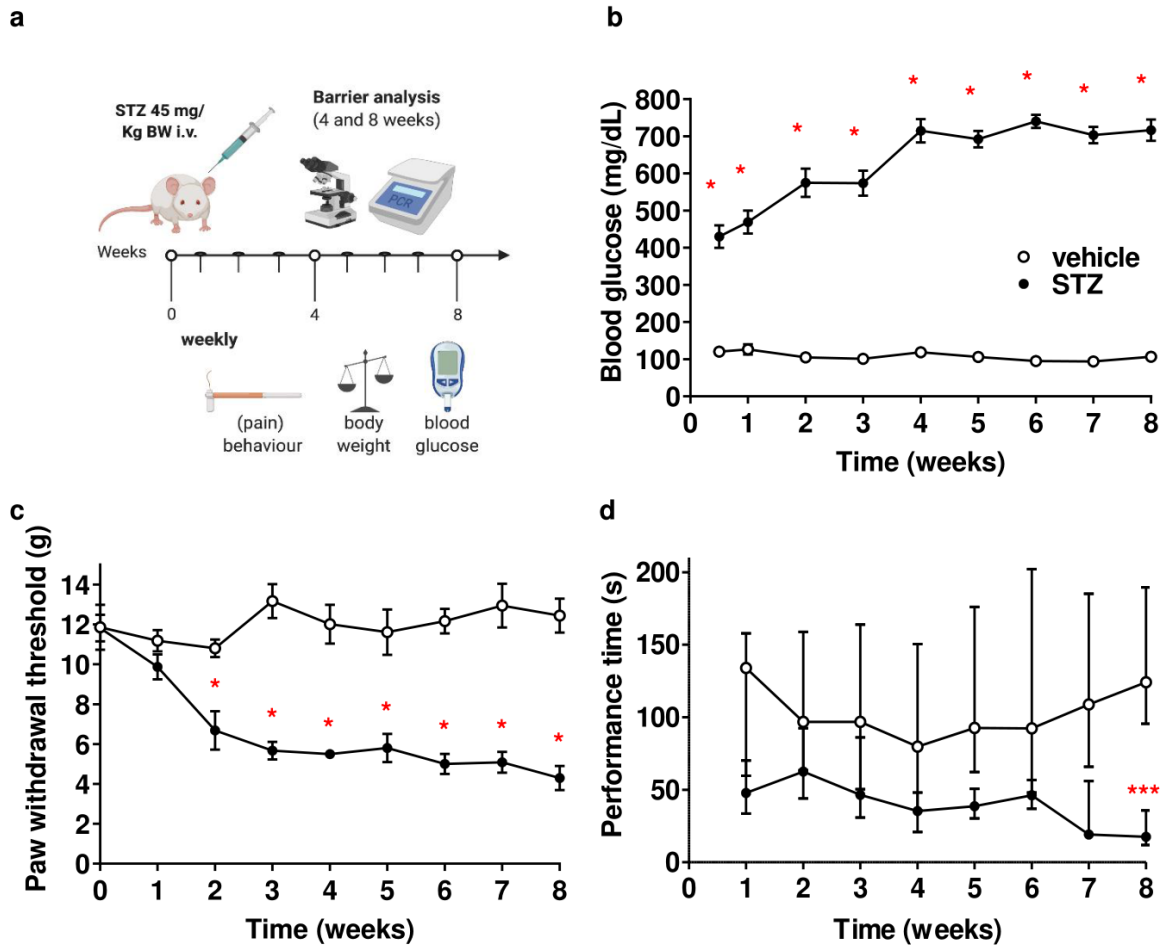

Fig. 9 Mechanical hypersensitivity and alteration of motor performance in STZ-induced diabetes type I in rats. (**a**) Male Wistar rats were treated with i.v. streptozotocin (STZ; once 45 mg/kg): experimental outline for tests and tissue harvest (created with Biorender SCR 018361). (**b**) Blood glucose in mg/dL, (**c**) mechanical allodynia measured by von Frey hairs (grams) and (d) motor function by Rotarod (sec). All data points represent mean ± SEM. *P < 0.05 (n = 6). Two-way repeated measurement ANOVA and Bonferroni post-hoc test for multiple comparisons. For Rotarod (**d**) data points represent median and interquartile range. ***P < 0.001 (n = 6); Friedman test and Dunn´s post hoc test for multiple comparison. Figure from Ben-Kraiem and colleagues., 2021: data collected by Sauer RS and analyzed by Ben-Kraiem A (Ben-Kraiem et al 2021)

Capillary, perineurial leakiness to small molecules and perineurial claudin-1 loss in STZ-induced DPN

At eight weeks after CCI, fluorescence in sciatic nerve endoneurium was enhanced after both *in vivo* (capillary barrier, **Fig. 10a-c**) and *ex vivo* (perineurial barrier, **Fig. 10d, e**) NaFlu application that indicate capillary and perineurial barrier leakiness for small molecules.

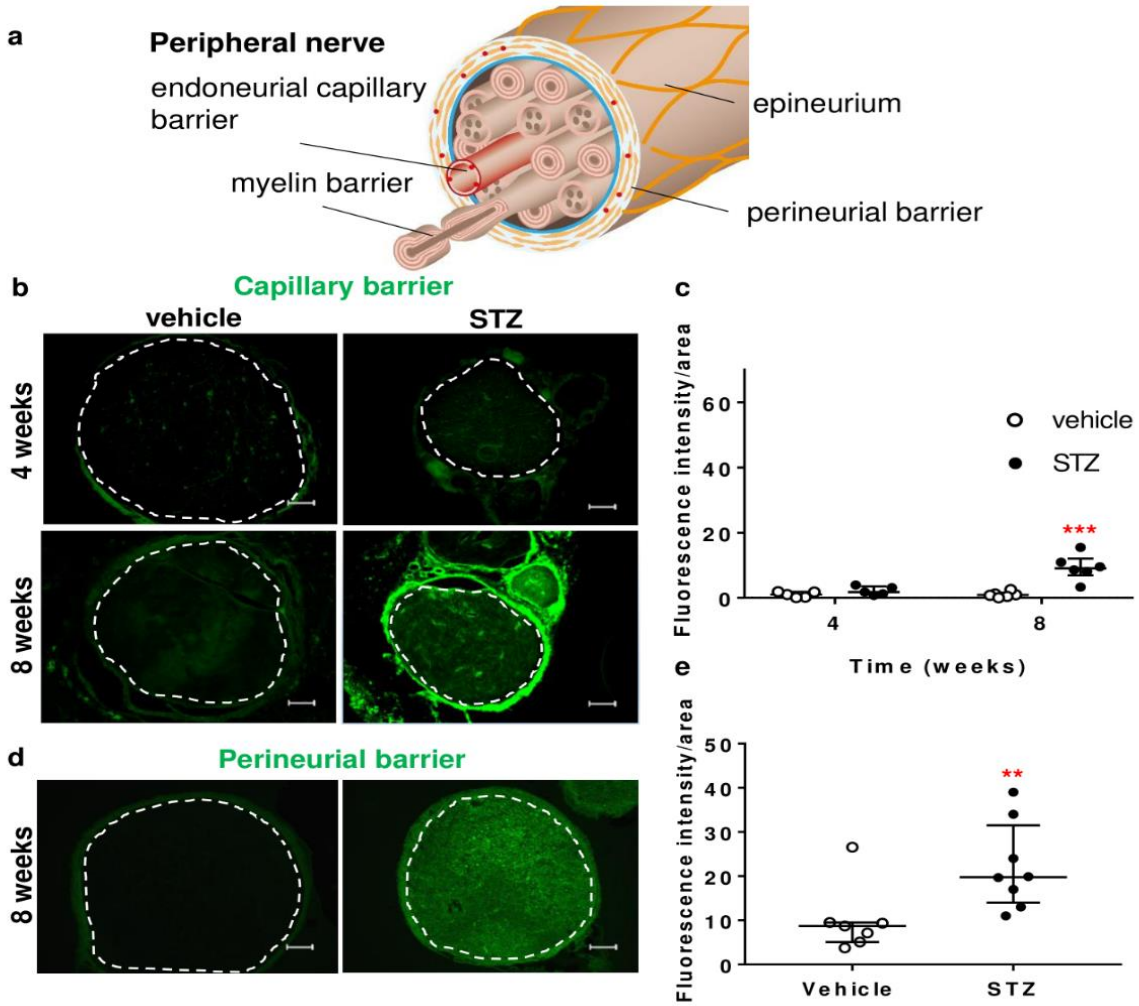

Fig. 10 Increased capillary and perineurial permeability for small molecules in prolonged STZ-induced DPN. (**a**) Barriers in the peripheral nerve. (**b, c**) Diabetic and non-diabetic male Wistar rats were treated with i.v sodium fluorescein (376 Da) 30 min before sacrifice to measure the tightness of the capillary barrier, n = 5-6. (**d, e**) Sciatic nerves were collected and immersed in 3% sodium fluorescein to analyze the perineurial barrier tightness, n = 7-8. Quantification of fluorescence intensity normalized by the stained area (dashed line) is depicted in c and e. Scale bars = 100 µm, dot plots represent median and interquartile range, C. two-way ANOVA, *** P < 0.001, E. Mann-Whitney test, **P < 0.01. Figure from Ben-Kraiem and colleagues., 2021: data collected by Norwig C and analyzed by Ben-Kraiem A (Ben-Kraiem et al 2021)

Interestingly, nerves stained for fibrinogen (340 kDa, capillary barrier) exhibited no differences (**Fig. 11a, b**). Likewise, incubated sciatic nerves with EBA (68 kDa) displayed no endoneurial diffusion (perineurial barrier, **Fig. 11c, d**) suggesting no leakiness for large molecules.

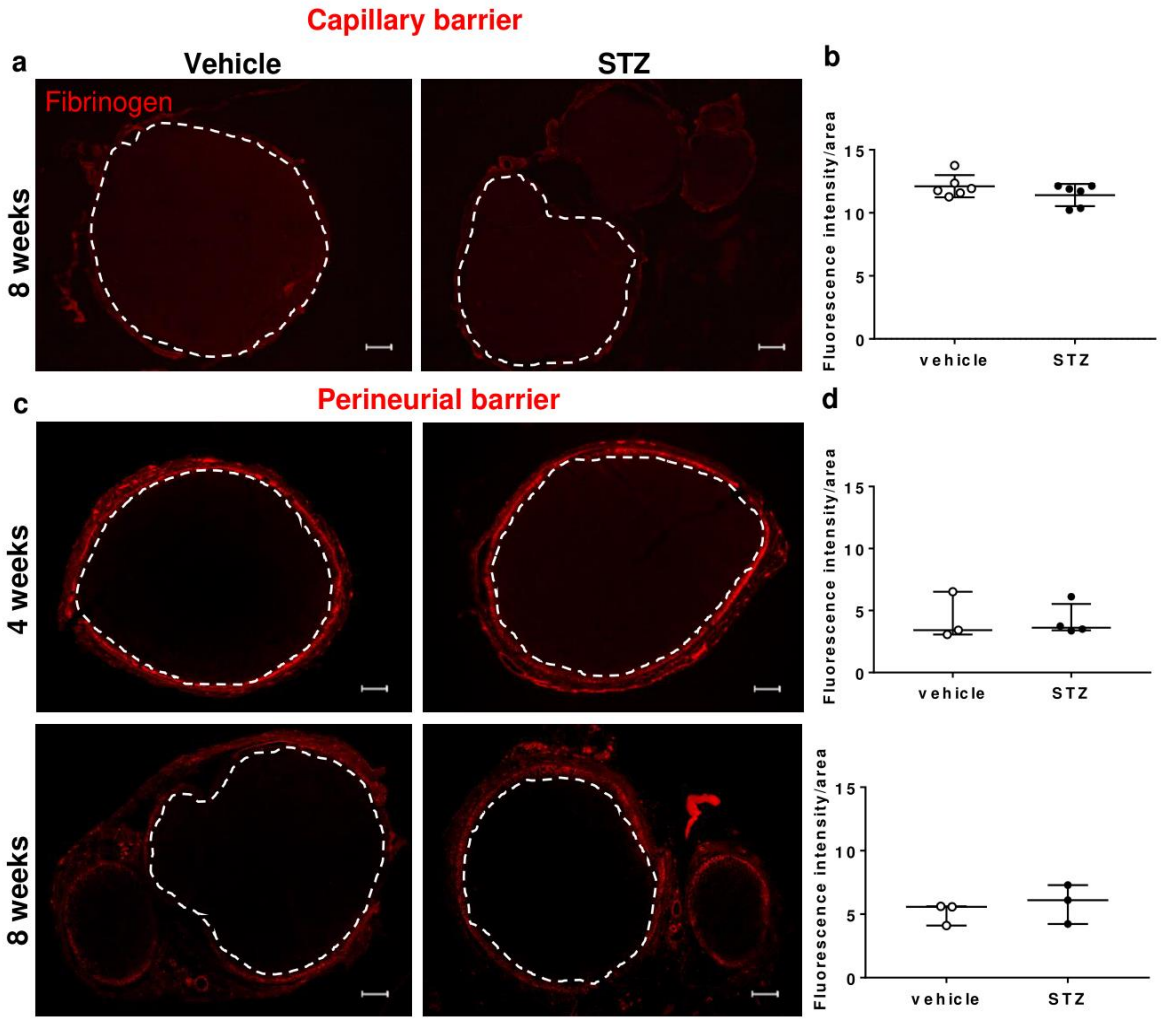

Fig. 11 Preserved blood-nerve barrier function for macromolecules in the sciatic nerve. Sciatic nerve from male Wistar rats were harvested and (**a, b**) stained against fibrinogen (340 kDa) or (**c, d**) incubated in Evans blue albumin (68 kDa) for 1 h. (**a**) Endoneurial immunoreactivity against fibrinogen 8 weeks after STZ or vehicle, n = 6. (**c**) Penetration of Evans blue albumin into the endoneurium 4 and 8 weeks after STZ, n = 3. Fluorescence intensity was quantified and normalized to the region of interest (dashed line). Scale bars = 100 µm. Figure from Ben-Kraiem and colleagues., 2021: data collected by Norwig C and analyzed by Ben-Kraiem A (Ben-Kraiem et al 2021)

To visualize the corresponding proteins, claudin-1 and -5 immunoreactivity was quantified in perineurium and endoneurium respectively. We noticed a lesser perineurial claudin-1 immunoreactivity at eight weeks STZ-induced DPN (**Fig. 12a, b**). Endoneurial claudin-5 immunoreactivity in the vWF positive capillaries was unaltered (**Fig. 12c, d**) which was validated by claudin-5 western blot presenting no difference between groups (**Fig. 12e**).

Decreased vessel-associated-macrophage number in STZ-induced diabetic neuropathy

In BNB the endoneurial capillaries have particular constitution: not only pericytes but also macrophages (vessel-associated-macrophages) prevent large molecule penetration (Malong et al 2019). In DPN, significantly less CD68+ macrophages were associated to vWF+ capillaries in eight weeks STZ rats in comparison to vehicle control (**Fig. 12f, g**). Vessel-associated macrophages could be further designated as CD206+ anti-inflammatory state macrophages (Koizumi et al 2019) neighboring RECA-1 positive endoneurial capillaries (Cattin et al 2015), and confirming the previous observations, eight weeks after STZ injection, the number of CD206+ vessel-associated-macrophages was reduced (**Fig. 12h, i**). As no claudin-5 expression changes but less vessel-associated-macrophages were detected, we highlighted here the importance of vessel-associated-macrophages in endoneurial barrier sealing.

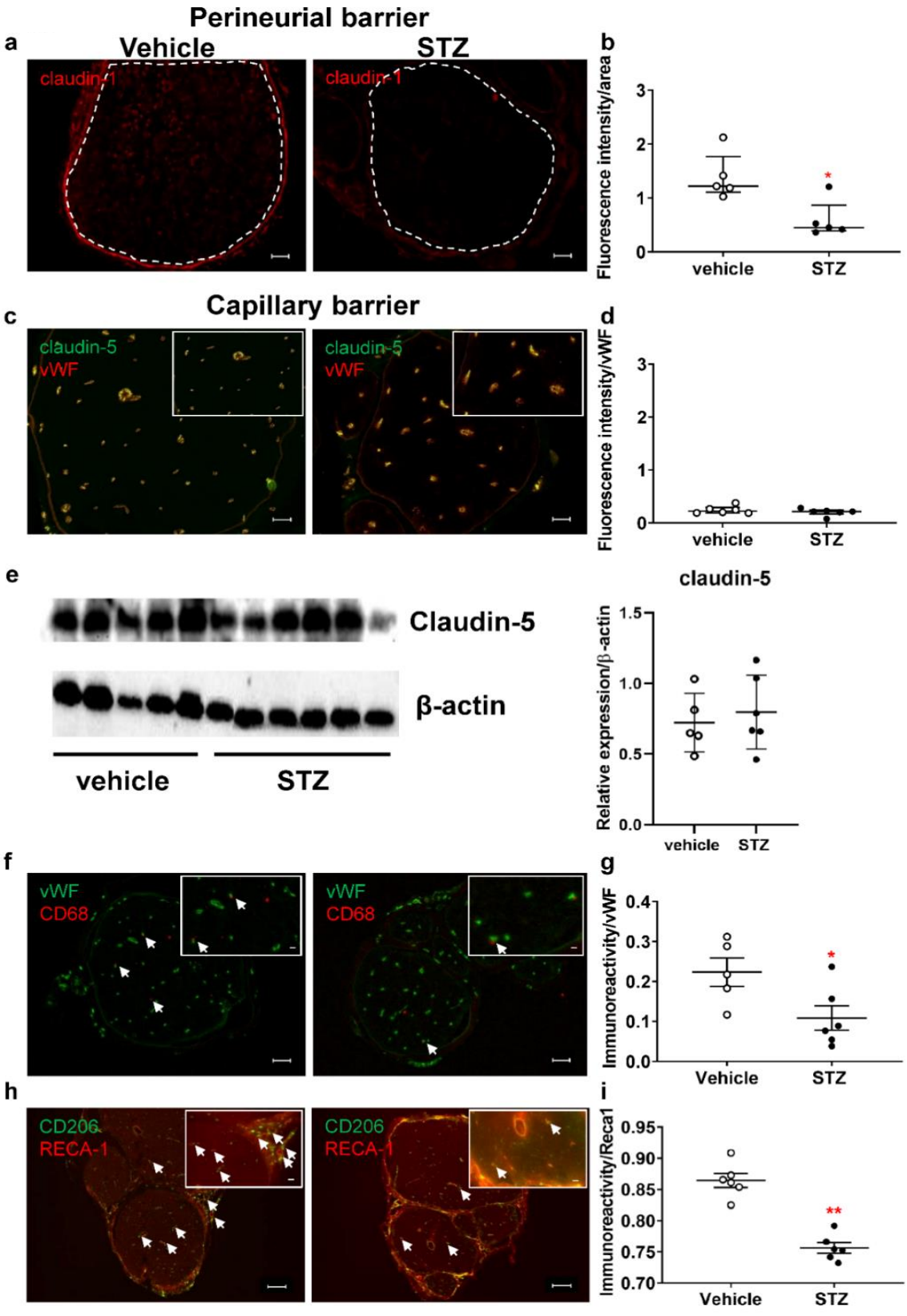

Fig. 12 Decreased claudin-1 immunoreactivity in the perineurium and vessel-associated-macrophages in prolonged STZ DPN. Sciatic nerve from male Wistar rats were stained with anti-claudin-1 (**a, b**), anti-claudin-5 + anti-von Willebrand factor (vWF, **c, d**). Claudin-5 was quantified relative to β-actin by Western blot (**e**). Vessel associated macrophages were

identified by immunolabeling with anti-CD68 and anti-vWF (**f, g**) or anti-CD206 and RECA-1 (**h, i**). Fluorescence intensity was quantified in the regions of interest (perineurium; **a, b**) and (vWF+ vessels; **c, d**) normalized to the area. (**f, g, h, i**) The total number of macrophages (CD68+ or CD206+) in proximity to blood vessels (vWF+ or RECA-1+) was counted and expressed relative to the total number of capillaries in the endoneurium. n = 5-6. Arrows depict examples. Scale bars = 100 µm and 20 µm in the insert, dot plots represent medians and interquartile range, Mann Whitney test for comparison. *****P < 0.05 and ******P < 0.01. Figure from Ben-Kraiem and colleagues., 2021 data collected by Bettenhausen AL (a), Sobhy Atalla M (b) and Ben-Kraiem A (c-i) and then all analyzed by Ben-Kraiem A (Ben-Kraiem et al 2021)

In the present part, we provide evidence for small molecules BNB leakiness in STZ-induced DPN: decreased perineurial claudin-1 explains a higher perineurial permeability, while decreased vessel-associated macrophages could be responsible for enhanced endothelial diffusion. BNB remained sealed for larger molecules. Moreover, all observed barrier changes occurred between four and eight weeks – long after the first detection of mechanical hypersensitivity. Consequently, a destabilized BNB could be responsible for maintaining - rather than initiating - neuropathic pain as well as further nerve damage.

Characterization of the chronic constriction injury (CCI) model of neuropathic pain and SPMs treatment to accelerate pain resolution

No sexual dimorphism in mechanical allodynia and thermal hypersensitivity resolution after CCI injury

Male and female are sexually dimorphic in neuropathic pain thus it was important to include both sexes in the study (Boullon et al 2021). We first characterized the behavioral phenotype after CCI injury. Starting with reflexive tests namely von Frey hair test and Hargreaves test assessing respectively mechanical allodynia and thermal allodynia (**Fig. 13a-c**), we observed maximal hypersensitivity at 1 week and a resolution that start from three weeks and completes between five to six weeks after injury in male and female rats (Fig. 13 a-b) for both mechanical and thermal hyperalgesia. As no difference in both mechanical and thermal hypersensitivity was observed between male and females (Fig. 13c), we then decided to proceed only with male rats assuming that in other behaviors and aspects there will be no difference. Then we wanted to characterize quality of life using voluntary wheel running test. No difference was found in the covered distance in 24 h and the mean speed in 24 (**Fig. 13d**). During the motor activity assessment, other parameters respectively the maximum speed and the maximum acceleration were also measured (data not shown). These two parameters measure only a selected moment and do not give a long term analysis like mean speed and mean distance. We also recoreded different parameters only during the active phase (night) (data not shown). For all the measures no difference was observed between sham and CCI animals.

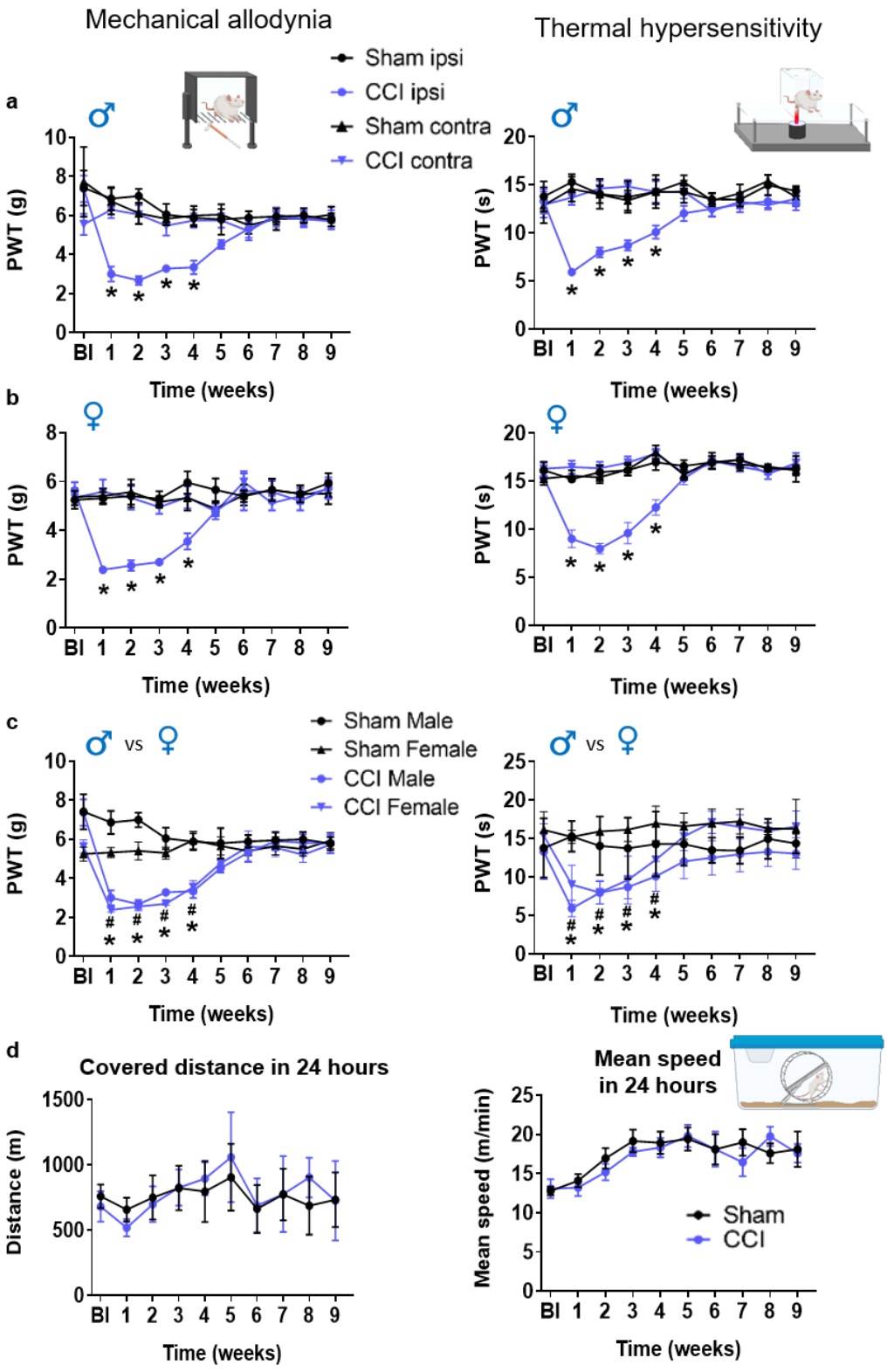

Fig. 13 Mechanical and thermal hypersensitivity resolution in six weeks CCI rats for both male and female rats. (**a**). Mechanical (von Frey) and thermal (Hargreaves test) hypersensitivity in CCI male rats. (**b**). mechanical and thermal hypersensitivity in CCI female rats. (**c**). mechanical and thermal hypersensitivity comparison between male and female CCI rats,; *P < 0.05 CCI male vs Sham male and female, # P < 0.05CCI female vs Sham male and female. (**d**). covered distance and mean speed during 24 h in the voluntary wheel running. All data points represent mean ± SEM. *P < 0.05 All n = 6 Two-way repeated measurement ANOVA and Bonferroni post-hoc test for multiple comparisons.

Pain resolution after fibrinogen removal in sciatic nerve of CCI rats

We next measured both perineurial and endoneurial permeability. For the perineurial barrier permeability we incubated harvested sciatic nerve in NaFlu (376 Da) and EBA (68 kDa) respectively measuring permeability for small and large molecules (**Fig. 14a**, **b** quantifications). We observed a persistent perineurium leakiness even at nine weeks after injury for both small and large molecules. To study endoneurial barrier leakiness, we stained for fibrinogen – a blood-borne protein that extravasates only if blood vessel barrier is not tight (**Fig. 14a**, and **b** for quantification). Until three weeks post injury, fibrinogen extravasated and leaked into the endoneurium space. From six weeks on, at the time of pain resolution fibrinogen is no more present indicating a degradation as well as a tightening of the endoneurial barrier blocking any new extravasation. Interstingly fibrinogen was also extravasating in the perineurium and the peripheral part of the nerve until three weeks and no more detectable from six weeks on. This underlie also a leakiness of peripheral blood vessel after CCI that normalizes with the resolution process. *Cldn1* was downregulated in all time points in accordance with the increased perineurial permeability observed (**Fig. 14c**). *Cldn5* was downregulated until six weeks and normalized at nine weeks (for both Cldn1 and Cldn5 raw data Ct and ΔCt are available in **Suppl. Table 1**). *Cldn5* expression at six weeks did not parallel resealing of the endoneurial barrier for fibrinogen.

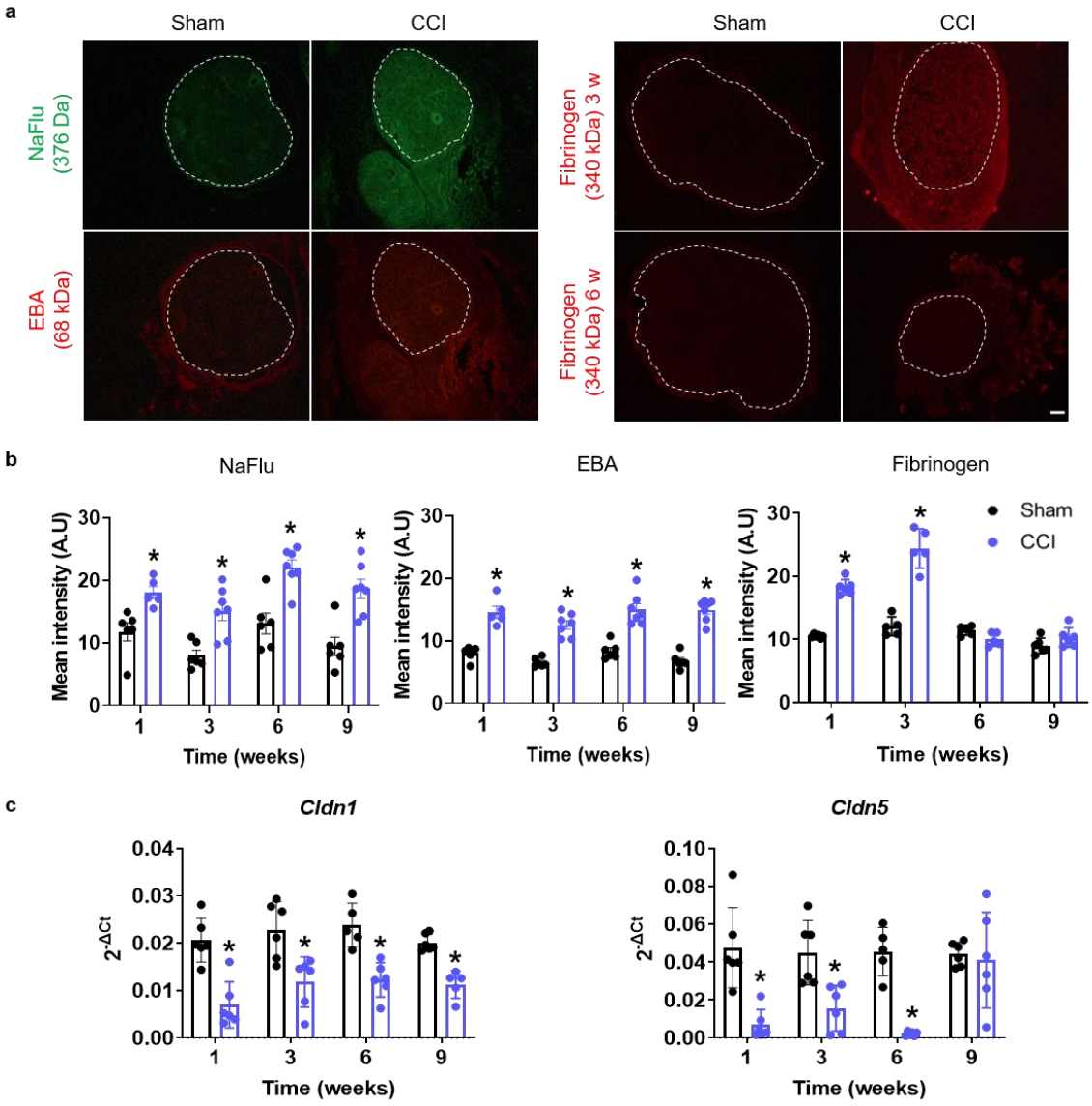

Fig. 14 Resealing of endoneurial barrier for large molecules in six weeks CCI rats. Sciatic nerve from male Wistar rats were harvested and (a) immersed in sodium fluorescein (NaFlu) and Evans blue albumin (EBA) to analyze the perineurial barrier leakiness after CCI, or stained against fibrinogen (340 kDa) to study endoneurial barrier permeability in CCI,; scale bars = 100 µm. (b) Fluorescence intensity of the barrier permeability testing was quantified in the region of interest (dashed line). (c) Gene expression of perineurial and endoneurial TJPs respectively *Cldn1* and *Cldn5* after CCI, All n= 6. Plots represent mean± SEM., two-way ANOVA, *P < 0.05.

Next, we screened the metabolome for SPMs after CCI injury. To do so, thanks to our collaboration with Dr. Marco Sisignano at the Pharmazentrum Frankfurt/ZAFES, Institute of Clinical Pharmacology, University Hospital, Goethe-University in Frankfurt am Main we could conduct some liquid chromatography tandem mass spectrometry (LC-MS/MS) on harvested sciatic nerve, dorsal root ganglia (DRGs), spinal cord (SPC), plantar skin, serum and plasma. of CCI male rats. No SPMs like resolvins could be detected. However, we measured several precursors of certain SPMs and other pro or anti-inflammatory derivates of fatty acids. Hence, we detected in the different tissues, various prostaglandins (PGs), respectively PGE2, PGF2α, PGD2, PJJ2, 6-keto prostaglandin F1α (6-ketoPGF1α). Other products such 5-HETE and thromboxane B2 (TXB2) were detected as well. In this group PGE2, PGF2α and 6-keto PGF1α are pro-inflammatory while prostaglandin PGD2 and PGJ2 are anti-inflammatory. 5–HETE is a precursor of leukotriene B4 (LTB4) and TXB2 is a product of degradation of thromboxane A2 (TXA2), both LTB4 and TXA2 are pro-inflammatory molecules. Interestingly, we detected in sciatic nerve at one week CCI, when both mechanical and thermal hypersensitivity are at maximum, an increased concentration of PGE2, PGF2α and while concentrations of PGD2 and was decreased. At three and six weeks concentrations were normalized, PGD2 is also decreased at six weeks. Both 6-keto PGF1α and PGJ2 were unaffected throughout the time points (**Table 1**). 5-HETE was increased at one week while TXB2 was increased from one to six weeks indicating an inflammatory status in sciatic nerve (**Table 1**). In other tissues (DRGs, SPC, skin, serum and plasma) no changes was observed in PGs and TXB2 concentrations, only PGD2 was decreased at one week in the skin of CCI rats (**Table 1**). In summary, only sciatic nerve presented PGs changes at one week after injury with pro-inflammatory PGs increase and anti-inflammatory decrease.

Table 1 Summary of measured lipids and SPMs precursor's and changes in their concentrations in different tissues after CCI

	Sciatic nerve			Dorsal root ganglia			Spinal cord		
	1 week	3 weeks	6 weeks	1 week	3 weeks	6 weeks	1 week	3 weeks	6 weeks
PGE2	↗ *P<0.05	→	→	→	→	→	→	→	→
PGF2α	↗ *P<0.05	→	→	→	→	→	→	→	→
PGD2	↘*P<0.05	→	↘*P<0.05	→	→	→	→	→	→
PGJ2	→	→	→	Undetected			Undetected		
6-keto-PGF1α	→	→	→	Undetected			Undetected		
TXB2	↗ *P<0.05	↗ *P<0.05	↗ *P<0.05	→	→	→	→	→	→
5-HETE	↗ *P<0.05	→	→	→	→	→	→	→	→
12-HETE	→	→	→	Undetected			↗ *P<0.05	→	→
15-HETE	→	↗ *P<0.05	→	→	→	→	→	→	→
17-HDHA	↗ *P<0.05	↗ *P<0.05	↗ *P<0.05	→	→	→	→	→	→
14-HDHA	↗ *P<0.05	→	↗ *P<0.05	→	→	→	→	→	→

	Plasma			Serum			Skin		
	1 week	3 weeks	6 weeks	1 week	3 weeks	6 weeks	1 week	3 weeks	6 weeks
PGE2	Undetected			→	→	→	→	→	→
PGF2α	Undetected			→	→	→	→	→	→
PGD2	Undetected			Undetected			↘*P<0.05	→	→
PGJ2	Undetected			Undetected			Undetected		
6-keto-PGF1α	→	→	→	→	→	→	→	→	→
TXB2	→	→	↗ *P<0.05	Undetected			→	→	→
5-HETE	→	→	→	→	→	→	→	→	→
12-HETE	Undetected			Undetected			→	→	→
15-HETE	→	→	→	→	→	→	→	→	→
17-HDHA	Undetected			→	→	→	→	→	→
14-HDHA	→	→	→	→	→	→	→	→	→

With focus on SPMs precursors, we noticed in sciatic nerve, increased concentrations of 15-HETE **–** the precursor of LXA4 – at three weeks after CCI at the start of the resolution phase and of 17-HDHA – the precursor of RvD1 – at one, three and six weeks after CCI before and during the resolution process. Also, from one to six weeks we observed an increased concentration of 14-HDHA an anti-inflammatory molecule produced during the metabolization of DHA **(Table 1 and Fig. 15).** No changes were observed in other tissues (**Table 1**). LXA_4 and RvD1 bind to a common receptor, the ALX/Fpr2 receptor. Interestingly the *Fpr2* expression was increased three weeks after CCI at the start of the resolution phase (**Fig. 15** raw Ct and ΔCt values in **Suppl. Table 2**). Not only *Fpr2* was upregulated, actually we also detected upregulation of *Chem23R* and *Gpr18* (**Suppl. Fig. 1** and respectively raw data in **Suppl. Table 3 and 4**), respectively coding for receptors of RvE1 and 2 and of RvD2 **(Fig. 8)**, from one to six weeks after CCI. At the opposite *Gpr37* and *Lgr6*, coding respectively for NPD1 and Mar1 receptors **(Fig. 8)**, were downregulated from one to six weeks after CCI (**Suppl. Fig. 1** and respectively raw data in **Suppl. Table 5 and 6**).

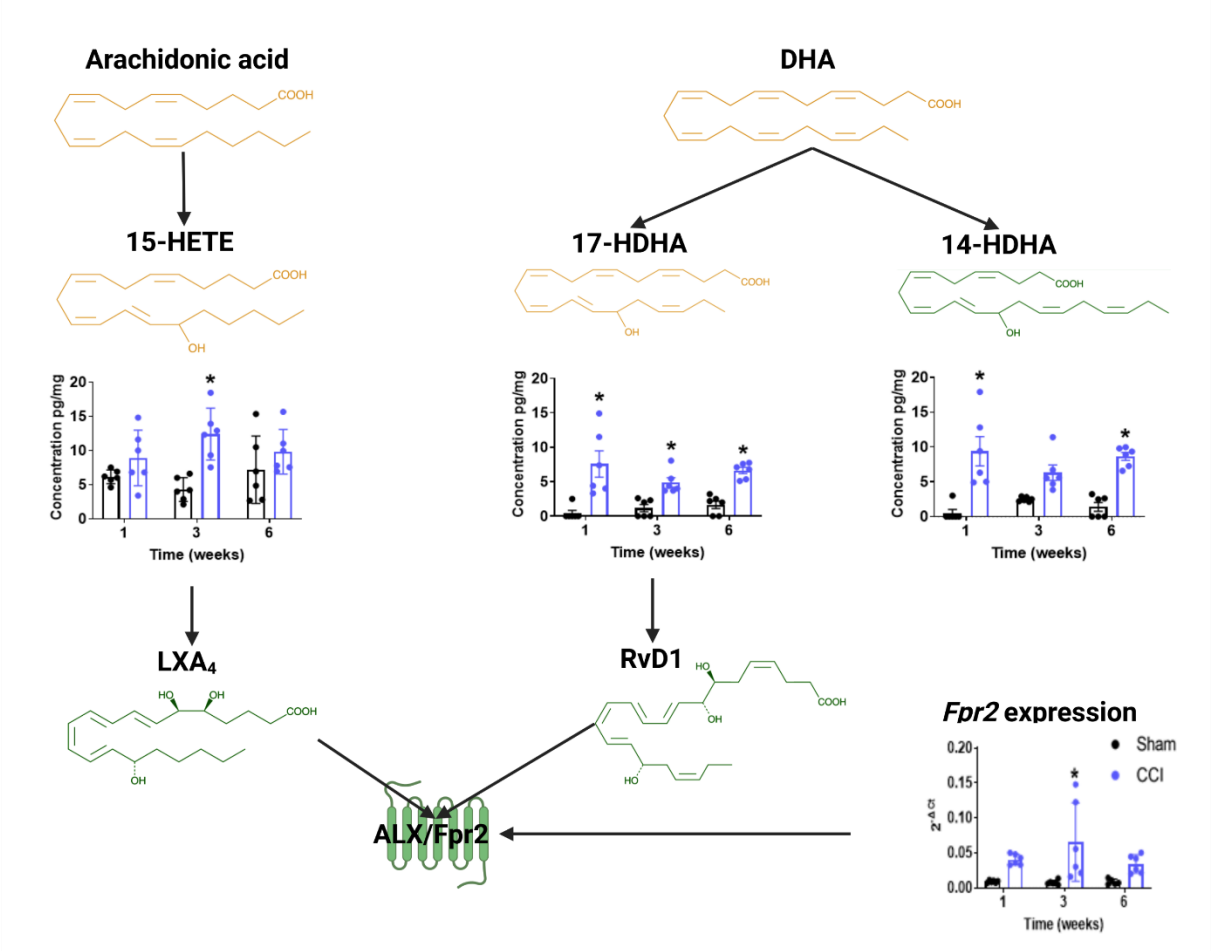

Fig. 15 Increased con centration of LXA4 and RvD1 precursors during the resolution phase, as well as upregulation of their receptor (Fpr2) after CCI. Sciatic nerve from male CCI rats, were harvested and analysed using liquid chromatography tandem mass spectrometry or for qRTPCR, n=6, plots represent mean ± SEM., two-way ANOVA, *P < 0.05

As we detected SPMs precursor increase at three weeks after CCI, the switching point toward the resolution, particularly precursors of LXA_4 and RvD1, SPMs known to have anti-inflammatory as well as an analgesic effect (Tao et al 2020) and are produced by neutrophils in the late phase of the inflammation just before the resolution (Serhan & Levy 2018). We therefore concluded that LXA_4 and RvD1 are involved in the endogenous pain resolution process after CCI.

Acceleration of pain resolution by resealing the endoneurial barrier and degrading fibrinogen in CCI rats after BML111 injections

Next, we wondered if local application of SPMs could accelerate pain resolution in CCI. We used for a first approach a synthetic agonist of the Fpr2, BML111 a stable LXA_4 analog (Xu et al 2022). During one week from 18 until day 24-post CCI rats were twice daily injected either

with vehicle solution (PBS) or with BML111. The first injection was done after the daily baseline measurement while the second was done after the last daily behavior test, six hours after the first injection (**Fig. 16a**). Injections started at day 18-post injury, before the beginning of the resolution phase and late enough to avoid effects of the initial inflammatory phase. BML111 had an acute antinociceptive effect starting 1 h and peaking 3 h after injection with PWT normalization. However six hours after injection, the antinociception was vanished (**Fig. 16b**). The two injection daily of BML111 resulted in a slow but steady persistent reversal of hyperalgesia. Remarkably, the effect lasted four days longer than the treatment (**Fig. 16c**). Both, mechanical and thermal allodynia, resolved at day 25-post injury after BML111 treatment (**Fig. 16c**). Thus, BML111 accelerates NP resolution. Moreover BML111 treatment induced fibrinogen degradation and prevented further fibrinogen deposition in the endoneurial space (**Fig. 16d**). We next measured the expression of both mRNA and protein of endoneurial barrier marker claudin-5. *Cldn5* and the protein were upregulated after BML111 treatment (**Fig. 16e, f,** all raw data: Ct and ΔCt for Cldn5 after BMl111 injections are shown in **Suppl. Table 7**).

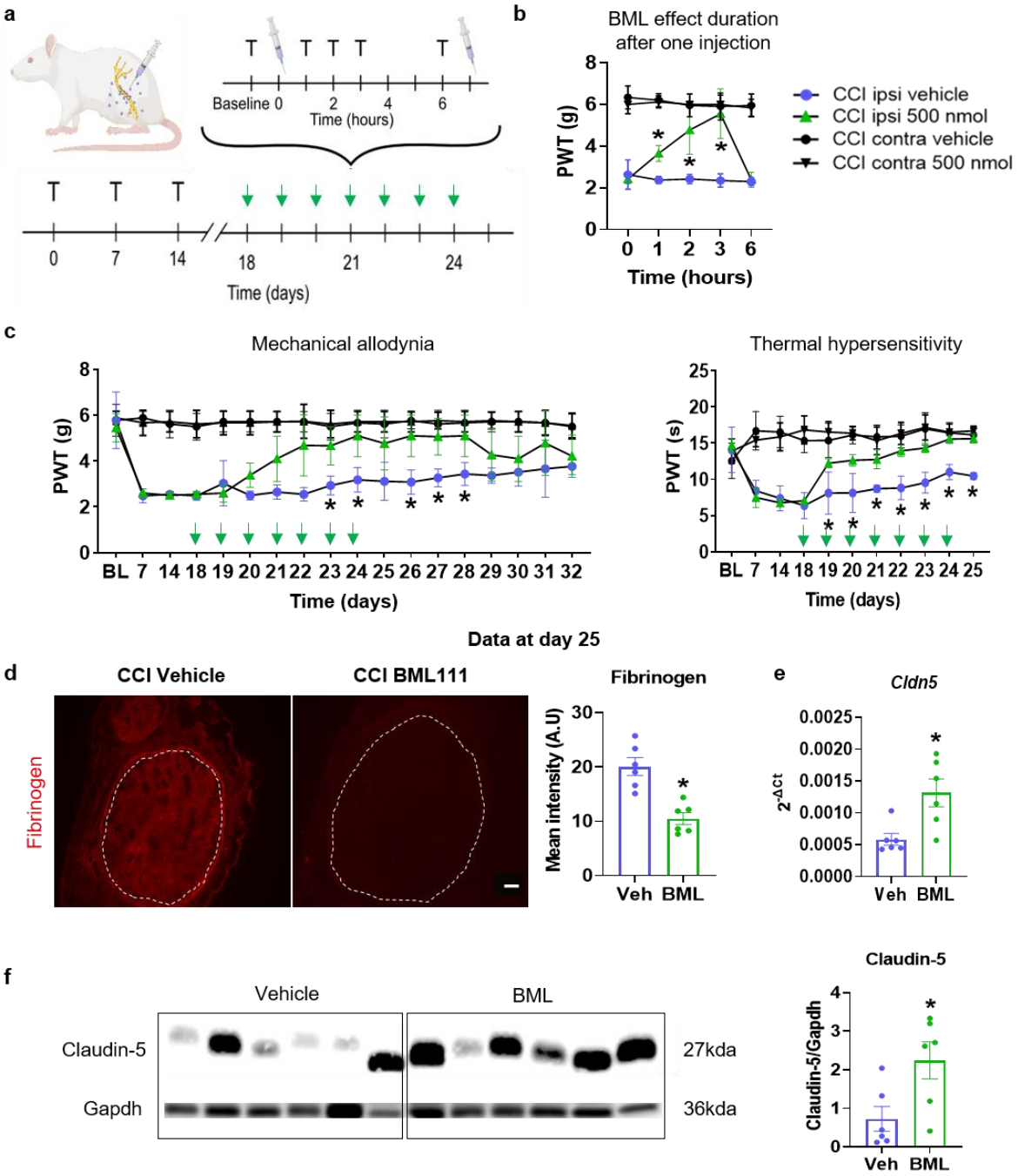

Fig. 16 BML111 accelerates pain resolution in CCI, sealing the endoneurial barrier and degradat-ing fibrinogen. (**a**) Experimental procedure: perineurial injection of BML111 twice daily. (**b**) Antinociceptive effect duration of BML111 after one injection. (**c**) Mechanical (von Frey) and thermal (Hargreaves test) hypersensitivity in CCI male rats treated or not with BML111, Two-way repeated measurement ANOVA and Bonferroni post-hoc test for multiple comparisons *P < 0.05 between vehicle ipsi and BML ipsi. (**d**) Fibrinogen extravasation and its quantification (fluorescence intensity of measured in the region of interest (dashed line)), scale bar = 100 µm. (**e**). Gene expression of endoneurial barrier TJP (*Cldn5*);. (**f**) Western blots showing the protein expression of endoneurial barrier TJP (claudin-5) and their quantification; All n = 6 ; from d to f t-test, *P < 0.05. All data points represent mean ± SEM.

Acceleration of pain resolution also by dgradating fibrinogen and resealing the endoneurial barrier in both male and female CCI rats after local RvD1 application

Native SPMs are unstable. Thanks to a collaboration with Dr. Andrés García we have been provided with PLGA-PEG nanoparticles (Quiros et al 2020) loaded with 500 nM RvD1. For this second aproach, based on the literature we injected once daily after the baseline measurement during one week. (**Fig. 17a**). We first measured RvD1 release from the nanoparticles in vitro: RvD1 was released for up to 72 h (**Fig. 17b**). In vivo, RvD1-loaded nanoparticles fastened pain resolution in male and female rats (**Fig.17c**). This treatment decreased fibrinogen immonoreactivity (**Fig 17d**) and upregulated *Cldn5* (**Fig. 17e**, raw data: Ct and ΔCt displayed in **Suppl. Table 8**). The same mechanism was found in female rats (**Fig. 17f, g**). In summary, SPMs (BML111 and RvD1) speed up the natural resolution process (fibrinolysis and endoneurial barrier resealing).

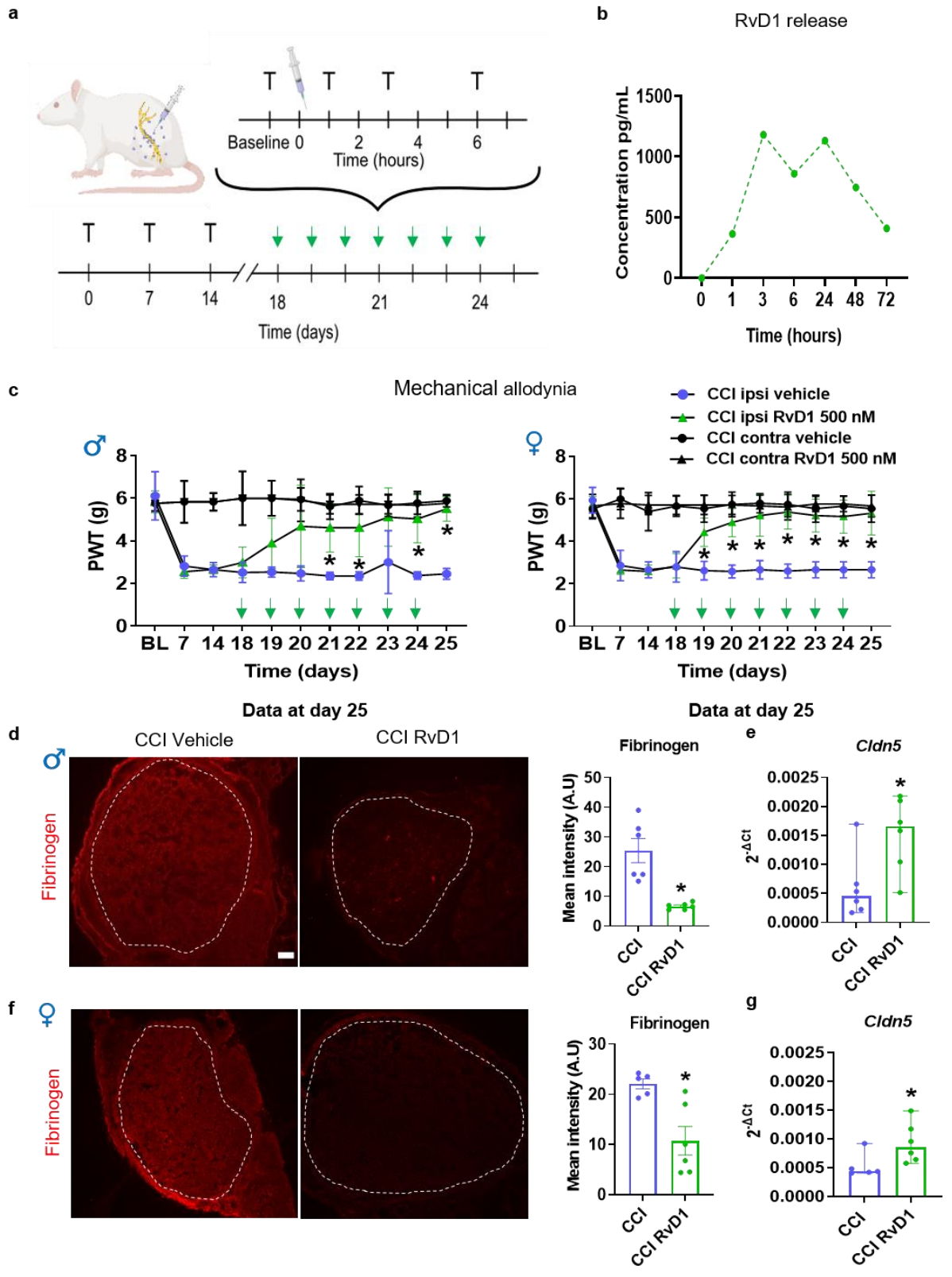

Fig. 17 RvD1 accelerates pain resolution in CCI and seal the endoneurial barrier for fibrinogen in both male and female rats. (**a**) Experimental procedure, perineurial injection of RvD1-loaded-Nps daily. (**b**) NPs dialysis: RvD1 release duration. (**c**) Mechanical (von Frey) hypersensitivity in CCI male and female rats treated or not with RvD1-loaded-NPs, Two-way repeated measurement ANOVA and Bonferroni post-hoc test for multiple comparisons *P < 0.05 between vehicle ipsi and RvD1 ipsi. (**d**) fibrinogen extravasation in CCI male rats treated

or not with RvD1 and its quantification (fluorescence intensity of measured in the region of interest (dashed line)). (**e**) Gene expression of endoneurial barrier TJP (*Cldn5*) in male CCI rats sciatic nerve after treatment or not with RvD1. (**f**) fibrinogen extravasation in CCI female rats treated or not with RvD1 and its quantification (fluorescence intensity of measured in the region of interest (dashed line)), n=6 RvD1 group and n=5 vehicle group; t-test *P < 0.05. (**g**). Gene expression of endoneurial barrier TJP (*Cldn5*) in female CCI rats sciatic nerve after treatment or not with RvD1, All n=6 RvD1 group and n=5 for female vehicle group; from d to g t-test, *P < 0.05. All data points represent mean ± SEM, scale bar = 100 µm.

Discussion

In our study, we demonstrated that in both DPN and CCI in rats the BNB is leaky. This includes the perineurial and endoneurial barrier. However, in DPN BNB is open only for small molecules and at a late time point after onset of hyperalgesia while in CCI, the BNB is leaky for small and large molecules at the onset of hyperalgesia. This indicates the BNB disruption is not the cause of NP in DPN, which is the opposite in CCI. BNB leakiness is due to loss of perineurial claudin-1 and blood-vessel-associated macrophages in DPN when it is probably due to loss of perineurial claudin-1 and endoneurial claudin-5 in CCI. Furthermore, in CCI a resolution occurs between three to six weeks that is characterized by increased level of SPMs and their receptor in sciatic nerve followed by the endoneurial barrier resealing and fibrinolysis while perineurium is still leaky. So, the interaction between SPMs (LXA_4 and RvD1) and their receptor (Fpr2) could induce resolution by sealing the endoneurial barrier which was sufficient to alleviate hyperalgesia in CCI. Interestingly treating locally with SPMs (BML and RvD1) accelerated resolution (fibrinolysis and endoneurial resealing).

BNB in the STZ model of DPN

The BNB was partially leaky in DPN. Interestingly, BNB changes do not parallel the development of mechanical allodynia. This indicates that BNB alteration is not the main cause for the development of allodynia but rather a cause for maintaining it. Previous studies also described increased peripheral nerve permeability for small but not macromolecules in STZ-induced diabetes after nine months (Rechthand et al 1987). Additionally, endoneurial edema was an early sign of STZ-induced diabetes (Wang et al 2015), but not in all studies and models (Schwarz et al 2020). Therefore, our results are in accordance with some previous smaller studies. Permeability for large molecules has been observed in type 1 diabetes rat models (Seneviratne 1972) and type 2 diabetes (Chapouly et al 2016), but not in other studies (Richner et al 2018). So, these studies are different from our results. A longer disease duration as in type 2 diabetes could led to large molecule leakiness.

Perineurial leakiness for small molecules arises from perineurial loss of claudin-1, a major sealing TJP of the perineurium. No other studies found this before. Some microvascular changes in DPN have been described such degradation of paracellular TJs, loss of pericytes, increased basement membrane thickness, fibrin positive blood vessels as well as endothelial cell hyperplasia (Richner et al 2018). Microvessels are sealed by TJPs, particularly claudin-5. Surprisingly, claudin-5 was not affected in DPN. In search of alternative mechanisms, we detected less blood-vessel associated-macrophages in endoneurium. This could explain the

increased small molecule endothelial permeability as hinted in the preprint study from Malong and colleagues (Malong et al 2019) in synergy with pericytes (Richner et al 2018, Shimizu et al 2011).

Which mechanisms could underlie decreased *Cldn1* in the perineurium as well as loss of vessel-associated macrophages in the endoneurium impairing the BNB function? It is known that, the wnt pathway (Sauer et al 2014), metalloproteinases and low-density lipoprotein receptor-related protein-1 (Zwanziger et al 2012) as well as microRNA (miR)-155 (Reinhold et al 2019), miR-21 and miR-183 (Yang et al 2016) regulate *Cldn1*. Moreover, restoration of blood-vessel-associated-macrophages could reinstate endothelial barrier function. Thus, not only TJPs, but also recruitment of macrophages could be regulated by common pathways. Treatment with e.g. glycogen-synthase-kinase-3β inhibitors (Ramirez et al 2013, Sauer et al 2014), miR-155 antagomirs (Chen et al 2019) or hedgehog fusion proteins (Calcutt et al 2003) could promote BNB sealing in DPN. Some of these inhibitors are currently under investigation for diabetes treatment (Calcutt et al 2003, Lux et al 2019, MacAulay & Woodgett 2008).

BNB after traumatic nerve injury (CCI)

In CCI, we described a natural resolution phase (normalization of both mechanical and thermal hypersensitivity) after a traumatic nerve injury. A similar time course was observed before by Sommer et al. (Sommer et al 1995). Interestingly, no alteration of motor activity in the voluntary wheel running was seen in our study. Although one could expect a loss of motor activity after CCI, this has not been thoroughly documented before. A previous study showed that rats after CCI injury decrease their motor activity only during the active phase (night for rodents) (Green-Fulgham et al 2022). These results were observed in an experiment procedure where rats were monitored for 42 d in a row while we monitored animals once a week for 24 h. Moreover, Green-Fulgham and colleagues used Fisher 344 rats while we were using Wistar rats. Different animal strain used have a different phenotype after nerve injury. For example, Contreras and colleagues studed motor activity in different pain models in two different mouse strains. They observed different results between strains. C57B/6J mice male and female mice lost motor activity after a daily CFA intra-plantar injection while in DBA/2J male and female mice did not. CCI in mice lead to a reduced motor activity only in C57B/6J females (Contreras et al 2021). So, the difference between our results and the ones by Green-Fulgham could be explained by the strain used and that for this experiment we used only male Wistar rats.

We also characterized the BNB after CCI as both perineurial and endoneurial barriers were leaky. Notably fibrinogen extravasated into the endoneurial compartment which is in line with

the observation of Lim et al. They documented in mice fibrinogen extravasation in the endoneurial compartment after PSNL injury, a milder model than CCI (Lim et al 2014). This results confirm that a direct mechanical insult to the nerve induces endoneurial barrier leakiness. Endoneurial permeability normalized at six weeks as fibrinogen could not be detected anymore. This indicates that the extravasated fibrinogen got degraded and in parallel the endoneurial barrier got resealed avoiding new extravasation. Our observation show that fibrinogen also extravasated in the peripheral part of the nerve and normalized after the resolution indicating that not only the endoneurial blood vessels were affected but also the external ones. Unexpectedly, perineurial permeability was still increased at 9 weeks CCI when the pain resolution is completed. Increased perineurial permeability matched with *Cldn1* downregulation at 9 weeks. This is the first characterization of perineurium permeability after CCI for such a long period. In fact, the perineurium is directly in contact with the ligations, thus the permanent mechanical strain of the perineurium does probably not allow perineurial recovery. Taken together these results indicate that endoneurial barrier resealing is sufficient for resolution. At the mRNA level, *Cldn5* was still dowregulated at 6 weeks and normalized only at 9 weeks, after the resolution is completed. This result seems contradictory at the first however; Moreau and colleagues described a *Cldn5* downregulation still at 60 days (almost 9 weeks) post CCI in rats (Moreau et al 2016). Thus, the role of claudin-5 as to be clarified with further experiments evaluating the protein expression. Indeed, mRNA level is not always a predictor for protein abundance (Koussounadis et al 2015, Wang 2008). It is possible that claudin-5 is restored in TJs earlier to allow sealing or other TJP could be responsible.

Looking for plausible mechanisms underlying pain resolution after CCI injury, we noticed the elevation LXA_4 and RvD1 precursors, 15-HETE and 17-HDHA, respectively in CCI sciatic nerve at three weeks after injury when the resolution phase starts. Interestingly 17-HDHA itself as a precursor is associated with less pain scores in osteoarthritis in human notably in heat pain (Serhan & Levy 2018, Valdes et al 2017). Moreover, the final products of these precursors, LXA_4 and RvD1 alleviate hyperalgesia in injury models such the SNL, spinal cord injury and CCI (Lu et al 2018, Martini et al 2016, Wang et al 2022, Wang et al 2014). Thus, the detection of these precursors at the start of the resolution phase implies their participation to the recovery process. Not only these SPMs precursors were increased, but also *Fpr2,* coding for their receptor, got upregulated at 3 weeks after CCI injury. FPR2 receptor activation allows neural differentiation and regeneration and reverses neuroinflammation (Cussell et al 2020, Zhu et al 2021). *Fpr2* upregulation at the resolution start could indicate that it is part of the resolution process. Indeed, RvD1 alleviates mechanical hypersensitivity via FPR2 in rats after SNL injury

(Wang et al 2022). So we postulate that the resolution in CCI involves the interaction of SPMs (LXA_4 and RvD1) with their receptor (FPR2).

BNB in CCI after SPM treatment

We studied the effect of FPR2 activation using two agonists, BML111 a stable analog of LXA_4 and RvD1 (Wang et al 2022, Xu et al 2022).We first injected BML111 on site of injury and observed an analgesic effects for six hours with a peak at three hours post injection. Previous studies showed analgesic and anti-inflammatory effect of BML111 in rats after spinal cord injury or in arthritis (Jaén et al 2020, Liu et al 2020). However, these studies were based on a short-term observation with a single systemic injection. In another study on CCI mice BML111 injected intrathecally at day 10 post-CCI reduced thermal hyperalgesia for one day (Colucci et al 2022). The effect was longer compared to our observation with a local injection.

Our study was designed for a longer term observation and with two injection daily for seven days, we elicited a cumulative effect on both mechanical and thermal hyperalgesia and thus also few days after treatment suspension. In summary, repetitive long-term treatment is antinociceptive beyond the expected duration of action arguing for structural changes. We also verified that activating FPR2 could accelerate pain resolution in case of nerve traumatic injury. Apart from nocifensive behaviors we assessed the endoneurial barrier and documented the decreased extravasation of fibrinogen after BML111 treatment. Assessing the resealing of the barrier we observed an upregulated *Cldn5* expression in BML111 treated nerves in comparison to vehicle injected nerves. Here the *Cldn5* upregulation was compared to CCI rats treated with solvent and not to Sham controls as in the study by Moreau et al. (Moreau et al 2016). It is possible that the upregulation by BML111 does not reach the normal expression in Sham controls. We however confirmed claudin-5 reinstatement by western blot. So FPR2 activation induces pain resolution and recovery of claudin-5 expression.

We further confirmed this using RvD1. As RvD1 is unstable and is quickly metabolized in the body environment (Li et al 2020), we used NPs to have a stable effect as described by Quiros and colleagues (Quiros et al 2020).We determined that the NPs released RvD1 for 72 h and allows a stable effect. Our result confirms what was shown by Quiros et al, a release of RvE1 until 3d after injection (Quiros et al 2020). We assessed mechanical hyperalgesia in both male and female rats and we noticed a significant analgesic effect at day 21-post surgery for males and already at day 19-post surgery for females. We here again verified that activating FPR2 accelerated resolution by resealing the endoneurial barrier and removing fibrinogen. Our study is the first that implemented and studied prolonged RvD1 treatment using NPs. We

demonstrated that there is a possibility to stabilize and prolong SPMs effect which is important for developing a treatment strategy.

Use of SPMs in DPN

As demonstrated in the CCI model SPMs seal the BNB and allow for pain resolution. In DPN resealing the BNB could be a therapeutic option. Indeed some treatment with e.g. glycogen-synthase-kinase-3β inhibitors (Ramirez et al 2013, Sauer et al 2014), miR-155 antagomirs (Chen et al 2019) or hedgehog fusion proteins (Calcutt et al 2003) could promote BNB sealing in DPN. Some of these inhibitors are currently under investigation for diabetes treatment (Calcutt et al 2003, Lux et al 2019, MacAulay & Woodgett 2008). One could also think about using SPMs in order to seal the BNB in DPN. Some studies have studied effects of SPMs in diabetic complications: They focused on diabetes associated atherosclerosis and diabetic kidney disease (Brennan et al 2018a, Brennan et al 2018b). Brennan and colleagues noticed increased expression of *FPR2* in aortic tissue of STZ-induced-diabetes mice, moreover injecting LXA_4 intra-peritoneally in STZ mice did not affect blood glucose but improved significantly blood vessels inflammation status and reduced aortic arch plaque development (Brennan et al 2018a). They also showed that LXA_4 reverses established renal damage and attenuates the development of proteinuria and glomerular injury in diabetic mice (Brennan et al 2018b). Other studies focused on Ω3-poly-unsaturated-fatty- acids and SPMs effect in DPN. In STZ-diabetic rats giving docosahexaenoic acid (DHA) reduced both mechanical and thermal hyperalgesia and also reversed neural hyperexcitability in dorsal root ganglia (Heng et al 2015). In a mouse model of type 2 diabetes, giving either fish oil or RvD1 or RvE1 reduced both mechanical and thermal hyperalgesia and improved neural transduction and innervation of skin and cornea (Obrosov et al 2017). Moreover, 17-HDHA is reduced in diabetes and its reinstatement reduces inflammation and improves glucose tolerance (Neuhofer et al 2013). It clearly appears that SPMs and more specially LXA_4/RvD1 have a wide range of application in diabetes complications but still it is to understand the mechanisms underlying their effects. We propose here that resolution can arise from sealing the BNB in DPN however; this could be a totally different mechanism or even many mechanisms in parallel involving sealing the BNB and attenuating inflammatory status for example. Indeed, understanding such mechanisms would offer many innovative and various treatment possibilities and alternatives to only focusing on regulating blood glucose level as implemented nowadays.

Other diabetes models

In our study we used a type 1 diabetes model, however most patients have type 2 diabetes mellitus. The BNB hast been studied in preclinical model there as well: $Lepr^{db/db}$ mice have increased BNB permeability due to claudin-5 downregulation (Chapouly et al 2016). This observation differs from our work. This underlies already a different mechanism. In type 1 diabetes endoneurial permeability seems to depend on blood vessel-associated macrophages while it arises from claudin-5 downregulation in type 2 diabetes. Of course, it shows the importance of also studying type 2 diabetes models. More characterization of TJPs regulation have been made in $Lepr^{db/db}$ type 2 diabetic mice and both *Cldn5* and *Tjp1* are regulated by the sonic hedgehog pathway (Chapouly et al 2016) and activating the sonic hedgehog pathway restores endothelial barrier function in diabetic neuropathy (Kusano et al 2004). Interestingly after nerve injury (CCI) alterations of the sonic hedgehog pathway elicit BNB disruption through downregulation of *Cldn5* and other TJPs (Moreau et al 2016). This calls for a shared regulatory mechanism in diabetes type 2 and the CCI model. Indeed, this can also be put in perspective with the few studies that looked into the effects of SPMs in DPN. SPMs, namely LXA_4 and RvD1 improve significantly the DPN status in both type1 and type 2 diabetes (Heng et al 2015, Obrosov et al 2017). Regarding the similarities observed in diabetes type 2 model and in CCI, we should consider to study fibrinogen extravasation in the endoneurium in type 2 diabetes and verify if resealing the endoneurial barrier and degrading extravasated fibrinogen would have an effect on DPN. This could be a base to develop new strategies to treat both traumatic nerve neuropathy and DPN. These observations rise the role of the hedgehog pathways in the regulation of TJPs and in the BNB structure maintenance. Indeed, further investigation regarding the effects of SPMs on the sonic hedgehog pathway would be of importance as it could allow us to describe an entire mechanism and identify different targets.

Other nerve injury models

As we studied the CCI model and that there are many nerve injury models that has been established with wide range of procedure going from the nerve crush to the nerve transection that would be interesting to have a comparative analysis of what happen after injury induction in these different models. Of course, following the nature of the induced injury the regeneration and the resolution would need different time frame (Abboud et al 2021). In these different models, resolution could follow a general main pattern or different mechanisms following the model. It appears reasonable to think that as nerve injury models present direct mechanical insult of the nerve, they all suffer destabilization of the BNB. In the PSNL model Lim and

colleagues observed an increased permeability of the endoneurial barrier with extravasation of fibrinogen in the endoneurium (Lim et al 2014). In this study Lim and colleagues associated the increased permeability to loss of tjp1 a scaffold protein anchoring and maintaining TJPs such claudin-5 or occludin in the blood vessels (Lim et al 2014). No data was shown regarding claudin-5 in this study; however, one can assume that as tjp1 is lost the same could occur to claudin-5 and if not, claudin-5 would not be able to function properly and seal the barrier. In that sense Hirakawa and colleagues noted after sciatic nerve crush injury in rats, a loss of TJPs, namely claudin-1, 5 and occludin, thus one day after injury associated with an increased permeability. Both TJPs and permeability normalized seven-day post-injury (Hirakawa et al 2003). Another study using the crush nerve injury in mice demonstrated endoneurial barrier leakiness but no alteration of the TJPs expression pattern (Dong et al 2018). Between these two studies the difference lays on the species used respectively rats and mice but also on the crush injury itself. In Hirakawa's study, crush injury consisted of a ligation of the nerve with one ligature for 24 h while in Dong performed crush injury by crushing the sciatic nerve with forceps for two seconds (Dong et al 2018, Hirakawa et al 2003). This shows that a more standardized procedure should be followed between studies, nevertheless it also clearly shows that following nerve injury the BNB is destabilized and restoring its function would be part of the resolution process. In CCI hedgehog pathways regulate TJPs and after injury alteration of such pathways induce TJPs (*Cldn5*) downregulation and thus BNB disruption leading to hyperalgesia (Moreau et al 2016). Interestingly in other nerve injury models sonic hedgehog take also part in the regeneration and resolution process. In mice after crush injury (sciatic nerve crushed for 15 s with forceps), stimulating sonic hedgehog pathway locally with estradiol accelerated the nerve regeneration and restored capillaries (Sekiguchi et al 2012). In a more serious injury model (the sciatic nerve transection), blocking sonic hedgehog pathway impaired the sciatic nerve regeneration in rats (Martinez et al 2015). In sciatic nerve transection model, regeneration is dependant on schwann cells (Arthur-Farraj et al 2012). Sonic hedgehog is regulated by c-Jun and in this study Arthur-Farraj and colleagues demonstrated c-jun activity in Schwann cells after injury, induces regeneration (Arthur-Farraj et al 2012). This correlates with the previous cited results from Sekiguchi and colleagues regarding the acceleration of the nerve regeneration following a local stimulation of the sonic hedgehog pathway (Sekiguchi et al 2012). All this data underlies the role of the sonic hedgehog pathway in nerve regeneration and in the BNB structure and function. It also enlightens the role of Schwann cells in the regeneration and resolution process, as they appear to be responsible for the resolution onset (Hashimoto et al 2008).

Schwann cells and resolution

Mechanical nerve injury destabilizes the BNB and lead to the downregulation of the sonic hedgehog pathway that reduces expression of TJPs in the endoneurial blood vessels inducing permeability and hyperalgesia (Moreau et al 2016). Then Schwann cell – via activation of the sonic hedgehog pathway – could initiate TJP expression for restoration of the barrier function and thus pain resolution (Arthur-Farraj et al 2012, Hashimoto et al 2008). In our case using BML111 and RvD1 resealed the endoneurial barrier and following the other groups observations we assume that both BML111 and RvD1 allowed the activation of sonic hedgehog pathway by Schwann cells initiating endoneurial resealing. So far, there is no described activation of the sonic hedgehog pathway following the use of SPMs. Thus, further investigation towards effects of SPMs on Schwann cells and the sonic hedgehog pathway are needed. Some hints indicate that SPMs particularly LXA_4/RvD1 could directly act on Schwann cells. Xia and colleagues described FPR2 expression on Schwann cells (Xia et al 2020). In this study activating FPR2 in Schwann cells after facial nerve injury led to Schwann cells proliferation and remyelination followed by a nerve regeneration (Xia et al 2020). However, this study did not check the activation of the sonic hedgehog pathway after activation of the FPR2 receptor. This has still to be done in the future.

In the resolution process, we described fibrinogen removal as an important part. Fibrinolysis involves several actors, first tissue plasminogen activator cleaves plasminogen into plasmin, fibrinogen is depolymerized in fibrin thanks to thrombin and then plasmin degrades fibrin in fibrin degradation products that are then cleared (Kaufman et al 2018, Yepes et al 2021). Reports indicate that mature myelinated Schwann cells produce and release tissue plasminogen activator (Castorina et al 2015). Moreover release of tissue plasminogen activator by Schwann cells after nerve crush injury in mice induced fibrinolysis protecting against axonal degeneration (Akassoglou et al 2000). In another study the application of exogenous tissue plasminogen activator enhanced nerve regeneration after crush injury in mice (Zou et al 2006). These data suggest that Schwann cells not only initiate BNB resealing after injury but also initiate fibrinolysis. This would designate Schwann cells as the key player of the resolution process.

Schwann cells are possibly the main hub for resolution after nerve injury; could this be the case in DPN? As said previously, there are common grounds to type 2 diabetes models and nerve injury models, especially regarding the role of sonic hedgehog pathway in regulating TJPs expression and restoring the BNB function. Unfortunately in DPN and in both type 1 or type 2 diabetes Schwann cells are subjected to schwannopathies and are not able to fulfill their

function as they undergo various cycles of myelination and demyelination with segmental full demyelination and also have some oxidative stress due to mitochondrial impairments (Gonçalves et al 2017). Restoring Schwann cells function in DPN could allow them to start a resolution process (Belavgeni et al 2022, Guo et al 2022). Also treating with exogenous sonic hedgehog could be a solution for BNB resealing in DPN (Kusano et al 2004). LXA_4/RvD1 have positive effects in DPN (Heng et al 2015, Obrosov et al 2017), which raise the question if these SPMs act directly on Schwann cells as hinted earlier (Xia et al 2020) or if they are acting on other actors upstream to restore Schwann cells function leading to resolution. This question is also applicable in case of nerve injury. Such intermediate actors could be macrophages known to express and carry FPR2 receptors and participate in many resolution processes (Filiberto et al 2022, García et al 2021, Maderna et al 2010). Still, a lot need to be done to understand resolution, the actors involved, their interactions and the role of SPMs between all these actors.

Developing treatment strategies

SPMs (LXA_4/RvD1) present hyperalgesia-resolving effects in both DPN and nerve injury using them as treatment could be an option. Only one has to think of the administration method as injecting patients regularly could be uncomfortable. One could think of using pumps as for insulin in case of type 1 diabetes mellitus. Another important element is to administrate stabilized SPMs molecules, this could be done using nanoparticles as in our study or some stabilized SPMs are available on the market such 17-oxo-RvD1, benzo-RvD1 or $BLXA_4$ (Serhan & Levy 2018). More than SPMs action we also observed the resolution process and described mechanisms that form this process, targeting these mechanisms using other molecules as treatment could also lead to resolution. A closer look to TJPs expression regulation allow us to think of using glycogen-synthase-kinase-3β inhibitors as wnt pathway inhibits TJPs expression (MacAulay & Woodgett 2008), or using sonic hedgehog as it is clear that it participate and favour the resolution through the TJPs upregulation after nerve injury and DPN (Arthur-Farraj et al 2012, Calcutt et al 2003, Sekiguchi et al 2012). It appears that glucocorticoids could be of good help for restoring the BNB function. Some studies have shown that glucocorticoids are stimulating claudin-5 expression and endogenously produced glucocorticoids improve myelination of Schwann cells after crush injury in mice (Greene et al 2019, Morisaki et al 2010). Moreover, it has been shown that glucocorticoids reduced pain in rats after spinal nerve ligation (Li et al 2007). However, it was also described that glucocorticoids could participate in NP (Wang et al 2004). Thus, more investigation are needed.

Stimulating fibrinolysis in addition to restoring BNB function would also accelerate pain resolution. To that end one has to notice that a protein tetranectin stimulate the plasminogen system leading to fibrinolysis (Lin et al 2022). In this study Lin and colleagues treated cellular models of Parkinson's disease with exogenous tetranectin and observed activation of the plasminogen/plasmin system. Interestingly in neurodegenerative diseases such Alzheimer and Parkinson's disease, destabilization of the BBB is accompanied with fibrinogen extravasation in the brain (Marques et al 2013, Ruan et al 2022, Sweeney et al 2018). Moreover tetranectin is found in cerebrospinal fluid of multiple sclerosis patients (Stoevring et al 2006) where BBB disruption and fibrinogen deposits in brain tissue play an important role in its pathophysiology (Davalos et al 2019). An application of tetranectin locally after nerve injury could initiate fibrinolysis and associated with one of the possible BNB resealing methods would initiate resolution and alleviate NP. Not only tetranectin but also tissue plasminogen activator could be used to induce fibrinolysis in a coupled strategy in order to resolve NP after nerve injury.

With this project managed to have a better understanding natural resolution process, identifying some mechanisms behind it. More studies are needed to fully describe the exact pathways involved and their interactions. We also pave the way for developing new treatment strategies for NP using SPMs targeting and accelerating the mechanism involved in the resolution process.

References

Abboud C, Duveau A, Bouali-Benazzouz R, Massé K, Mattar J, et al. 2021. Animal models of pain: Diversity and benefits. *J. Neurosci. Methods* 348: 108997

Akassoglou K, Kombrinck KW, Degen JL, Strickland S. 2000. Tissue plasminogen activator-mediated fibrinolysis protects against axonal degeneration and demyelination after sciatic nerve injury. *J. Cell Biol.* 149: 1157-66

Alanne MH, Pummi K, Heape AM, Grènman R, Peltonen J, Peltonen S. 2009. Tight junction proteins in human Schwann cell autotypic junctions. *J. Histochem. Cytochem.* 57: 523-9

Arthur-Farraj PJ, Latouche M, Wilton DK, Quintes S, Chabrol E, et al. 2012. c-Jun reprograms Schwann cells of injured nerves to generate a repair cell essential for regeneration. *Neuron* 75: 633-47

Authier N, Gillet JP, Fialip J, Eschalier A, Coudore F. 2003. A new animal model of vincristine-induced nociceptive peripheral neuropathy. *Neurotoxicology* 24: 797-805

Bang S, Yoo S, Yang TJ, Cho H, Kim YG, Hwang SW. 2010. Resolvin D1 attenuates activation of sensory transient receptor potential channels leading to multiple anti-nociception. *Br. J. Pharmacol.* 161: 707-20

Belavgeni A, Maremonti F, Stadtmüller M, Bornstein SR, Linkermann A. 2022. Schwann cell necroptosis in diabetic neuropathy. *Proc. Natl. Acad. Sci. U. S. A.* 119: e2204049119

Ben-Kraiem A, Sauer R-S, Norwig C, Popp M, Bettenhausen A-L, et al. 2021. Selective blood-nerve barrier leakiness with claudin-1 and vessel-associated macrophage loss in diabetic polyneuropathy. *J. Mol. Med.*

Bennett GJ, Xie YK. 1988. A peripheral mononeuropathy in rat that produces disorders of pain sensation like those seen in man. *Pain* 33: 87-107

Biessels GJ, Bril V, Calcutt NA, Cameron NE, Cotter MA, et al. 2014. Phenotyping animal models of diabetic neuropathy: a consensus statement of the diabetic neuropathy study group of the EASD (Neurodiab). *J. Peripher. Nerv. Syst.* 19: 77-87

Binder A, Baron R. 2016. The Pharmacological Therapy of Chronic Neuropathic Pain. *Dtsch Arztebl International* 113: 616-26

Bouhassira D. 2019. Neuropathic pain: Definition, assessment and epidemiology. *Rev. Neurol. (Paris)* 175: 16-25

Boullon L, Finn DP, Llorente-Berzal Á. 2021. Sex Differences in a Rat Model of Peripheral Neuropathic Pain and Associated Levels of Endogenous Cannabinoid Ligands. *Front Pain Res (Lausanne)* 2: 673638

Brennan EP, Mohan M, McClelland A, de Gaetano M, Tikellis C, et al. 2018a. Lipoxins Protect Against Inflammation in Diabetes-Associated Atherosclerosis. *Diabetes* 67: 2657-67

Brennan EP, Mohan M, McClelland A, Tikellis C, Ziemann M, et al. 2018b. Lipoxins Regulate the Early Growth Response-1 Network and Reverse Diabetic Kidney Disease. *J. Am. Soc. Nephrol.* 29: 1437-48

Calcutt NA, Allendoerfer KL, Mizisin AP, Middlemas A, Freshwater JD, et al. 2003. Therapeutic efficacy of sonic hedgehog protein in experimental diabetic neuropathy. *J. Clin. Invest.* 111: 507-14

Castorina A, Waschek JA, Marzagalli R, Cardile V, Drago F. 2015. PACAP interacts with PAC1 receptors to induce tissue plasminogen activator (tPA) expression and activity in schwann cell-like cultures. *PLoS One* 10: e0117799

Cattin AL, Burden JJ, Van Emmenis L, Mackenzie FE, Hoving JJ, et al. 2015. Macrophage-Induced Blood Vessels Guide Schwann Cell-Mediated Regeneration of Peripheral Nerves. *Cell* 162: 1127-39

Chapouly C, Yao Q, Vandierdonck S, Larrieu-Lahargue F, Mariani JN, et al. 2016. Impaired Hedgehog signalling-induced endothelial dysfunction is sufficient to induce neuropathy: implication in diabetes. *Cardiovasc. Res.* 109: 217-27

Chattopadhyay R, Raghavan S, Rao GN. 2017. Resolvin D1 via prevention of ROS-mediated SHP2 inactivation protects endothelial adherens junction integrity and barrier function. *Redox Biol* 12: 438-55

Chen J, Li C, Liu W, Yan B, Hu X, Yang F. 2019. miRNA-155 silencing reduces sciatic nerve injury in diabetic peripheral neuropathy. *J. Mol. Endocrinol.* 63: 227-38

Clauw DJ, Essex MN, Pitman V, Jones KD. 2019. Reframing chronic pain as a disease, not a symptom: rationale and implications for pain management. *Postgrad. Med.* 131: 185-98

Cohen SP, Vase L, Hooten WM. 2021. Chronic pain: an update on burden, best practices, and new advances. *Lancet* 397: 2082-97

Colucci M, Stefanucci A, Mollica A, Aloisi AM, Maione F, Pieretti S. 2022. New Insights on Formyl Peptide Receptor Type 2 Involvement in Nociceptive Processes in the Spinal Cord. *Life (Basel)* 12

Contreras KM, Caillaud M, Neddenriep B, Bagdas D, Roberts JL, et al. 2021. Deficit in voluntary wheel running in chronic inflammatory and neuropathic pain models in mice: Impact of sex and genotype. *Behav. Brain Res.* 399: 113009

Costa B, Trovato AE, Colleoni M, Giagnoni G, Zarini E, Croci T. 2005. Effect of the cannabinoid CB1 receptor antagonist, SR141716, on nociceptive response and nerve demyelination in rodents with chronic constriction injury of the sciatic nerve. *Pain* 116: 52-61

Cussell PJG, Gomez Escalada M, Milton NGN, Paterson AWJ. 2020. The N-formyl peptide receptors: contemporary roles in neuronal function and dysfunction. *Neural Regen Res* 15: 1191-98

Davalos D, Mahajan KR, Trapp BD. 2019. Brain fibrinogen deposition plays a key role in MS pathophysiology - Yes. *Mult. Scler.* 25: 1434-35

Deacon RM. 2013. Measuring motor coordination in mice. *J Vis Exp*: e2609

Decosterd I, Woolf CJ. 2000. Spared nerve injury: an animal model of persistent peripheral neuropathic pain. *Pain* 87: 149-58

Deeds MC, Anderson JM, Armstrong AS, Gastineau DA, Hiddinga HJ, et al. 2011. Single dose streptozotocin-induced diabetes: considerations for study design in islet transplantation models. *Lab. Anim.* 45: 131-40

Deuis JR, Dvorakova LS, Vetter I. 2017. Methods Used to Evaluate Pain Behaviors in Rodents. *Front. Mol. Neurosci.* 10: 284

Dong C, Helton ES, Zhou P, Ouyang X, d'Anglemont de Tassigny X, et al. 2018. Glial-derived neurotrophic factor is essential for blood-nerve barrier functional recovery in an experimental murine model of traumatic peripheral neuropathy. *Tissue Barriers* 6: 1-22

Drel VR, Mashtalir N, Ilnytska O, Shin J, Li F, et al. 2006. The leptin-deficient (ob/ob) mouse: a new animal model of peripheral neuropathy of type 2 diabetes and obesity. *Diabetes* 55: 3335-43

Filiberto AC, Ladd Z, Leroy V, Su G, Elder CT, et al. 2022. Resolution of inflammation via RvD1/FPR2 signaling mitigates Nox2 activation and ferroptosis of macrophages in experimental abdominal aortic aneurysms. *FASEB J.* 36: e22579

Finnerup NB, Attal N, Haroutounian S, McNicol E, Baron R, et al. 2015. Pharmacotherapy for neuropathic pain in adults: a systematic review and meta-analysis. *Lancet Neurol.* 14: 162-73

Finnerup NB, Haroutounian S, Kamerman P, Baron R, Bennett DLH, et al. 2016. Neuropathic pain: an updated grading system for research and clinical practice. *Pain* 157: 1599-606

Finnerup NB, Johannesen IL, Fuglsang-Frederiksen A, Bach FW, Jensen TS. 2003. Sensory function in spinal cord injury patients with and without central pain. *Brain* 126: 57-70

Fox A, Eastwood C, Gentry C, Manning D, Urban L. 1999. Critical evaluation of the streptozotocin model of painful diabetic neuropathy in the rat. *Pain* 81: 307-16

Furman BL. 2015. Streptozotocin-Induced Diabetic Models in Mice and Rats. *Curr. Protoc. Pharmacol.* 70: 5.47.1-5.47.20

García RA, Lupisella JA, Ito BR, Hsu MY, Fernando G, et al. 2021. Selective FPR2 Agonism Promotes a Proresolution Macrophage Phenotype and Improves Cardiac Structure-Function Post Myocardial Infarction. *JACC Basic Transl Sci* 6: 676-89

Gonçalves NP, Vægter CB, Andersen H, Østergaard L, Calcutt NA, Jensen TS. 2017. Schwann cell interactions with axons and microvessels in diabetic neuropathy. *Nat. Rev. Neurol.* 13: 135-47

Goto Y, Kakizaki M, Masaki N. 1976. Production of spontaneous diabetic rats by repetition of selective breeding. *Tohoku J. Exp. Med.* 119: 85-90

Green-Fulgham SM, Ball JB, Maier SF, Rice KC, Watkins LR, Grace PM. 2022. Suppression of active phase voluntary wheel running in male rats by unilateral chronic constriction injury: Enduring therapeutic effects of a brief treatment of morphine combined with TLR4 or P2X7 antagonists. *J. Neurosci. Res.* 100: 265-77

Greene C, Hanley N, Campbell M. 2019. Claudin-5: gatekeeper of neurological function. *Fluids Barriers CNS* 16: 3

Gregory NS, Harris AL, Robinson CR, Dougherty PM, Fuchs PN, Sluka KA. 2013. An overview of animal models of pain: disease models and outcome measures. *J. Pain* 14: 1255-69

Guo J, Guo Z, Huang Y, Ma S, Yan B, et al. 2022. Blockage of MLKL prevents myelin damage in experimental diabetic neuropathy. *Proc. Natl. Acad. Sci. U. S. A.* 119: e2121552119

Hackel D, Brack A, Fromm M, Rittner HL. 2012a. Modulation of tight junction proteins in the perineurium for regional pain control. *Ann. N. Y. Acad. Sci.* 1257: 199-206

Hackel D, Krug SM, Sauer RS, Mousa SA, Bocker A, et al. 2012b. Transient opening of the perineurial barrier for analgesic drug delivery. *Proc. Natl. Acad. Sci. U. S. A.* 109: E2018-E27

Hargreaves K, Dubner R, Brown F, Flores C, Joris J. 1988. A new and sensitive method for measuring thermal nociception in cutaneous hyperalgesia. *Pain* 32: 77-88

Hashimoto M, Ishii K, Nakamura Y, Watabe K, Kohsaka S, Akazawa C. 2008. Neuroprotective effect of sonic hedgehog up-regulated in Schwann cells following sciatic nerve injury. *J. Neurochem.* 107: 918-27

Heng LJ, Qi R, Yang RH, Xu GZ. 2015. Docosahexaenoic acid inhibits mechanical allodynia and thermal hyperalgesia in diabetic rats by decreasing the excitability of DRG neurons. *Exp. Neurol.* 271: 291-300

Hirakawa H, Okajima S, Nagaoka T, Takamatsu T, Oyamada M. 2003. Loss and recovery of the blood-nerve barrier in the rat sciatic nerve after crush injury are associated with expression of intercellular junctional proteins. *Exp. Cell Res.* 284: 196-210

Ho Kim S, Mo Chung J. 1992. An experimental model for peripheral neuropathy produced by segmental spinal nerve ligation in the rat. *Pain* 50: 355-63

Huang J, Burston JJ, Li L, Ashraf S, Mapp PI, et al. 2017. Targeting the D Series Resolvin Receptor System for the Treatment of Osteoarthritis Pain. *Arthritis Rheumatol* 69: 996-1008

Huang L, Wang CF, Serhan CN, Strichartz G. 2011. Enduring prevention and transient reduction of postoperative pain by intrathecal resolvin D1. *Pain* 152: 557-65

Jaén RI, Fernández-Velasco M, Terrón V, Sánchez-García S, Zaragoza C, et al. 2020. BML-111 treatment prevents cardiac apoptosis and oxidative stress in a mouse model of autoimmune myocarditis. *FASEB J.* 34: 10531-46

Ji RR, Xu ZZ, Strichartz G, Serhan CN. 2011. Emerging roles of resolvins in the resolution of inflammation and pain. *Trends Neurosci.* 34: 599-609

Kaufman C, Kinney T, Quencer K. 2018. Practice Trends of Fibrinogen Monitoring in Thrombolysis. *J Clin Med* 7

King AJ. 2012. The use of animal models in diabetes research. *Br. J. Pharmacol.* 166: 877-94

Koizumi T, Kerkhofs D, Mizuno T, Steinbusch HWM, Foulquier S. 2019. Vessel-Associated Immune Cells in Cerebrovascular Diseases: From Perivascular Macrophages to Vessel-Associated Microglia. *Front. Neurosci.* 13: 1291

Koussounadis A, Langdon SP, Um IH, Harrison DJ, Smith VA. 2015. Relationship between differentially expressed mRNA and mRNA-protein correlations in a xenograft model system. *Sci. Rep.* 5: 10775

Kucenas S, Takada N, Park H-C, Woodruff E, Broadie K, Appel B. 2008. CNS-derived glia ensheath peripheral nerves and mediate motor root development. *Nat. Neurosci.* 11: 143-51

Kusano KF, Allendoerfer KL, Munger W, Pola R, Bosch-Marce M, et al. 2004. Sonic hedgehog induces arteriogenesis in diabetic vasa nervorum and restores function in diabetic neuropathy. *Arterioscler. Thromb. Vasc. Biol.* 24: 2102-7

Li C, Wu X, Liu S, Shen D, Zhu J, Liu K. 2020. Role of Resolvins in the Inflammatory Resolution of Neurological Diseases. *Front. Pharmacol.* 11: 612

Li H, Xie W, Strong JA, Zhang JM. 2007. Systemic antiinflammatory corticosteroid reduces mechanical pain behavior, sympathetic sprouting, and elevation of proinflammatory cytokines in a rat model of neuropathic pain. *Anesthesiology* 107: 469-77

Lim JY, Park CK, Hwang SW. 2015. Biological Roles of Resolvins and Related Substances in the Resolution of Pain. *Biomed Res Int* 2015: 830930

Lim TK, Shi XQ, Martin HC, Huang H, Luheshi G, et al. 2014. Blood-nerve barrier dysfunction contributes to the generation of neuropathic pain and allows targeting of injured nerves for pain relief. *Pain*

Lima-Garcia JF, Dutra RC, da Silva K, Motta EM, Campos MM, Calixto JB. 2011. The precursor of resolvin D series and aspirin-triggered resolvin D1 display anti-hyperalgesic properties in adjuvant-induced arthritis in rats. *Br. J. Pharmacol.* 164: 278-93

Lin H, Tang R, Fan L, Wang E. 2022. Exogenous Tetranectin Alleviates Pre-formed-fibrils-induced Synucleinopathies in SH-SY5Y Cells by Activating the Plasminogen Activation System. *Neurochem. Res.* 47: 3192-201

Liu J, Peng L, Li J. 2020. The Lipoxin A4 Receptor Agonist BML-111 Alleviates Inflammatory Injury and Oxidative Stress in Spinal Cord Injury. *Med. Sci. Monit.* 26: e919883

Liu ZH, Miao GS, Wang JN, Yang CX, Fu ZJ, Sun T. 2016. Resolvin D1 Inhibits Mechanical Hypersensitivity in Sciatica by Modulating the Expression of Nuclear Factor-κB, Phospho-extracellular Signal-regulated Kinase, and Pro- and Antiinflammatory Cytokines in the Spinal Cord and Dorsal Root Ganglion. *Anesthesiology* 124: 934-44

Lu T, Wu X, Wei N, Liu X, Zhou Y, et al. 2018. Lipoxin A4 protects against spinal cord injury via regulating Akt/nuclear factor (erythroid-derived 2)-like 2/heme oxygenase-1 signaling. *Biomed. Pharmacother.* 97: 905-10

Lux TJ, Hu X, Ben-Kraiem A, Blum R, Chen JT, Rittner HL. 2019. Regional Differences in Tight Junction Protein Expression in the Blood-DRG Barrier and Their Alterations after Nerve Traumatic Injury in Rats. *Int. J. Mol. Sci.*

MacAulay K, Woodgett JR. 2008. Targeting glycogen synthase kinase-3 (GSK-3) in the treatment of Type 2 diabetes. *Expert Opin. Ther. Targets* 12: 1265-74

Maderna P, Cottell DC, Toivonen T, Dufton N, Dalli J, et al. 2010. FPR2/ALX receptor expression and internalization are critical for lipoxin A4 and annexin-derived peptide-stimulated phagocytosis. *FASEB J.* 24: 4240-9

Malong L, Napoli I, White IJ, Stierli S, Bossio A, Lloyd AC. 2019. Macrophages Enforce the Blood Nerve Barrier. *bioRvix*

Manglik A, Lin H, Aryal DK, McCorvy JD, Dengler D, et al. 2016. Structure-based discovery of opioid analgesics with reduced side effects. *Nature* 537: 185-90

Marmiroli P, Riva B, Pozzi E, Ballarini E, Lim D, et al. 2017. Susceptibility of different mouse strains to oxaliplatin peripheral neurotoxicity: Phenotypic and genotypic insights. *PLoS One* 12: e0186250

Marques F, Sousa JC, Sousa N, Palha JA. 2013. Blood-brain-barriers in aging and in Alzheimer's disease. *Mol. Neurodegener.* 8: 38

Martinez JA, Kobayashi M, Krishnan A, Webber C, Christie K, et al. 2015. Intrinsic facilitation of adult peripheral nerve regeneration by the Sonic hedgehog morphogen. *Exp. Neurol.* 271: 493-505

Martini AC, Berta T, Forner S, Chen G, Bento AF, et al. 2016. Lipoxin A4 inhibits microglial activation and reduces neuroinflammation and neuropathic pain after spinal cord hemisection. *J. Neuroinflammation* 13: 75

Mogil JS, Davis KD, Derbyshire SW. 2010. The necessity of animal models in pain research. *Pain* 151: 12-17

Moreau N, Mauborgne A, Bourgoin S, Couraud PO, Romero IA, et al. 2016. Early alterations of Hedgehog signaling pathway in vascular endothelial cells after peripheral nerve injury elicit blood-nerve barrier disruption, nerve inflammation, and neuropathic pain development. *Pain* 157: 827-39

Morisaki S, Nishi M, Fujiwara H, Oda R, Kawata M, Kubo T. 2010. Endogenous glucocorticoids improve myelination via Schwann cells after peripheral nerve injury: An in vivo study using a crush injury model. *Glia* 58: 954-63

Mukherjee PK, Marcheselli VL, Serhan CN, Bazan NG. 2004. Neuroprotectin D1: a docosahexaenoic acid-derived docosatriene protects human retinal pigment epithelial cells from oxidative stress. *Proc. Natl. Acad. Sci. U. S. A.* 101: 8491-6

Nakhooda AF, Like AA, Chappel CI, Wei CN, Marliss EB. 1978. The spontaneously diabetic Wistar rat (the "BB" rat). Studies prior to and during development of the overt syndrome. *Diabetologia* 14: 199-207

Neuhofer A, Zeyda M, Mascher D, Itariu BK, Murano I, et al. 2013. Impaired local production of proresolving lipid mediators in obesity and 17-HDHA as a potential treatment for obesity-associated inflammation. *Diabetes* 62: 1945-56

Ni S, Ling Z, Wang X, Cao Y, Wu T, et al. 2019. Sensory innervation in porous endplates by Netrin-1 from osteoclasts mediates PGE2-induced spinal hypersensitivity in mice. *Nat Commun* 10: 5643

Noble J, Munro CA, Prasad VS, Midha R. 1998. Analysis of upper and lower extremity peripheral nerve injuries in a population of patients with multiple injuries. *J. Trauma* 45: 116-22

Obrosov A, Coppey LJ, Shevalye H, Yorek MA. 2017. Effect of Fish Oil vs. Resolvin D1, E1, Methyl Esters of Resolvins D1 or D2 on Diabetic Peripheral Neuropathy. *J. Neurol. Neurophysiol.* 8

Odusanwo O, Chinthamani S, McCall A, Duffey ME, Baker OJ. 2012. Resolvin D1 prevents TNF-α-mediated disruption of salivary epithelial formation. *Am. J. Physiol. Cell Physiol.* 302: C1331-45

Orr PM, Shank BC, Black AC. 2017. The Role of Pain Classification Systems in Pain Management. *Crit. Care Nurs. Clin. North Am.* 29: 407-18

Pitzer C, Kuner R, Tappe-Theodor A. 2016. EXPRESS: Voluntary and evoked behavioral correlates in neuropathic pain states under different housing conditions. *Mol. Pain* 12

Preguiça I, Alves A, Nunes S, Fernandes R, Gomes P, et al. 2020. Diet-induced rodent models of obesity-related metabolic disorders-A guide to a translational perspective. *Obes. Rev.* 21: e13081

Quiros M, Feier D, Birkl D, Agarwal R, Zhou DW, et al. 2020. Resolvin E1 is a pro-repair molecule that promotes intestinal epithelial wound healing. *Proc. Natl. Acad. Sci. U. S. A.* 117: 9477-82

Ramirez SH, Fan S, Dykstra H, Rom S, Mercer A, et al. 2013. Inhibition of glycogen synthase kinase 3beta promotes tight junction stability in brain endothelial cells by half-life extension of occludin and claudin-5. *PLoS One* 8: e55972

Raputova J, Srotova I, Vlckova E, Sommer C, Üçeyler N, et al. 2017. Sensory phenotype and risk factors for painful diabetic neuropathy: a cross-sectional observational study. *Pain* 158: 2340-53

Rechthand E, Smith QR, Latker CH, Rapoport SI. 1987. Altered blood-nerve barrier permeability to small molecules in experimental diabetes mellitus. *J. Neuropathol. Exp. Neurol.* 46: 302-14

Reinhold AK, Rittner HL. 2017. Barrier function in the peripheral and central nervous system-a review. *Pflugers Arch.* 469: 123-34

Reinhold AK, Yang S, Chen JT, Hu L, Sauer RS, et al. 2019. Tissue plasminogen activator and neuropathy open the blood-nerve barrier with upregulation of microRNA-155-5p in male rats. *Biochim Biophys Acta Mol Basis Dis* 1865: 1160-69

Richner M, Ferreira N, Dudele A, Jensen TS, Vaegter CB, Goncalves NP. 2018. Functional and Structural Changes of the Blood-Nerve-Barrier in Diabetic Neuropathy. *Front. Neurosci.* 12: 1038

Rittner HL, Hackel D, Voigt P, Mousa S, Stolz A, et al. 2009. Mycobacteria attenuate nociceptive responses by formyl peptide receptor triggered opioid peptide release from neutrophils. *PLoS Pathog.* 5: e1000362

Romano M, Cianci E, Simiele F, Recchiuti A. 2015. Lipoxins and aspirin-triggered lipoxins in resolution of inflammation. *Eur. J. Pharmacol.* 760: 49-63

Ruan Z, Zhang D, Huang R, Sun W, Hou L, et al. 2022. Microglial Activation Damages Dopaminergic Neurons through MMP-2/-9-Mediated Increase of Blood-Brain Barrier Permeability in a Parkinson's Disease Mouse Model. *Int. J. Mol. Sci.* 23

Sałat K. 2020. Chemotherapy-induced peripheral neuropathy: part 1-current state of knowledge and perspectives for pharmacotherapy. *Pharmacol. Rep.* 72: 486-507

Sauer RS, Kirchner J, Yang S, Hu L, Leinders M, et al. 2017. Blood-spinal cord barrier breakdown and pericyte deficiency in peripheral neuropathy. *Ann. N. Y. Acad. Sci.* 1405: 71-88

Sauer RS, Krug SM, Hackel D, Staat C, Konasin N, et al. 2014. Safety, efficacy, and molecular mechanism of claudin-1-specific peptides to enhance blood-nerve-barrier permeability. *Journal of controlled release : official journal of the Controlled Release Society* 185: 88-98

Schwarz D, Hidmark AS, Sturm V, Fischer M, Milford D, et al. 2020. Characterization of experimental diabetic neuropathy using multicontrast magnetic resonance neurography at ultra high field strength. *Sci. Rep.* 10: 7593

Sekiguchi H, Ii M, Jujo K, Renault MA, Thorne T, et al. 2012. Estradiol triggers sonic-hedgehog-induced angiogenesis during peripheral nerve regeneration by downregulating hedgehog-interacting protein. *Lab. Invest.* 92: 532-42

Seltzer Z, Dubner R, Shir Y. 1990. A novel behavioral model of neuropathic pain disorders produced in rats by partial sciatic nerve injury. *Pain* 43: 205-18

Seneviratne KN. 1972. Permeability of blood nerve barriers in the diabetic rat. *J. Neurol. Neurosurg. Psychiatry* 35: 156-62

Serhan CN. 2004. A search for endogenous mechanisms of anti-inflammation uncovers novel chemical mediators: missing links to resolution. *Histochem. Cell Biol.* 122: 305-21
Serhan CN, Chiang N. 2013. Resolution phase lipid mediators of inflammation: agonists of resolution. *Curr. Opin. Pharmacol.* 13: 632-40
Serhan CN, Levy BD. 2018. Resolvins in inflammation: emergence of the pro-resolving superfamily of mediators. *J. Clin. Invest.* 128: 2657-69
Shimizu F, Sano Y, Haruki H, Kanda T. 2011. Advanced glycation end-products induce basement membrane hypertrophy in endoneurial microvessels and disrupt the blood-nerve barrier by stimulating the release of TGF-β and vascular endothelial growth factor (VEGF) by pericytes. *Diabetologia* 54: 1517-26
Siemionow M, Brzezicki G. 2009. Chapter 8: Current techniques and concepts in peripheral nerve repair. *Int. Rev. Neurobiol.* 87: 141-72
Sommer C, Lalonde A, Heckman HM, Rodriguez M, Myers RR. 1995. Quantitative neuropathology of a focal nerve injury causing hyperalgesia. *J. Neuropathol. Exp. Neurol.* 54: 635-43
Stanos S, Brodsky M, Argoff C, Clauw DJ, D'Arcy Y, et al. 2016. Rethinking chronic pain in a primary care setting. *Postgrad. Med.* 128: 502-15
Stoevring B, Jaliashvili I, Thougaard AV, Ensinger C, Høgdall CK, et al. 2006. Tetranectin in cerebrospinal fluid of patients with multiple sclerosis. *Scand. J. Clin. Lab. Invest.* 66: 577-83
Sweeney MD, Sagare AP, Zlokovic BV. 2018. Blood-brain barrier breakdown in Alzheimer disease and other neurodegenerative disorders. *Nat. Rev. Neurol.* 14: 133-50
Tao X, Lee MS, Donnelly CR, Ji RR. 2020. Neuromodulation, Specialized Proresolving Mediators, and Resolution of Pain. *Neurotherapeutics* 17: 886-99
Tiwari V, Anderson M, Yang F, Tiwari V, Zheng Q, et al. 2018. Peripherally Acting μ-Opioid Receptor Agonists Attenuate Ongoing Pain-associated Behavior and Spontaneous Neuronal Activity after Nerve Injury in Rats. *Anesthesiology* 128: 1220-36
Toewe A, Balas L, Durand T, Geisslinger G, Ferreirós N. 2018. Simultaneous determination of PUFA-derived pro-resolving metabolites and pathway markers using chiral chromatography and tandem mass spectrometry. *Anal. Chim. Acta* 1031: 185-94
Valdes AM, Ravipati S, Menni C, Abhishek A, Metrustry S, et al. 2017. Association of the resolvin precursor 17-HDHA, but not D- or E- series resolvins, with heat pain sensitivity and osteoarthritis pain in humans. *Sci. Rep.* 7: 10748
Ventzel L, Madsen CS, Karlsson P, Tankisi H, Isak B, et al. 2018. Chronic Pain and Neuropathy Following Adjuvant Chemotherapy. *Pain Med.* 19: 1813-24
Wang C, Chen P, Lin D, Chen Y, Lv B, et al. 2021. Effects of varying degrees of ligation in a neuropathic pain model induced by chronic constriction injury. *Life Sci.* 276: 119441
Wang D. 2008. Discrepancy between mRNA and protein abundance: insight from information retrieval process in computers. *Comput. Biol. Chem.* 32: 462-8
Wang D, Zhang X, Lu L, Li H, Zhang F, et al. 2015. Assessment of diabetic peripheral neuropathy in streptozotocin-induced diabetic rats with magnetic resonance imaging. *Eur. Radiol.* 25: 463-71
Wang JC, Strichartz GR. 2017. Prevention of Chronic Post-Thoracotomy Pain in Rats By Intrathecal Resolvin D1 and D2: Effectiveness of Perioperative and Delayed Drug Delivery. *J. Pain* 18: 535-45
Wang S, Lim G, Zeng Q, Sung B, Ai Y, et al. 2004. Expression of central glucocorticoid receptors after peripheral nerve injury contributes to neuropathic pain behaviors in rats. *J. Neurosci.* 24: 8595-605
Wang YH, Gao X, Tang YR, Chen FQ, Yu Y, et al. 2022. Resolvin D1 Alleviates Mechanical Allodynia via ALX/FPR2 Receptor Targeted Nod-like Receptor Protein 3/Extracellular

Signal-Related Kinase Signaling in a Neuropathic Pain Model. *Neuroscience* 494: 12-24

Wang ZF, Li Q, Liu SB, Mi WL, Hu S, et al. 2014. Aspirin-triggered Lipoxin A4 attenuates mechanical allodynia in association with inhibiting spinal JAK2/STAT3 signaling in neuropathic pain in rats. *Neuroscience* 273: 65-78

Xia W, Zhu J, Wang X, Tang Y, Zhou P, et al. 2020. ANXA1 directs Schwann cells proliferation and migration to accelerate nerve regeneration through the FPR2/AMPK pathway. *FASEB J.* 34: 13993-4005

Xie W, Wang H, Wang L, Yao C, Yuan R, Wu Q. 2013. Resolvin D1 reduces deterioration of tight junction proteins by upregulating HO-1 in LPS-induced mice. *Lab. Invest.* 93: 991-1000

Xu F, Zhang J, Zhou X, Hao H. 2022. Lipoxin A(4) and its analog attenuate high fat diet-induced atherosclerosis via Keap1/Nrf2 pathway. *Exp. Cell Res.* 412: 113025

Xu ZZ, Zhang L, Liu T, Park JY, Berta T, et al. 2010. Resolvins RvE1 and RvD1 attenuate inflammatory pain via central and peripheral actions. *Nat. Med.* 16: 592-7, 1p following 97

Yamamoto S, Kawashiri T, Higuchi H, Tsutsumi K, Ushio S, et al. 2015. Behavioral and pharmacological characteristics of bortezomib-induced peripheral neuropathy in rats. *J. Pharmacol. Sci.* 129: 43-50

Yang S, Krug SM, Heitmann J, Hu L, Reinhold AK, et al. 2016. Analgesic drug delivery via recombinant tissue plasminogen activator and microRNA-183-triggered opening of the blood-nerve barrier. *Biomaterials* 82: 20-33

Ye J, Ding H, Ren J, Xia Z. 2018. The publication trend of neuropathic pain in the world and China: a 20–years bibliometric analysis. *The Journal of Headache and Pain* 19: 110

Yepes M, Woo Y, Martin-Jimenez C. 2021. Plasminogen Activators in Neurovascular and Neurodegenerative Disorders. *Int. J. Mol. Sci.* 22

Zhang L, Terrando N, Xu ZZ, Bang S, Jordt SE, et al. 2018. Distinct Analgesic Actions of DHA and DHA-Derived Specialized Pro-Resolving Mediators on Post-operative Pain After Bone Fracture in Mice. *Front. Pharmacol.* 9: 412

Zhu J, Li L, Ding J, Huang J, Shao A, Tang B. 2021. The Role of Formyl Peptide Receptors in Neurological Diseases via Regulating Inflammation. *Front. Cell. Neurosci.* 15: 753832

Zou T, Ling C, Xiao Y, Tao X, Ma D, et al. 2006. Exogenous tissue plasminogen activator enhances peripheral nerve regeneration and functional recovery after injury in mice. *J. Neuropathol. Exp. Neurol.* 65: 78-86

Zwanziger D, Hackel D, Staat C, Bocker A, Brack A, et al. 2012. A peptidomimetic tight junction modulator to improve regional analgesia. *Mol. Pharm.* 9: 1785-94

Curriculum vitae

M. Sc. Adel Ben-Kraiem
Born the 3rd of November 1993 in Toulouse, France

Education

2018-2023	**PhD Neuroscience, Pain research: Center for Interdisciplinary Pain Medicine, Dept Anesthesiology, Intensive Care, Emergency and Pain Medicine, University Hospital Würzburg, Germany**
2015-2016	**Master 2, Neuroscience, Behavior, Cognition, University of Paul Sabatier, Toulouse, FRANCE.** *Grade average of 14.9 of the 20 possible, Rank: 6th among 18 candidates* *Topics: Cognition, neuroethology and ethology, tools in neurosciences (practical, plasticity and memory process, statistics analysis*
2014-2015	**Master 1 Biology & Health Neuroscience and Behavior, University of Paul Sabatier, Toulouse, FRANCE.** Grade average of 12.8 of the 20 possible *(33rd among 146 candidates) topics: Cognitive neuroscience, Neuroethology and Neurogenetics, Animal Cognition, Neurogenesis and Neurodegeneration, Advance Imaging in Biology, Fundamental and Clinical Pharmacology*
2013-2014	**Bachelor Degree Cellular and Molecular Biology and Physiology, University of Paul Sabatier Toulouse, FRANCE.** *Grade average of 14.1 of the 20 possible (7th among 190 candidates). Topic: Integrated Nerve Function*.
2011	**Baccalaureate (High School Diploma) in Science major Biology, Lycee Sainte Marie des Champs, Toulouse, FRANCE.** *Grade average 14.6 of the 20 possible.*

Work experience

09.2018 - 11.2018	**Scientific assistant Universitätsklinikum Würzburg, Zentrum für interdiszplinäre Schmerzmedizin, Klinik für Anästhesiologe, Intensivmedizin, Notfallmedizin und Schmerztherapie, Würzburg Germany.** Advisor: Prof. Dr. Heike RITTNER
2016-2017	First year of PhD, Stereotaxic viral injection in mice hippocampus and arc in situ hybridization in mice, in LIN, Magdeburg, Germany

Research experience:

Ph.D. Project: Temporal characterisation of the blood nerve barrier and specialized pro resolving mediators as therapeutic targets in neuropathy *Supervisor:* Prof. Dr. Heike RITTNER, AG Molekulare Schmerzforschung

Master Project**:** Role of co-repressor Sin3A in aging. *Supervisor:* Dr Cédrick FLORIAN, CRCA Laboratory (Centre de Recherches sur la Cognition Animale, CNRS UMR 5169), Remember Team, Toulouse, France.

Grants

- 12.2018-11.2021 Stipend funding the PhD project Resolvins for nerve barrier sealing and pain control in neuropathic pain, to be completed. (Promotionsstipendium des Evanglischen Studienwerk Villigst)
- 12.2021-02.2022 DAAD Stipend (Stipendium des deutschen akademischen Austauchdienstes)

Place, date: Würzburg, 02.22.2023 signature

Affidavit

I hereby confirm that my thesis entitled **Temporal characterization of the blood nerve barrier and specialized pro resolving mediators as therapeutic targets in neuropathy** is the result of my own work. I did not receive any help or support from commercial consultants. All sources and / or materials applied are listed and specified in the thesis.

Furthermore, I confirm that this thesis has not yet been submitted as part of another examination process neither in identical nor in similar form.

Würzburg, 02.22.2023

Place, Date Signature

Eidesstattliche Erklärung

Hiermit erkläre ich an Eides statt, die Dissertation **Zeitliche Charakterisierung der Funktion der Blut-Nerven-Schranke und der entzündungsauflösenden Lipide als Targets bei Neuropathie** eigenständig, d.h. insbesondere selbständig und ohne Hilfe eines kommerziellen Promotionsberaters, angefertigt und keine anderen als die von mir angegebenen Quellen und Hilfsmittel verwendet zu haben.

Ich erkläre außerdem, dass die Dissertation weder in gleicher noch in ähnlicher Form bereits in einem anderen Prüfungsverfahren vorgelegen hat.

Würzburg, 22.02.2023

Ort, Datum Unterschrift

Publication list

1. Lux TJ, Hu X, **Ben-Kraiem A**, Blum R, Chen JT, Rittner HL: **Regional Differences in Tight Junction Protein Expression in the Blood-DRG Barrier and Their Alterations after Nerve Traumatic Injury in Rats**. *International Journal of Molecular Sciences* 2019.

2. Oehler B, Kloka J, Mohammadi M, **Ben-Kraiem A**, Rittner HL: **D-4F, an ApoA-I mimetic peptide ameliorating TRPA1-mediated nocifensive behaviour in a model of neurogenic inflammation**. *Molecular Pain* 2020.

3. Sauer RS, Krummenacher I, Bankoglu EE, Yang S, Oehler B, Schoppler F, Mohammadi M, Guntzel P, **Ben-Kraiem A**, Holzgrabe U *et al*: **Stabilization of delphinidin in a complex with sulfobutylether-beta-cyclodextrin allows for antinociception in inflammatory pain**. *Antioxidants and Redox Signaling* 2020.

4. **Ben-Kraiem A**, Sauer R-S, Norwig C, Popp M, Bettenhausen A-L, Atalla MS, Brack A, Blum R, Doppler K, Rittner HL: **Selective blood-nerve barrier leakiness with claudin-1 and vessel-associated macrophage loss in diabetic polyneuropathy**. *Journal of Molecular Medicine* 2021.

5. Hartmannsberger B, **Ben-Kraiem A**, Kramer S, Thomas D, Sisignano M, Kalelkar P, Garcia A, Brack A, Sommer C, Rittner HL: **Formylpeptirecepor 2 (FPR2) activation alievates pain and induces fibrinogen degradation after traumatic nerve injury: in preparation**

Supplementary data

Sham				CCI			
Samples	Ct *Gapdh*	Ct *Cldn1*	ΔCt	Samples	Ct *Gapdh*	Ct *Cldn1*	ΔCt
Sham 1w 1	27.1756924	32.8412923	5.6655999	CCI 1w 1	21.3876512	29.6979774	8.3103262
Sham 1w 2	26.9321669	32.3581111	5.4259442	CCI 1w 2	21.3750848	29.1131915	7.7381068
Sham 1w 3	26.3034038	31.9875520	5.6841482	CCI 1w 3	22.0931110	28.0556811	5.9625701
Sham 1w 4	27.2009483	33.3168500	6.1159017	CCI 1w 4	19.9765637	27.5508532	7.5742895
Sham 1w 5	30.5531421	36.2644440	5.7113020	CCI 1w 5	21.0341744	27.8449780	6.8108035
Sham 1w 6	26.0650192	31.2155205	5.1505013	CCI 1w 6	19.4844832	27.4849145	8.0004313
Sham 3w 1	24.0544620	29.9473262	5.8928642	CCI 3w 1	23.3975516	29.4923572	6.0948055
Sham 3w 2	29.7659445	35.8037563	6.0378118	CCI 3w 2	23.1620108	30.1708897	7.0088789
Sham 3w 3	25.5468768	30.7729777	5.2261009	CCI 3w 3	20.5617664	26.6085565	6.0467900
Sham 3w 4	23.7121302	29.2712622	5.5591320	CCI 3w 4	21.5637667	27.7031015	6.1393348
Sham 3w 5	23.2513693	28.4217515	5.1703822	CCI 3w 5	20.5384185	26.4803063	5.9418878
Sham 3w 6	28.2255667	33.3148582	5.0892915	CCI 3w 6	19.1557197	27.5960856	8.4403659
Sham 6w 1	24.4631536	29.7092914	5.2461378	CCI 6w 1	20.8003520	26.6819789	5.8816270
Sham 6w 2	31.0981671	36.8509320	5.7527649	CCI 6w 2	19.9601391	26.4711773	6.5110381
Sham 6w 3	25.6727317	31.2254659	5.5527342	CCI 6w 3	21.9051544	29.2311469	7.3259925
Sham 6w 4	24.5492791	30.0178256	5.4685466	CCI 6w 4	21.8585034	28.2118476	6.3533442
Sham 6w 5	29.5048299	34.5434607	5.0386309	CCI 6w 5	19.2448696	25.5540342	6.3091646
Sham 6w 6	undetermined			CCI 6w 6	19.3630270	25.4557849	6.0927579
Sham 9w 1	22.9909890	28.4900342	5.4990452	CCI 9w 1	22.0771876	28.3851401	6.3079525
Sham 9w 2	23.0588083	28.7290537	5.6702454	CCI 9w 2	20.7481705	27.9986311	7.2504606
Sham 9w 3	23.6769093	29.4397172	5.7628078	CCI 9w 3	23.9914438	30.5540542	6.5626104
Sham 9w 4	24.0631029	29.7744838	5.7113809	CCI 9w 4	22.9043998	29.2089376	6.3045378
Sham 9w 5	25.1981393	30.6666858	5.4685466	CCI 9w 5	25.1981393	undetermined	
Sham 9w 6	23.6928365	29.4258050	5.7329685	CCI 9w 6	23.2969673	29.4587577	6.1617904

Sham				CCI			
Samples	Ct *Gapdh*	Ct *Cldn5*	ΔCt	Samples	Ct *Gapdh*	Ct *Cldn5*	ΔCt
Sham 1w 1	27.0339217	32.3915693	5.3576476	CCI 1w 1	21.0512563	29.6076911	8.5564348
Sham 1w 2	26.0420446	30.6898552	4.6478105	CCI 1w 2	21.0489685	28.9023487	7.8533801
Sham 1w 3	25.9631389	30.1627393	4.1996004	CCI 1w 3	22.1142290	28.8448248	6.7305958
Sham 1w 4	26.5329133	30.0698482	3.5369349	CCI 1w 4	19.7688062	25.2747050	5.5058987
Sham 1w 5	25.9640590	30.6218998	4.6578408	CCI 1w 5	20.7666908	29.8624460	9.0957552
Sham 1w 6	26.4329047	31.0293606	4.5964559	CCI 1w 6	19.9920078	28.3731434	8.3811356
Sham 3w 1	25.1842239	29.3835529	4.1993290	CCI 3w 1	23.1832291	28.3336829	5.1504538
Sham 3w 2	27.8062184	32.7467824	4.9405640	CCI 3w 2	22.3009651	31.7301822	9.4292171
Sham 3w 3	24.7946911	29.9040508	5.1093597	CCI 3w 3	20.4881499	29.3211534	8.8330036
Sham 3w 4	24.5406175	28.3818258	3.8412083	CCI 3w 4	21.5212205	27.0087160	5.4874955
Sham 3w 5	23.9435103	29.0352215	5.0917111	CCI 3w 5	20.4386364	25.6530691	5.2144327
Sham 3w 6	27.0542609	31.2492388	4.1949779	CCI 3w 6	21.6848741	27.9547393	6.2698652
Sham 6w 1	24.2644626	28.5053681	4.2409055	CCI 6w 1	20.5039367	29.7859632	9.2820265
Sham 6w 2	29.5334529	34.7549758	5.2215229	CCI 6w 2	20.2812671	28.3336972	8.0524301
Sham 6w 3	26.0022526	30.6106729	4.6084203	CCI 6w 3	21.6519857	31.5579218	9.9059361
Sham 6w 4	35.9263056	40.3498468	4.4235412	CCI 6w 4	21.6859556	30.1279905	8.4420349
Sham 6w 5	28.2774913	32.3243779	4.0468866	CCI 6w 5	19.7218606	29.5530213	9.8311607
Sham 6w 6	undetermined			CCI 6w 6	19.9750083	28.3319939	8.3569856
Sham 9w 1	25.4249749	29.7015430	4.2765681	CCI 9w 1	22.1298176	27.0304083	4.9005907
Sham 9w 2	25.3520279	30.0801172	4.7280893	CCI 9w 2	23.1637556	26.8821889	3.7184332
Sham 9w 3	24.0687753	28.4478289	4.3790536	CCI 9w 3	21.6568047	26.1853805	4.5285757
Sham 9w 4	24.8317134	29.3973074	4.5655941	CCI 9w 4	20.2684915	25.5266802	5.2581887
Sham 9w 5	25.8579971	30.1897338	4.3317367	CCI 9w 5	20.2161770	27.6759630	7.4597860
Sham 9w 6	24.5782007	29.3411360	4.7629353	CCI 9w 6	22.9975338	25.5266802	2.5291464

Suppl. Table 1 Raw Ct and ΔCt values for *Cldn1* and *Cldn5*

Sham				CCI			
Samples	Ct *Gapdh*	Ct *Fpr2*	ΔCt	Samples	Ct *Gapdh*	Ct *Fpr2*	ΔCt
Sham 1w 1	25.9750578	33.0729146	7.0978568	CCI 1w 1	21.4543861	25.7677675	4.3133814
Sham 1w 2	26.2528246	33.3723080	7.1194835	CCI 1w 2	21.1910501	25.5698668	4.3788167
Sham 1w 3	25.7405134	32.6621345	6.9216212	CCI 1w 3	21.9933546	26.9021252	4.9087706
Sham 1w 4	26.5832467	33.2306661	6.6474193	CCI 1w 4	19.9591875	24.4940145	4.5348271
Sham 1w 5	25.9033412	32.3338852	6.4305439	CCI 1w 5	20.7895442	25.5810103	4.7914661
Sham 1w 6	26.5065960	33.0972007	6.5906047	CCI 1w 6	19.9897789	24.9125280	4.9227491
Sham 3w 1	25.3474863	31.5523620	6.2048757	CCI 3w 1	23.6181106	26.3736030	2.7554924
Sham 3w 2	28.0612111	34.9432085	6.8819973	CCI 3w 2	22.5369715	26.7035025	4.1665310
Sham 3w 3	24.6070449	31.7880000	7.1809552	CCI 3w 3	20.4813999	23.5075266	3.0261267
Sham 3w 4	24.5257722	32.3480468	7.8222746	CCI 3w 4	21.4787122	26.5253010	5.0465888
Sham 3w 5	23.7585472	31.0116609	7.2531137	CCI 3w 5	20.2485831	26.2069828	5.9583997
Sham 3w 6	27.0128835	34.3332025	7.3203190	CCI 3w 6	21.6678456	27.2160943	5.5482487
Sham 6w 1	24.7230853	31.2347538	6.5116684	CCI 6w 1	19.9237905	25.1586584	5.2348680
Sham 6w 2	29.6091828	37.2482889	7.6391061	CCI 6w 2	20.2966773	24.7771188	4.4804416
Sham 6w 3	25.9149016	33.0369237	7.1220221	CCI 6w 3	21.5799930	27.1085134	5.5285205
Sham 6w 4	34.7105752	42.1386773	7.4281021	CCI 6w 4	21.8450650	27.4721237	5.6270587
Sham 6w 5	27.7137538	33.8303692	6.1166155	CCI 6w 5	20.0150524	24.5857898	4.5707374
Sham 6w 6	undetermined			CCI 6w 6	19.9062395	24.2156707	4.3094312

Suppl. Table 2 Raw Ct and ΔCt values for *Fpr2*

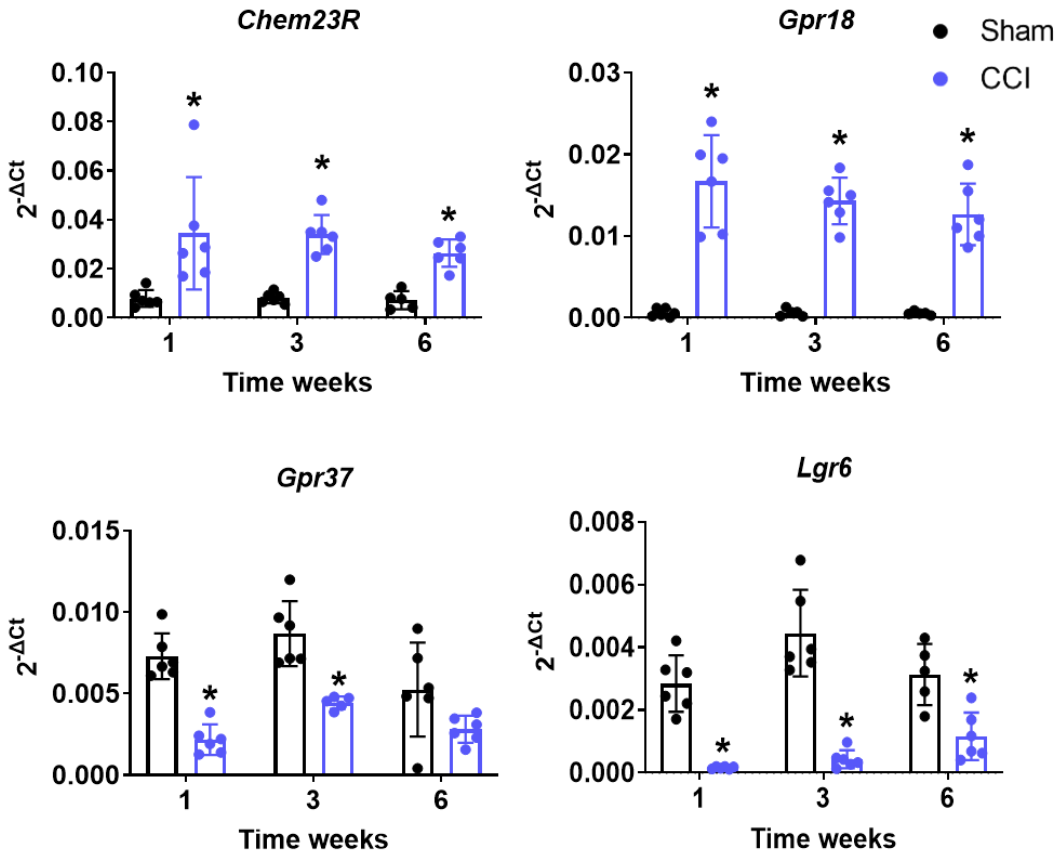

Suppl. Fig. 1 Gene expression of SPMs receptors after CCI

Sham				CCI			
Samples	Ct *Gapdh*	Ct *Chem23R*	ΔCt	Samples	Ct *Gapdh*	Ct *Chem23R*	ΔCt
Sham 1w 1	27.2325740	34.5378584	7.3052844	CCI 1w 1	21.5387939	26.7836575	5.2448636
Sham 1w 2	26.6407012	33.9239016	7.2832004	CCI 1w 2	21.1529084	25.8863323	4.7334238
Sham 1w 3	26.1595627	32.2965110	6.1369483	CCI 1w 3	22.1152114	25.7803368	3.6651254
Sham 1w 4	26.6111608	34.4948336	7.8836728	CCI 1w 4	19.8723416	25.6260340	5.7536924
Sham 1w 5	25.9140103	33.0884217	7.1744114	CCI 1w 5	20.9259680	26.0426483	5.1166803
Sham 1w 6	26.7791307	33.5184984	6.7393677	CCI 1w 6	20.0072091	25.8901111	5.8829021
Sham 3w 1	25.6425358	32.7355676	7.0930317	CCI 3w 1	23.4679399	28.3849711	4.9170312
Sham 3w 2	30.5475808	38.0654971	7.5179163	CCI 3w 2	20.8743827	26.0349877	5.1606050
Sham 3w 3	24.7309897	31.1630222	6.4320325	CCI 3w 3	21.5815157	26.8998963	5.3183806
Sham 3w 4	25.4396996	32.2822772	6.8425775	CCI 3w 4	20.2519686	25.0854257	4.8334571
Sham 3w 5	23.6147197	30.8792571	7.2645374	CCI 3w 5	21.5845084	26.4239612	4.8394529
Sham 3w 6	27.2710812	34.0385649	6.7674837	CCI 3w 6	22.8457433	27.2261126	4.3803693
Sham 6w 1	29.5052693	37.7200245	8.2147551	CCI 6w 1	20.5701307	25.5921465	5.0220158
Sham 6w 2	26.1898581	33.2124758	7.0226177	CCI 6w 2	19.9298695	24.8474798	4.9176103
Sham 6w 3	37.8247290	44.7731230	6.9483940	CCI 6w 3	21.6374127	27.4935141	5.8561014
Sham 6w 4	27.6419729	33.9507107	6.3087378	CCI 6w 4	20.2528482	25.3848312	5.1319830
Sham 6w 5	27.7305077	35.6092949	7.8787872	CCI 6w 5	20.0044466	25.3490835	5.3446370
Sham 6w 6	25.0228614	29.5 (outlier)	4.5651514	CCI 6w 6	20.9333328	26.2950395	5.3617067

Suppl. Table 3 Raw Ct and ΔCt values for *Chem23R*

Sham				CCI			
Samples	Ct *Gapdh*	Ct *Gpr18*	ΔCt	Samples	Ct *Gapdh*	Ct *Gpr18*	ΔCt
Sham 1w 1	27.0083333	36.6470446	9.6387114	CCI 1w 1	9574395864	27.1013369	5.9055930
Sham 1w 2	26.1389692	36.9399878	10.8010185	CCI 1w 2	21.0412494	26.4213208	5.3800715
Sham 1w 3	25.2896245	34.9686765	9.6790520	CCI 1w 3	22.1667636	27.8469018	5.6801382
Sham 1w 4	26.7925861	36.4773841	9.6847980	CCI 1w 4	20.0419403	26.6511878	6.6092476
Sham 1w 5	25.9497708	41.0903397	15.1405689	CCI 1w 5	20.8067373	26.4527906	5.6460533
Sham 1w 6	26.5920213	37.9073815	11.3153602	CCI 1w 6	20.0406567	26.6968579	6.6562012
Sham 3w 1	26.0112756	38.1565757	12.1453001	CCI 3w 1	23.2753975	29.2814880	6.0060905
Sham 3w 2	27.8250854	undetermined		CCI 3w 2	20.5600470	26.7010309	6.1409839
Sham 3w 3	24.7463392	35.2098164	10.4634772	CCI 3w 3	21.6844487	27.9594264	6.2749777
Sham 3w 4	24.8775887	34.4421413	9.5645526	CCI 3w 4	20.2916459	26.3491563	6.0575104
Sham 3w 5	23.8257715	34.3284696	10.5026981	CCI 3w 5	21.7346764	28.4019597	6.6672834
Sham 3w 6	27.1202165	39.5015068	12.3812903	CCI 3w 6	22.6033029	28.3696345	5.7663315
Sham 6w 1	29.5038539	40.2468733	10.7430194	CCI 6w 1	19.8091774	26.6673987	6.8582213
Sham 6w 2	26.0768422	36.9563599	10.8795177	CCI 6w 2	20.2205165	25.9592977	5.7387812
Sham 6w 3	34.5950676	46.3260111	11.7309435	CCI 6w 3	21.8007862	28.4410903	6.6403041
Sham 6w 4	27.8084719	38.7900073	10.9815354	CCI 6w 4	21.9587044	27.9684342	6.0097297
Sham 6w 5	24.7228141	34.8318140	10.1090000	CCI 6w 5	19.9722708	26.3475610	6.3752902
Sham 6w 6	undetermined			CCI 6w 6	20.0315715	26.5373867	6.5058152

Suppl. Table 4 Raw Ct and ΔCt values for *Gpr18*

Sham				CCI			
Samples	Ct *Gapdh*	Ct *Gpr37*	ΔCt	Samples	Ct *Gapdh*	Ct *Gpr37*	ΔCt
Sham 1w 1	27.2325740	34.5378584	7.3052844	CCI 1w 1	21.5387939	31.1598354	9.6210415
Sham 1w 2	26.6407012	33.8691826	7.2284814	CCI 1w 2	21.1529084	30.1828201	9.0299117
Sham 1w 3	26.1595627	32.8219382	6.6623755	CCI 1w 3	22.1152114	30.1341236	8.0189122
Sham 1w 4	26.6111608	33.9660727	7.3549119	CCI 1w 4	19.8723416	29.3639955	9.4916539
Sham 1w 5	25.9140103	33.0884217	7.1744114	CCI 1w 5	20.9259680	29.7440313	8.8180634
Sham 1w 6	26.7791307	33.7665476	6.9874169	CCI 1w 6	20.0072091	28.6981047	8.6908956
Sham 3w 1	25.6425358	32.3349998	6.6924640	CCI 3w 1	23.4679399	31.4832712	8.0153313
Sham 3w 2	30.5475808	37.6714521	7.1238713	CCI 3w 2	20.8743827	28.5746342	7.7002516
Sham 3w 3	24.7309897	31.8593177	7.1283280	CCI 3w 3	21.5815157	29.3625900	7.7810743
Sham 3w 4	25.4396996	31.8206054	6.3809057	CCI 3w 4	20.2519686	28.1265867	7.8746181
Sham 3w 5	23.6147197	30.7924133	7.1776936	CCI 3w 5	21.5845084	29.3094188	7.7249104
Sham 3w 6	27.2710812	34.0385649	6.7674837	CCI 3w 6	22.8457433	27.22 (outlier)	4.3803693
Sham 6w 1	29.5052693	36.6278050	7.1225357	CCI 6w 1	20.5701307	29.8870100	7.3859182
Sham 6w 2	26.1898581	33.7334043	7.5435463	CCI 6w 2	19.9298695	27.9560489	10.3032869
Sham 6w 3	37.8247290	44.6220851	6.7973561	CCI 6w 3	21.6374127	30.2331564	6.7859222
Sham 6w 4	27.6419729	35.3665984	7.7246255	CCI 6w 4	20.2528482	28.4233349	8.5101833
Sham 6w 5	25.0228614	32.7136960	7.6908346	CCI 6w 5	20.0044466	28.7630315	9.2600317
Sham 6w 6	27.7305077	38.9312230	11.2007153	CCI 6w 6	20.9333328	29.2644783	8.3311455

Suppl. Table 5 Raw Ct and ΔCt values for *Gpr37*

Sham				CCI			
Samples	Ct *Gapdh*	Ct *Lgr6*	ΔCt	Samples	Ct *Gapdh*	Ct *Lgr6*	ΔCt
Sham 1w 1	27.3861641	35.2790413	7.8928772	CCI 1w 1	23.8460198	36.5903040	12.7442842
Sham 1w 2	26.5994114	34.8874396	8.2880282	CCI 1w 2	24.1456024	37.2722383	13.1266359
Sham 1w 3	26.1526388	34.8288284	8.6761896	CCI 1w 3	24.6189602	36.9153030	12.2963427
Sham 1w 4	27.0274786	35.8487811	8.8213025	CCI 1w 4	22.7406973	35.6987316	12.9580343
Sham 1w 5	25.2857438	34.4760380	9.1902942	CCI 1w 5	23.3415038	35.7686780	12.4271742
Sham 1w 6	26.1690704	34.4183359	8.2492655	CCI 1w 6	22.5904954	34.9230829	12.3325875
Sham 3w 1	26.9046223	34.1086012	7.2039789	CCI 3w 1	23.9480387	35.5484058	11.6003671
Sham 3w 2	25.3882366	33.6409887	8.2527521	CCI 3w 2	23.0003917	34.2082499	11.2078582
Sham 3w 3	26.8194798	34.8952591	8.0757793	CCI 3w 3	23.2356711	35.0869004	11.8512293
Sham 3w 4	26.6866566	34.8344855	8.1478289	CCI 3w 4	8813135534	39.0906456	12.9025142
Sham 3w 5	30.6821591	38.6681547	7.9859955	CCI 3w 5	5258944267	34.4990841	11.0464946
Sham 3w 6	26.5668412	34.0785103	7.5116691	CCI 3w 6	0648575660	37.7203629	10.0138772
Sham 6w 1	24.8540726	33.9732939	9.1192213	CCI 6w 1	1486589572	32.0252037	8.7103378
Sham 6w 2	25.5319989	34.1256792	8.5936804	CCI 6w 2	22.5903973	33.2446352	10.6542379
Sham 6w 3	26.2905374	34.3508134	8.0602760	CCI 6w 3	2160887621	33.9004209	11.2788120
Sham 6w 4	36.6900776	44.5520904	7.8620128	CCI 6w 4	7027810971	33.1816102	10.5113321
Sham 6w 5	29.3851879	37.6524791	8.2672912	CCI 6w 5	22.5619230	31.7722240	9.2103010
Sham 6w 6	undetermined			CCI 6w 6	22.7201164	32.4618014	9.7416850

Suppl. Table 6 Raw Ct and ΔCt values for *Lgr6*

CCI vehicle				CCI BML111			
Samples	Ct *Gapdh*	Ct *Cldn5*	ΔCt	Samples	Ct *Gapdh*	Ct *Cldn5*	ΔCt
CCI vehicle 1	23.0847149	34.2729645	11.1882496	CCI BML 1	22.2598267	32.2360497	9.9762230
CCI vehicle 2	22.5693798	33.5396080	10.9702282	CCI BML 2	22.7513180	30.8910980	8.1397800
CCI vehicle 3	23.2764797	34.2052481	10.9287684	CCI BML 3	21.8097248	33.5699654	11.7602406
CCI vehicle 4	23.0807266	34.1147078	11.0339812	CCI BML 4	22.0991955	33.1398506	11.0406551
CCI vehicle 5	23.1936703	34.2066623	11.0129920	CCI BML 5	22.1819534	33.4230080	11.2410545
CCI vehicle 6	22.8220768	33.7056770	10.8836002	CCI BML 6	22.9742661	32.5433159	9.5690498

Suppl. Table 7 Raw Ct and ΔCt values for *Cldn5* in CCI after BML111 injections

Male							
CCI vehicle				CCI RvD1			
Samples	Ct *Gapdh*	Ct *Cldn5*	ΔCt	Samples	Ct *Gapdh*	Ct *Cldn5*	ΔCt
CCI vehicle 1	23.8563175	34.7274437	10.8711262	CCI RvD1 1	23.1113796	32.0065308	8.1502132
CCI vehicle 2	22.9803104	32.1836700	9.2033596	CCI RvD1 2	22.9130917	32.2161369	9.2358265
CCI vehicle 3	23.2857533	33.8435936	10.5578403	CCI RvD1 3	22.9691620	31.8103275	8.5245743
CCI vehicle 4	21.6022186	34.1267815	12.5245628	CCI RvD1 4	23.3042603	32.4789810	10.8767624
CCI vehicle 5	21.7156124	33.8269768	12.1113644	CCI RvD1 5	21.1421223	32.0627594	10.3471470
CCI vehicle 6	23.4933414	34.9015236	11.4081821	CCI RvD1 6	22.6378307	32.5405464	9.0472050
Female							
CCI vehicle				CCI RvD1			
Samples	Ct *Gapdh*	Ct *Cldn5*	ΔCt	Samples	Ct *Gapdh*	Ct *Cldn5*	ΔCt
CCI vehicle 1	21.8067398	32.8164063	11.0096664	CCI RvD1 1	22.8926468	32.6229782	9.7303314
CCI vehicle 2	22.1232185	33.2792015	11.1559830	CCI RvD1 2	21.6769638	32.4261322	10.7491684
CCI vehicle 3	22.8366432	32.9165459	10.0799026	CCI RvD1 3	22.2307320	32.2549210	10.0241890
CCI vehicle 4	21.9648609	33.2213957	11.2565348	CCI RvD1 4	21.9772682	32.5789642	10.6016960
CCI vehicle 5	22.4381771	33.6370460	11.1988689	CCI RvD1 5	21.9059410	32.2691498	10.3632088
				CCI RvD1 6	22.2543297	31.6447372	9.3904076

Suppl. Table 8 Raw Ct and ΔCt values for *Cldn5* in CCI male and female rats after RvD1 loaded NPs injections

List of abreviations

NP	Neuropathic pain
QST	Quantitative sensory testing
NPSI	Neuropathic pain symptom inventory
SNRI	Serotonin-noradrenaline-reuptake-inhibitors
NNT	Number needed to treat
TRPV1	Transient receptor potential vanilloid 1
TRPA1	Transient receptor potential ankyrin 1
CGRP	Calcitonin generated peptide
CFA	Complete Freund’s adjuvant
CIPN	Chemotherapy-induced peripheral neuropathy
DPN	Diabetic polyneuropathy
DRG	Dorsal root ganglia
STZ	Streptozotocin
CCI	chronic constriction injury
PSNL/PNI	Partial sciatic nerve ligation/partial nerve injury
SNL	Spinal nerve ligation
SNI	Spared nerve injury
BBB	Blood brain barrier
BSCB	Blood spinal cord barrier
BDRGB	Blood dorsal root ganglion barrier
BNB	Blood nerve barrier
CNS	Central nervous system
PNS	Peripheral nervous system
TJPs	Tight junction proteins
SPMs	Specialised proresolving mediators

PUFAs	ω-3 polyunsaturated fatty acids
EPA	Eicosapentaenoic acid
DHA	Docosahexaenoic acid
RvE	Resolvin-E-series
RvD	Resolvin-D-series
Mar	Maresin
NPD1	Neuroprotectin D1
RvD1	Resolvin D1
PGE2	Prostaglandin E2
IL-1	Interleukin-1
IL-1β	Interleukin 1 beta
IL-10	Interleukin 10
TNF-α	Tumor necrosis factor alpha
TGF-β1	Tumor growth factor beta1
NF-kB/p65	Nuclear factor kappa-light-chain-enhancer of activated B cells
IBA-1	Ionized calcium-binding adapter molecule 1
17(R)-HDHA	17(R)-hydroxy docosahexaenoic acid
LXA_4	Lipoxin-A4
ALX/FPR2	lipoxin A4/annexin-A1 7 receptor/formyl-peptide receptor 2
GPR18, 32, 37	G-protein-coupled-receptor 18, 32, 37
ChemR23	Chemerin receptor
PEG-PLGA acid	Biotinylated polymeric polyethylene glycol–poly lactic acid-coglycolic
ZO-1	Zonula occludens 1
mRNA	messenger ribonucleic acid
Cldn1	claudin-1 mRNA
Cldn5	claudin-5 mRNA
Fpr2	Formyl-peptide receptor 2 mRNA

LC-MS/MS	Liquid chromatography tandem mass spectrometry
NaFlu	Sodium fluorescein
EBA	Evans blue albumin
BSA	Bovine serum albumin
PBS	Phosphate buffered saline
SDS	Sodium dodecyl sulfate
RECA-1	Rat Endothelial Cell Antigen 1
vWF	von Willebrand factor

Material list

Antibodies			
Antibody	reference	company	RRID
Claudin-1	37-4900	Thermo Fisher	AB_2533323
Claudin-5	35-2500	Thermo Fisher	AB_2533200
von Willebrand factor (vWF)	A0082	Agilent (formerly DAKO)	AB_2315602
RECA-1	MA1-81510	Thermo Fisher	AB_935279
CD68	MCA341R	Bio-Rad	AB_2291300
CD206	ab64693	Abcam	AB_1523910
Fibrinogen	ABIN458743	Antibodies-Online	AB_10787808
β-actin	A3854	Sigma-Aldrich	AB_262011
Gapdh	MAB374	Millpore	AB_2107445
Donkey anti-mouse Alexa Fluor 555	A-31570	Thermo Fisher	AB_2536180
Goat anti-mouse FITC	F0257	Sigma-Aldrich	AB_259378
Donkey anti-rabbit Alexa Fluor 555	A-31572	Thermo Fisher	AB_162543
Donkey anti-rabbit Alexa Fluor 488	A-21206	Thermo Fisher	AB_2535792
Donkey anti goat Alexa fluor 594	A32758	Thermo Fisher	AB_2762828
Mouse IgG HRP conjugated	7076	Cell Signaling Technology	AB_330924

TaqMan probes		
Probe	Reference	Company
Gapdh	Rn01462662_g1	Thermo Fisher
Cldn1	Rn00581740_m1	Thermo Fisher
Cldn5	Rn01753146_s1	Thermo Fisher
Fpr2	Rn03037051_gH	Thermo Fisher

Chemicals and reagents		
Product	Reference	Company
Evans blue Albumine (EBA)	E2129	Sigma-Aldrich
Sodium Fluorescein (NaFlu)	F6377	Sigma-Aldrich
BML111	SML0215	Sigma-Aldrich
Resolvin D1	10012554	Cayman Chemical
Phosphate buffered saline (PBS)	D8537	Sigma-Aldrich
Nonfat dried milk powder	A0830	ITW Reagents
Triton™ X-100	T8787	Sigma-Aldrich
TWEEN®20	P7949	Sigma-Aldrich
DAPI	D9542	Sigma-Aldrich
N,N,N',N'-Tetramethylethylenediamine (TEMED)	T9281	Sigma-Aldrich
2-Mercaptoethanol	M7154	Sigma-Aldrich
Ambion™ Nuclease free water	AM9937	Thermo Fisher
2-Propanol	I9516	Sigma-Aldrich
Chkoroform	32211	Sigma-Aldrich
Ethanol	32205	Sigma-Aldrich
Paraformaldehyde	A3813,500	ITW Reagents
Pierce™ BCA protein assay kit	23225	Thermo Fisher
TaqMan™ Fast advanced master mix	4444557	Thermo Fisher
cOmplete Ultra tablets, mini, EASYpack (protease inhibitor)	05 892 970 001	Roche
NaCl 0.9% saline solution	235 0778	BRAUN

Chemicals and reagents		
Distilled water: Ampuwa® 1000mL Pöastipur®	1088811	Fresenius Kabi
SDS ultrapure	A1112.0500	ITW Reagents
Tris ultrapure	A1086,1000	ITW Reagents
Sodium-deoxycholate	D6750	Sigma-Aldrich
Sodium-chloride	31434	Sigma-Aldrich
Glycine	131340.1211	ITW Reagents
Glycerol	A3552,1000	ITW Reagents
Bromophenol blue	114391	Sigma-Aldrich
Nonidet®P40 (NP40)	A1694.0250	ITW Reagents
Hydrogen peroxyde	216763	Sigma-Aldrich
Luminol/Aminophital hydrazide	123072	Sigma-Aldrich
Coumaric-acid	C9008	Sigma-Aldrich
Dimethylsulfoxid (DMSO)	D2650	Sigma-Aldrich
ROTIPHORESE®GEL 30: Acrylamide	3029.2	ROTH
Hydrochloric acid	T134.1	ROTH
Sodium hydroxide solution	1.09137.1000	Sigma-Aldrich
Acetone	32201	Sigma-Aldrich
Methanol	32213	Sigma-Aldrich
PageRuler Plus Prestained Protein Ladder	26620	Thermo Fisher
Donkey serum	D9663	Sigma-Aldrich
QIAzol® Lysis reagent (trizol)	5,346,994	QIAGEN
High-Capacity cDNA reverse transcription kit with Rnase inhibitor	4374966	Thermo Fisher

Solutions		
Solution	Reagents	Purpose
3M Tris PH 8.8	Tris	Enter in the composition of other buffers and solutions
	Hydroclhoric acid	
	Distilled water	
1M Tris PH 6.8	Tris	
	Hydroclhoric acid	
	Distilled water	
SDS 10%	SDS	
	Distilled water	
RIPA buffer	0.1% SDS	Lysis buffer
	150 mM Sodium-chloride	
	0.5% Sodium-deoxycholate	
	1% NP40	
	Distilled water	
RIPA buffer + protease inhibitor	1 tablet protease inhibitor	Lysis buffer for protein extraction
	10 mL RIPA buffer	
PFA 4%	Paraformaldehyde	Tissue fixation
	PBS	
	Hydroclhoric acid	
	Sodium hydroxide solution	
	Distilled water	

Solutions		
Laemmli	SDS	Protein loading marker during electrophoresis
	Glycerol	
	Bromophenol blue	
	1M Tris PH6.6	
Electrophoresis buffer	Tris 8.8	Western blot, electrophoresis, protein migration
	Glycine	
	SDS	
	Distilled water	
Towbin buffer	Tris	Western blot, protein transfer from gel to membrane
	Glycine	
	Methanol	
	SDS 10%	
	Distilled water	

Softwares		
Software	Company	RRID
GraphPad Prism 9.1.1 (225)	Graphpad vy dotmatics	SCR_002798
Fiji ImageJ	National Institutes of Health	SCR_002285
Biorender	Biorender	SCR_018361

Acknowledgements

I would like to thank in the first place my supervisor, **Prof. Dr. Heike Rittner**, for her permanent support, skilled guidance, and teaching. It was an honor and a satisfaction to work with you and in your group, where surfaces curiosity, precision, and eagerness. Surely are grateful those who had, have, and will have the chance to be under your supervision.

Many thanks to the members of my thesis committee, Prof. Dr. Robert Blum, Prof. Dr. Claudia Sommer, and Prof. Dr. Paul Pauli, for their constant support and feedback regarding my work.

Special thanks to Dr. Solange Reine Sauer and Dr. Beate Hartmannsberger for their practical teachings, help and supervision in the lab.

Warm thanks to the Evangelisches Studienwerk Villigst that supported me financially and without whom I would never been able to carry on the project.

To all lab members and alumni: Dr. Annemarie Aue, Dr. Jeremy Chen, Dr. Ann-Kristin Reinhold, Dr. Juliane Becker, Dr. Sofia Kramer, Dr Gudrun-Karin Kindl, Carla Norwig, Thomas Lux, Christopher Dietz, Anna-Lena Bettenhausen, Lea Schmitt, Sabrina Scriba, Katharina Mehling, Mariam Sobhy Atalla, Julius Verse, Bruno Rogalla von Bieberstein, Philipp Wenzel and many others. Thank you all for being such kind and helpful colleagues, allowing a stimulating and driving team atmosphere.

To all our collaborators who took part in the project: PD Dr. Marco Sissignano, Dr. Dominique Thomas, Prof. Dr. Andrés García and Dr. Pranav Kalelkar. Thanks a lot, without your contributions the project would not have been completed.

To Dr. Mohammed Hankir I would like to thank you and express my gratitude for language editing and for all the interesting discussions and advice, scientific or not, we had during all these years.

Finally, I would like to thank my family, relatives, and friends for their amazing and invaluable support throughout good and bad times and thus from abroad.